Collecting Quality Echosounder Data in Inclement Weather

Volume 352 I December 2021

ICES COOPERATIVE RESEARCH REPORT

RAPPORT
DES RECHERCHES
COLLECTIVES

ICES INTERNATIONAL COUNCIL FOR THE EXPLORATION OF THE SEA
CIEM CONSEIL INTERNATIONAL POUR L'EXPLORATION DE LA MER

International Council for the Exploration of the Sea
Conseil International pour l'Exploration de la Mer

H. C. Andersens Boulevard 44–46
DK-1553 Copenhagen V
Denmark
Telephone (+45) 33 38 67 00
Telefax (+45) 33 93 42 15
www.ices.dk
info@ices.dk

Series editor: Emory Anderson
Prepared under the auspices of ICES Working Group on Fisheries Acoustics, Science, and Technology (WGFAST), ICES Workshop on Collecting Quality Underwater Acoustic Data in Inclement Weather (WKQUAD), and ICES Topic Group on Collecting Quality Underwater Acoustic Data in Inclement Weather (TGQUAD)
Peer-reviewed by Julia Clemons (NOAA Fisheries, USA), and Lars G. Rudstam (Cornell University, USA)

ISBN number: 978-87-7482-751-1
ISSN number: 2707-7144

ICES Cooperative Research Report

Volume 352 I December 2021

Collecting Quality Echosounder Data in Inclement Weather

Authors

J. Michael Jech ● Matthias Schaber ● Martin Cox ● Pablo Escobar-Flores ● Sven Gastauer ● Kunnath Haris ● John Horne ● Toby Jarvis ● Yoann Ladroit ● Richard O'Driscoll ● Geir Pedersen ● Marian Peña ● Tim Ryan ● Serdar Sakinan ● Rebecca Thomas ● Haley Viehman ● Carrie Wall ● Timothy Whitton

Recommended format for purpose of citation:

Jech, J. M., Schaber, M., Cox, M., Escobar-Flores, P., Gastauer, S., Haris, K., Horne, J., *et al.* 2021. Collecting quality echosounder data in inclement weather. ICES Cooperative Research Report, Vol. 352. 108 pp. https://doi.org/10.17895/ices.pub.7539

ICES International Council for the Exploration of the Sea
CIEM Conseil International pour l'Exploration de la Mer

Contents

I Summary

Echosounder data are widely collected and employed to address multitude scientific questions, from characterizing pelagic marine ecosystems, to investigating the behaviour and dynamics of marine organisms, and estimating the abundance and biomass of marine resources.

Acoustic data are collected from a variety of platforms that are influenced in different ways by the environment, weather, and sea state. These factors can affect vessel motion in many ways, which, in turn, affects the quality of echosounder data through (i) the movement of the transducer emitting sound pulses into the water column, (ii) bubbles at the transducer face, and (iii) increased electrical, mechanical, and acoustic noise.

A reduction in data quality will directly affect the outcome of quantitative estimates based on echosounder data, such as stock assessments. Therefore, procedures for collecting and processing quality echosounder data in inclement weather situations need to be developed. However, the diversity of platforms employed for collecting echosounder data, and the enormous variability of individual platform responses to inclement weather, render it highly challenging and complicated to develop a universal set of procedures and recommendations that can be applied to all platforms. Accordingly, all recommendations need to be driven by acoustic data, rather than by weather conditions or the response of individual platforms to such conditions.

The practical aims of this CRR are to (i) review current knowledge and experience on the impact of weather conditions on acoustic data collected with a variety of echosounders operating on research vessels at common acoustic frequencies used in fisheries acoustics; (ii) develop standard procedures and methods for identifying unsuitable survey conditions, i.e. situations that are considered too degraded to continue collecting acoustic data; and (iii) propose methods for dealing with degraded data.

II Foreword

To meet the goals of this CRR, the Working Group on Fisheries Acoustics, Science, and Technology (WGFAST) conducted a Workshop on Collecting Quality Underwater Acoustic Data in Inclement Weather (WKQUAD) during the 2017 meeting in Nelson, New Zealand. During this initial meeting, vessel-independent metrics were developed and examined to determine which could feasibly be used as criteria for identifying reduced data quality. WKQUAD quickly identified the complexity of deriving such universal, data-driven metrics from data influenced by a variety of environmental effects. Subsequently, after this problem was scoped, a Topic Group on Collecting Quality Underwater Acoustic Data in Inclement Weather (TGQUAD) was created. TGQUAD met in conjunction with the annual WGFAST meetings the following three years, to develop a set of recommendations and write this CRR.

The authors hope that this CRR will be a helpful guide for users and operators of echosounders, and survey scientists alike, but also recognize that with the deployment of an increasing variety of such echosounders on an increasing variety of platforms, all metrics and recommendations provided in this report will require continuous updates and refinements. These updates and refinements may come as updates to survey protocols [e.g. ICES Survey Protocols published within the ICES Techniques in marine Environmental Science (TIMES) series], WGFAST and other ICES expert group annual reports (published in the ICES Scientific Reports series), and/or ICES expert group GitHub[1] sites.

[1] https://github.com/ices-eg. Last accessed 9 November 2021.

1 Introduction

This CRR focuses on developing standard procedures and methods to identify unsuitable survey conditions, propose methods for dealing with degraded data, and compare procedures and methods on selected datasets. This introduction provides the rationale, scope, and outline of the CRR.

1.1 Rationale

High-quality echosounder data are essential to quantitative fisheries assessments. Three common scenarios for the collection of echosounder data during a ship-based survey are:

i) one or more trained acousticians onboard with the skills and experience to make real-time decisions about the echosounder data quality;

ii) scientists onboard without the skills and experience to make real-time decisions about the echosounder data quality; or

iii) no scientists onboard, and the vessel captain makes decisions about the survey (e.g. opportunistic echosounder data collected during commercial fishing operations).

These three scenarios influence the data quality. Data quality is a continuum from high to low, with implications for quantitative and qualitative applications, such as estimating abundance, input to ecological models, and describing spatio-temporal distributions of marine resources.

The scientific utility of echosounder data would be improved if recommendations could be provided for the collection of high-quality echosounder data under any given survey scenario.

1.2 Scope

Given the importance of weather conditions (e.g. windspeed or sea state) on collecting quality echosounder data, the scope of this CRR was constrained to recommendations for the collection of data that are used for abundance estimates in stock assessments or ecosystem models.

Different data-quality outcomes can arise under similar weather conditions. For example, under the same weather conditions, a well-designed research vessel with motion stabilization and the transducers mounted on a retractable centre board is likely to obtain different echosounder data quality than a small fishing boat. Similarly, the same vessel may obtain different results under the same weather conditions when running with the seas or into it. Due to this variability of platform response to inclement weather, recommendations were formulated based on diagnostic information and metrics of data quality.

Given these constraints, decisions were made about which echosounder types, platform types, and specific echosounder measurements to consider.

1.2.1 Acoustic systems

At the time of writing, only narrow bandwidth (narrowband) single-beam echosounders are used for quantitative fisheries assessments. Therefore, this report only provides recommendations for these systems, focusing on the common narrowband frequencies centred at 18, 38, 70, 120, 200, and 333 kHz.

We do not address wide bandwidth (wideband), single-beam echosounders, multibeam echosounders (including two-dimensional swathe systems for water column or seabed, two-dimensional high-resolution imaging sonars and three-dimensional omnidirectional systems), or Acoustic Doppler Current Profilers (ADCPs).

1.2.2 Platforms

At the time of writing, the vast majority of quantitative fisheries assessments using echosounders are carried out from downward-facing transducers mounted on research platforms travelling on the sea surface. We, therefore, provide recommendations for mobile surface platforms, including research vessels (RVs), fishing vessels (FVs), and autonomous surface vehicles (ASVs).

We do not provide recommendations for towed bodies, autonomous underwater vehicles (AUVs), moorings, fish attraction devices (FADs), or other fixed surface or subsurface platforms. However, data from some of these platforms were useful for our analyses (see sections 4 and 5).

1.2.3 Echosounder measurements

Analyses and recommendations are constrained to *in situ* measurements of volume backscatter data (S_v; dB re 1 m^{-1}) collected during acoustic/trawl surveys, and derived area backscatter [s_a (m^2 m^{-2}) or s_A (m^2 nautical mile^{-2})] that are used directly for estimating abundance for stock or ecosystem assessments (see MacLennan *et al*., 2002 for definitions of acoustic variables).

The data-quality threshold for accepting target strength data (TS; dB re 1 m^2) that are used for resource management is stringent. Therefore, it is recommended that TS data not be collected during inclement weather. We present TS data and analyses in this report only to provide examples and develop diagnostics.

1.3 Report outline

This report provides technical background to the topic of echosounder signal degradation, and recommendations for the collection of quality echosounder data in inclement weather for use in quantitative fisheries assessments.

Section 2 details the sources of echosounder data degradation. The introduction defines this report's use of signal (Section 2), noise (Section 2.2), and attenuation (Section 2.3), then details the different types and sources of noise and attenuation. The section wraps up with practical approaches to reducing noise and attenuation (i.e. data degradation; Section 2.4).

Section 3 addresses metadata considerations for echosounders and platforms used for fisheries surveys. Metadata are critical for the acoustic data to be useful not only for the intended survey, but, perhaps more importantly, also for applications beyond that first use when the data can be used for multiple purposes. Throughout the document, case studies are provided using data collected from a variety of platforms. Annex 4 provides pertinent metadata for those platforms so that readers can gauge their vessel or autonomous vehicle against those provided here.

Section 4 provides metrics and case studies for quantifying signal attenuation when using only echosounder data. In these cases, ancillary data describing meteorological conditions (e.g. windspeed and direction), oceanic conditions (e.g. sea state), and vessel conditions (e.g. heading and motion) are not available. Therefore, metrics based solely on the acoustic data, and products

from the acoustic data are used as indicators of data quality. Examples are provided here for seabed backscatter (Section 4.1), transducer ringing (Section 4.2), transducer impedance (Section 4.3), and comparisons among hull-mounted and towed vehicle/trawl or drop-keel mounted transducers (Section 4.4).

Section 5 provides metrics and case studies for quantifying signal attenuation using echosounder and ancillary data in combination. Windspeed (Section 5.1), relative wind heading (Section 5.2), and platform motion (Section 5.3), are examples of ancillary data that were explored as indicators of data quality.

Section 6 provides a synthesis of the results of the case studies and evaluations (i.e. comparisons) among the different metrics that were developed in sections 4 and 5. Summaries of metrics based on acoustic data alone (Section 6.1) and metrics based on a combination of acoustic and ancillary data (Section 6.2) are provided. The potential error due to inclement weather is related to the broader context of the overall error budget when collecting and processing acoustic data for fisheries surveys (Section 6.3). A workflow is proposed that can be used by researchers to evaluate and diagnose their data (Section 6.4).

Section 7 describes post-processing methods that can be applied when measures to eliminate or minimize noise and attenuation were not effective during data acquisition. Historical data are "you get what you get", in the sense that it is not possible to go back and change the way they were collected. Therefore, methods and algorithms have been developed to clean the data of background noise (Section 7.1), impulse noise (Section 7.2), transient noise (Section 7.3), signal attenuation due to bubbles (Section 7.4), signal attenuation due to transducer motion (Section 7.5), speckle noise (Section 7.6), transducer ringing (Section 7.7), and seabed aliases (Section 7.8). Many of the metrics depend on detection and enumeration of attenuated pings, so an initial comparison of the algorithms provided by different software packages was conducted to evaluate the effectiveness of the algorithms on a common dataset (Section 7.4.1).

Section 8 discusses the implications of the case studies and metrics on data quality, and develops data-quality flags (Section 8.1), criteria for accepting or rejecting data (Section 8.2), thresholds and diagnostics (Section 8.3), and applications of metrics and indicators (Section 8.4). A primary application for these metrics and indicators is developing strategies for data collection during surveys and for post-processing data (Section 8.5).

Section 9 summarizes this report and provides practical advice and recommendations to fisheries acousticians on how to evaluate data quality, collect clean data (or at least minimize data degradation), and what to do when data were collected under less than optimal conditions.

The annexes provide a glossary (Annex 2), a list of acronyms used throughout the document (Annex 3) and a table of platform metadata (Annex 4).

2 Sources of echosounder data degradation

Echosounders are remarkably sensitive. They convert the smallest amount of reflected sound (acoustic backscatter) to an electrical voltage, which is then processed to the digital data that are used for estimating abundance and biomass. Thus, it should not be surprising that echosounders are highly susceptible to external sources of unwanted sound (acoustic noise) and voltage (electrical noise; e.g. Simmonds and MacLennan, 2005; Wittje, 2020), in the forms of electrical or mechanical interference, acoustic cross-talk from high-energy pulses of other acoustic systems, and reductions in backscatter due to excess acoustic attenuation. For the purposes of this document, acoustic and electrical noise are the backscatter and voltage, respectively, which degrade data quality; and attenuation is the reduction in received backscatter, which also degrades data quality. Unless specified, we use noise as a generic term inclusive of both acoustic and electrical sources. Noise and attenuation can be highly dependent on weather conditions, and this document is structured around developing diagnostics, metrics, and indicators of data quality using measurements of noise and attenuation.

Degradation is a signal-processing term used to describe a reduction in the quality of a desired measurement (i.e. the signal). Degradation in echosounder data is due to noise and/or signal attenuation. Noise adds a positive bias to the data (i.e. an increase in electrical voltage that can be interpreted as an increase in acoustic energy), while attenuation adds a negative bias to the data (i.e. a decrease in electrical voltage that can be interpreted as a decrease in acoustic energy). Both noise and attenuation will often increase fluctuations in the data. Noise is independent of the echosounder transmit/receive cycle. The range at which the noise manifests in the echogram depends on the timing of the transmit/receive cycle in relation to the noise. If it appears in the echogram at short ranges, the noise may not be significant, but due to the time-varied-gain (TVG) function, it may dominate the data if it appears at longer ranges.

Adverse weather can increase noise from a variety of sources, including increased engine load, noise from the collapse of surface bubbles, and a generally noisier environment. Adverse weather can also cause attenuation of the transmitted and/or received acoustic backscatter due to the bubbles that are pushed beneath the hull as the vessel interacts with sea conditions (i.e. bubble sweep down; Delacroix *et al.*, 2016a), entrapment of air bubbles by breaking waves (Delacroix *et al.*, 2016b), and/or losses due to motion effects (Stanton, 1982; Dunford, 2005). Collectively, these are the degradation factors that determine data quality and, consequently, measurement uncertainty. A useful metric of data quality is the signal-to-noise ratio (SNR; Kieser *et al.*, 2005; Demer *et al.*, 2015), with higher SNR values representing better data quality. Since there are different sources of noise, descriptions of SNR need to be explicit (e.g. signal-to-acoustic noise and signal-to-background noise).

The focus of this CRR is on weather related sources of data degradation. However, degraded echograms can often contain a combination of artefacts that can be weather related or have another source. Therefore, a comprehensive approach is required that considers all sources of data degradation, regardless of origin. It is useful to consider the various sources of data degradation separately when seeking to minimize their influence during acquisition and post-processing. In this section, the potential sources of echosounder data degradation (Table 2.1; Figure 2.1) and the practical approaches to reduce their effects are reviewed, with a focus on downward-facing transducers mounted on a mobile surface platform. Section 7 describes post-processing methods to reduce the effects of degradation when mitigation methods were either not possible or not fully effective.

Table 2.1. Types and sources of echosounder data degradation for downward-facing transducers mounted on mobile surface platforms. See text for further details about each type.

Type	Weather-related sources?	Non-weather-related sources?
Platform design	Yes	Yes
Noise		
Background noise	Yes	Yes
Impulse noise	No	Yes
Transient noise	Yes	Yes
Multi-ping aliasing	No	Yes
Transducer ringing	Yes	Yes
Attenuation		
Bubble attenuation	Yes	Yes
Transducer motion	Yes	No

2.1 Platform design

Careful platform design and configuration can minimize and perhaps eliminate various sources of data degradation. In some cases, research vessels have been explicitly designed and built to meet a radiated noise specification (Mitson, 1995; Spence and Fischer, 2017). Hull design and, in particular, the use of transducers mounted on a retractable keel (i.e. protruding, drop keel, centre board; ICES, 1990; Shabangu *et al*., 2014) can greatly improve data quality and the range of weather conditions in which reliable acoustic data can be collected (Shabangu *et al*., 2014). Retractable keels often increase the transducer depth by 1–3 m below the keel depth, which can position the transducers below the bubble sweep of the hull, or below the bubble layer (see Section 2.2.5). Nevertheless, weather conditions can reach a point where the data quality of lowered keel systems is still compromised (Shabangu *et al*., 2014).

Modern research vessels have highly complex electrical systems that can produce broad-spectrum electromagnetic radiation. This can induce unwanted electrical noise in the transducer cables and transceiver wiring, which manifests itself in the acoustic data as noise. Thorough attention to electrical shielding is essential. Common strategies are running transducer cables in separate steel conduits that are physically located away from other cable runs, grounding the transducer and/or transceivers to the ship's ground and/or the sea, and turning off offending machinery, equipment, or instruments when collecting scientific data. Mechanical sources may also be problematic, with hydraulic pumps, electrical generators, refrigeration units, and other machinery generating noise that might interfere with the electrical signal.

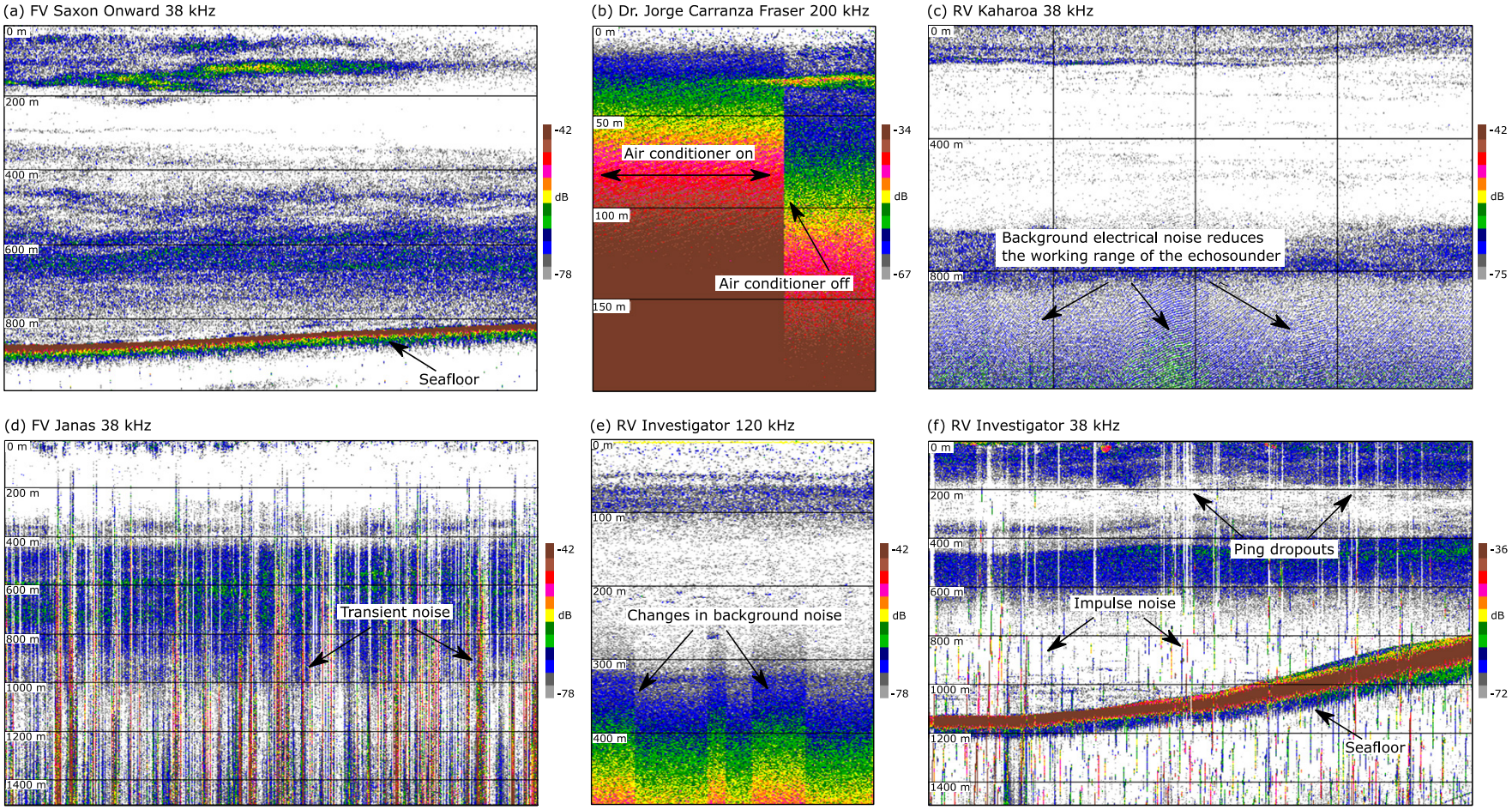

Figure 2.1. Examples of various types of data degradation. Echograms are S_v data, and colour scales represent S_v minimum and maximum thresholds. (a) Example of high-quality 38-kHz data from the FV Saxon Onward. (b) High level of background noise at 200 kHz on the RV Dr Jorge Carranza, which dropped by ca. 15 dB when an air conditioning unit on the bridge was turned off. (c) 38-kHz echogram from the RV Kaharoa showing background noise that is likely electrical in origin. (d) 38-kHz echogram from the FV Janas, recorded in poor weather, showing transient noise. (e) 120-kHz echogram from the RV Investigator showing similar changes in background noise as seen in panel (b). (f) 38-kHz echogram from the RV Investigator showing cross-talk impulse noise from multibeam or ADCP sounders as well as attenuated pings due to inclement weather.

2.2 Noise

In the context of an echosounder, noise can be either acoustic or electrical in origin. Acoustic noise enters the system at the transducer face, while electrical noise can be induced through the transceiver wiring or transducer cabling. In any case, noise is an unwanted signal that rises above the processing threshold applied to the S_v data.

Acoustic and electrical noise can be classified on the basis of amplitude and duration, resulting in the following common categorization scheme (De Robertis and Higginbottom, 2007; Ryan *et al.*, 2015; Peña, 2016):

- background noise, defined as low-amplitude, long-duration (minutes to hours) noise that is often amplified (e.g. by TVG);
- impulse noise, defined as high-amplitude, short-duration noise (less than one ping duration, typically in the order of milliseconds); or
- transient noise, defined as medium- to high-amplitude, medium-duration noise (persists over multiple pings).

2.2.1 Background noise

The total received acoustic backscatter contains contributions from acoustic backscatter plus noise. The acoustic backscatter component is reduced as a function of range due to absorption by seawater and beam spreading. Background noise, on the other hand, is independent of range and ping-duty cycle (i.e. ping duration and rate). Thus, the relative contribution of backscatter to the total signal will decrease with range, and the background noise will be progressively more dominant. At some point, the effective range of the data is reached, i.e. SNR decreases below an acceptable threshold. Note also that since attenuation increases with acoustic frequency, the effective range will also decrease with increasing frequency.

Background noise is a form of additive noise that can be introduced to the transmit signal (Simmonds and MacLennan, 2005; De Robertis and Higginbottom, 2007; Peña, 2016) and can vary in intensity and pattern with vessel speed, engine speed, propeller pitch, bottom depth, and/or other factors (Peña, 2016).

Sources of acoustic background noise include:

- radiated sound from the vessel's engine and other machinery;
- flow noise from water and bubbles moving across the hull as the vessel moves through the water;
- sound generated from collapsing bubbles (cavitation), due to the pitch, speed, and design of the vessel's propeller;
- biologically generated sounds in the environment, e.g. grazing sea urchins or snapping shrimp; and
- physically generated sounds in the environment, e.g. rain, wind, or sea ice abrasion.

Sources of electrical background noise include:

- thermally generated noise from the random motion of electrons in the transceiver;
- electrical interference from electrical instruments, e.g. power supplies, air-conditioning units, or microwave ovens; and

- multiple different ground connections within the transceiver and/or transducer circuit, causing ground loops with different voltages that result in voltage fluctuations.

These background noise sources can all be significant, and can vary over time in their amplitude, pattern, and frequency, resulting in variation in their contribution to S_v.

2.2.2 Impulse noise

Acoustic interference among systems with similar, overlapping, or harmonics of the echosounder frequencies (also termed cross-talk or impulse noise; Ryan *et al.*, 2015) is a common problem when a platform is running multiple acoustic systems, such as narrowband and/or broadband downward-facing echosounders, multibeam swathe systems, ADCPs, and omnidirectional sonars.

Sources of acoustic impulse noise include:

- transmit pulses from other acoustic instruments mounted on the same or other nearby platforms;
- echoes from strong targets due to the transmit pulse of other acoustic instruments; and
- sounds produced by marine mammals and other organisms.

Sources of electrical impulse noise include:

- DC-to-AC power inverters, where the rapid switching of the inverter's output alternating current (AC) from positive to negative voltage generates short voltage spikes at either 50 or 60 Hz; and
- AC circuits, which similarly generate voltage spikes.

Of these potential sources of impulse noise, the most common are cross-talk (Figure 2.1) from unsynchronized echosounders and inverter noise. Impulse noise is artificially amplified by the TVG function in the same way as background noise. Unlike background noise, impulse noise can be significant at all ranges when its amplitude is high, and can span a wide range of frequencies. This type of noise is often very obvious, in which case the transmit pulse of the other system(s) can be observed in the echograms and removed as impulse noise (Ryan *et al.*, 2015). In other cases, it can be more difficult to detect, and requires the analysis of echograms in passive mode (passive mode or listening mode, is when the transmit pulse is not transmitted, but the echosounder remains open to receive signals). Cross-talk can be severe in broadband data due to transmit pulses among unsynchronized sounders, and/or the harmonics of one frequency sweep being within the range of an adjacent bandwidth. Pings synchronization does not mitigate this issue, which is the primary reason why sequential pinging is used when recording broadband data (e.g. with the Simrad EK80).

Synchronization among acoustic instruments may minimize or even remove cross-talk. However, syncing instruments can be complicated, since there are often competing objectives for each system. Synchronization often requires compromises, and the ping rate of some instruments may need to be reduced or increased to stay in lock-step with other instruments.

2.2.3 Transient noise

Transient noise is a specific form of noise where additive noise is introduced to the received signal, which occurs at non-regular intervals and persists over a number of transmit/receive cycles (Figure 2.1; Ryan *et al.*, 2015). Transient noise may be present in as little as one ping cycle

or may persist for as long as 10–20 s. The mechanisms generating transient noise are often not clear, but sources of acoustic transient noise can be broad-spectrum high-energy or electrical.

Broad-spectrum high energy sources can include:

- radiated noise due to impacts on the hull, e.g. waves, sea ice, active ballast systems, and steam nozzles;
- radiated sound from the vessel's engine and other machinery; and
- sound generated from collapsing bubbles (cavitation), due to the pitch, speed, and design of the vessel's propeller.

Sources of electrical transient noise include:

- electromagnetic interference from electrical instruments, e.g. noisy power supplies, air-conditioning units, and microwave ovens.

Of these potential sources of transient noise, wave impacts on the hull and propeller cavitation are thought to be the most common during surface-vessel echosounder surveys.

Transient noise is artificially amplified by the TVG function in the same way as background and impulse noise. Depending on its initial amplitude, transient noise may be significant at any range (high amplitude noise) or only beyond a given range (medium amplitude noise).

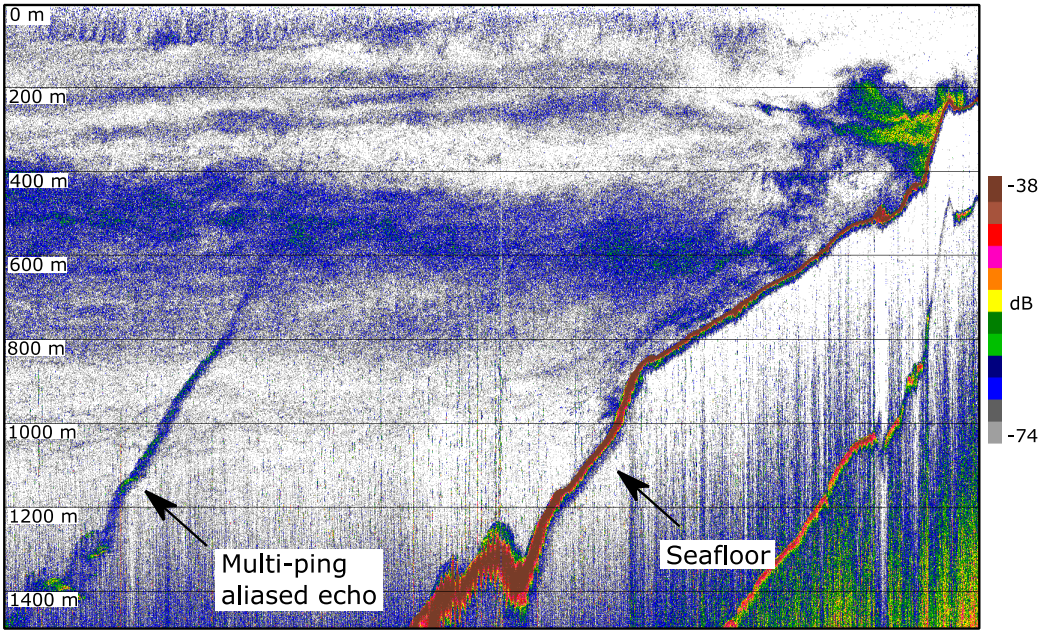

Figure 2.2. Example 38-kHz echogram with the seabed alias interference recorded by FV Paerangi. The colour bar represents the range of S_v values displayed in the echogram.

2.2.4 Multi-ping aliasing

Multi-ping aliasing can occur when strongly scattering targets along the propagation path of the transmitted pulse, such as the seabed, fish schools, or echoes from other sonars, generate echoes that can continue to reflect between scattering boundaries for a period of time (e.g. MacLennan *et al.*, 2004). While multi-ping aliasing is not weather-dependent (Table 2.1), it is a source of noise and needs to be addressed when post-processing water column data. Since the echo reflects at the boundaries multiple times, this is known as multipathing. For a downward-facing transducer, the most common multipathing scenario occurs when the transmitted pulse

reflects repeatedly between the bottom and either the water surface, the platform, or the transducer mounting plate. If the receive cycle is long enough, the multipathed bottom echo appears on the S_v echogram at twice the range of the original bottom echo. This is known as a second bottom echo and can be eliminated from the watercolumn data because it arrives after the primary seabed echo. In fact, there can be multiple bottom echoes, all of which arrive after the first seabed echo (e.g. right side of the echogram in Figure 2.2). However, if, during the current receive cycle, a subsequent ping is transmitted while the transmission immediately prior is still multipathing, the prior transmission may be detected if it encounters the transducer. The detection of an echo from the previous transmission during the current receive cycle is known as aliasing (Blackwell *et al*., 2019), and, when the echo is due to the seabed, it is often referred to as a ghost or false bottom echo (Figure 2.2; Tomczak *et al*., 2002; Bourguignon *et al*., 2009). This mixing of the seabed echo can be difficult to deal with. In some cases, it matches the seabed topography and is strong and readily identifiable, but in other situations, it can subtly mix with layers of backscatter.

Multi-ping aliasing most often occurs in deep water (> 1000 m), but depending on ping rate, it can occur in shallower water. This source of noise can be eliminated by controlling the ping repetition rate, either via an active supervision regime (Renfree and Demer, 2016) or via the use of a suitably slow ping rate.

2.2.5 Transducer ringing

The transmitted acoustic pulse is caused by precise vibration of the piezoelectric elements in the transducer. Following transmission, the elements take an amount of time to stop vibrating. This is referred to as ringing, the duration of which is determined by the damping characteristics of the transducer. Generally, a transducer will require a fixed number of wave periods to stop ringing. Since the wave period is a function of the transmit frequency, higher-frequency transducers will generally ring for less time. In addition, older transducers composed of tonpilz ceramic elements will ring for longer than newer transducers composed of composite ceramic elements.

As the elements continue to vibrate after pulse transmission, they contribute significantly to the received voltage via the piezoelectric effect. This manifests on an echogram as very high values within the first few samples, which then decrease rapidly as the vibration is reduced to zero (Figure 2.3). The SNR will be < 1 for these samples, hence they cannot be used for the detection of targets, such as entrained air bubbles (Section 2.3). For echograms generated from a downward-facing transducer, the time elapsed since transmission is translated to a depth value, hence the colloquial term ringdown.

2.3 Signal attenuation

The backscattered acoustic energy received at the transducer can be reduced (attenuated) by (1) scattering and absorption of the acoustic energy by strongly scattering targets (the sum of which is referred to as extinction), such as dense aggregations of animals (Foote, 1999) and clouds of air bubbles; and/or (2) by changes in the direction that the transducer is pointing between transmission and reception, such that the echo is received further off-axis and hence in a less sensitive part of the transducer beam pattern. Entrained air bubbles (Section 2.3.1) and changes in transducer pointing direction (i.e. transducer motion, Section 2.3.2) are both important manifestations of inclement weather. When compared with unaffected or less-affected pings on an S_v echogram, the effect of attenuation on a given ping can be seen as a vertical stripe of

samples with lower S_v values than those nearby (Figure 2.1). For this reason, an attenuated ping is often referred to as a ping dropout.

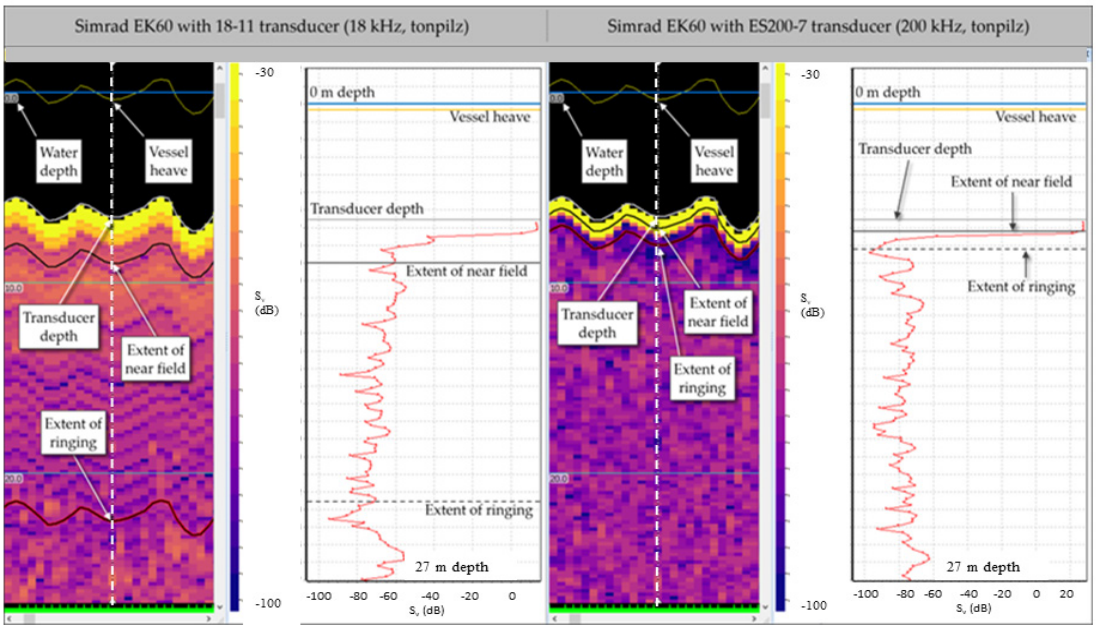

Figure 2.3. An example of transducer ringing for two different tonpilz transducers installed on the retractable keel of the RV GO Sars in 2013. A zoomed in view of the S_v echogram is shown for each transducer (to the left on each double panel), along with a plot of S_v vs. depth for the ping indicated by the vertical dotted line on the echogram (to the right on each double panel). The nearfield extent was calculated using the equation available at http://www2.dnr.cornell.edu/acoustics/SuggestedSOP.html (last accessed 9 November 2021). The ringing extent was estimated by eye from the echogram. Please note that (i) the ringing duration is shorter for the higher-frequency transducer, and (ii) the 18–kHz transducer has a short period of intense ringing followed by a longer period of lower-level oscillations.

2.3.1 Entrained air bubbles

Clouds of air bubbles at short range in front of a transducer can occur in two ways: (1) air bubbles can be entrained into the water column by breaking waves due to wind and water currents, or (2) when a surface vessel pitches and rolls, air bubbles can be entrained into the water column and swept under and along the hull as it moves forward (bubble sweep or sweep-down). The influence of entrained air bubbles on the echo integral has been characterized in a number of marine surveys from surface vessels and shown to be significant (Dalen and Løvik, 1981; Shabangu *et al.*, 2014; Delacroix *et al.*, 2016a, 2016b). It is possible to observe attenuated pings on an echogram without observing backscatter from close-range bubbles (Figure 2.4). This is thought to be due to bubble sweep-down. With wind-induced entrainment, the bubble backscatter is more likely to overlap completely in time with the transducer ringing (Section 2.2.5).

The level of signal attenuation caused by entrained air bubbles relates to their depth extent, number, density, and size distribution relative to the acoustic wavelength. Air bubbles will scatter sound most strongly at the boundary between Rayleigh and geometric scattering, when the bubble size and acoustic wavelength are similar (Simmonds and MacLennan, 2005). This peak in backscatter is referred to as resonance. For example, at 38 kHz, resonance will occur when the bubble diameter is ~12 mm. The effect of bubble attenuation has been well studied in the laboratory and controlled experiments (Clay and Medwin, 1977), but *in situ* studies are

hampered by the difficulty of independently measuring the size distribution of bubbles along the propagation path. Bubble size distributions and entrainment depth due to wind-induced waves have been modelled (Novarini and Bruno, 1982, 1983; Trevorrow, 2003; Weber, 2008), but with insufficient accuracy to permit reliable application to survey conditions. However, it is clear that as wind velocity and sea conditions deteriorate, entrained air bubbles increase in abundance, density, and depth penetration (Figure 2.5), and their size distribution widens (Novarini *et al*., 1998). The effect of tidal flows on echosounder data has also been demonstrated (e.g. Baschek *et al*., 2006; Fraser, 2017; Williamson *et al*., 2017). Tidally induced water currents can affect the data, not only through signal attenuation from entrained air bubbles, suspended sediment, and water-density gradients, but also through target-classification uncertainties when the targets and animals are in close proximity to each other.

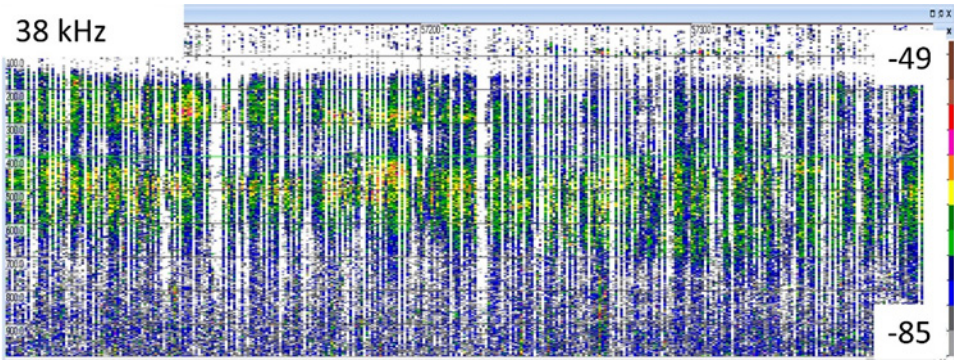

Figure 2.4. An example S_v echogram at 38-kHz from the icebreaker RV L'Astrolabe, showing extreme signal attenuation, but with no air-bubble backscatter apparent. The colour scale represents minimum and maximum S_v thresholds. Data provided by Commonwealth Scientific and Industrial Research Organization (CSIRO; Australia).

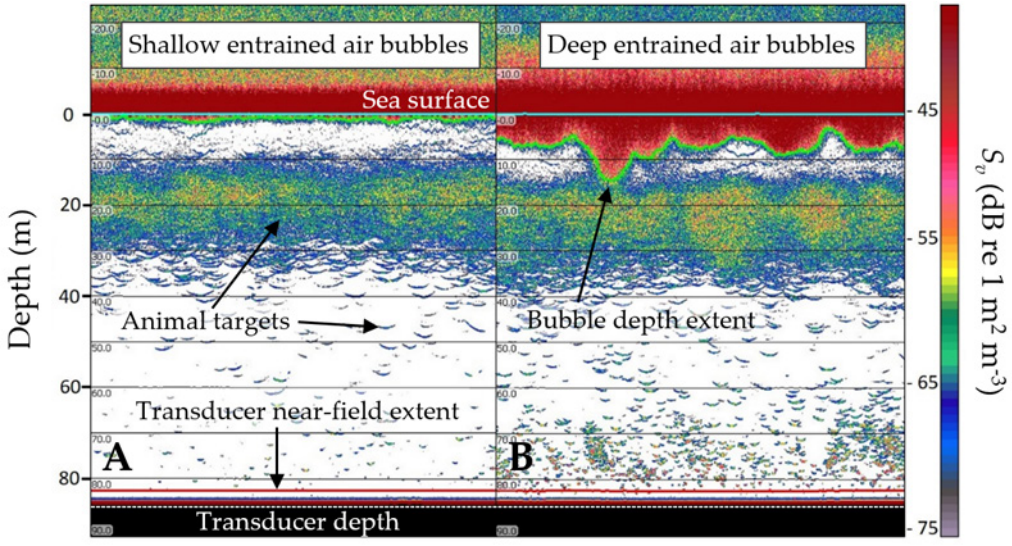

Figure 2.5. Calibrated measurements of S_v at 70 kHz from an upward-facing Simrad EK80 WBAT echosounder on the seabed at ~ 85 m depth in Holyhead Deep (Wales, UK). (A) A 5-min period of time on the 6th of October 2019, when the depth of entrained air bubbles (green line) was at a minimum. (B) A 5-min period of time on the 8th of October 2019, when the depth of entrained air bubbles (green line) extended to as much as ~ 15 m.

To quantify the influence of tidal currents on the depth of entrained air bubbles, 70-kHz data from an upward-facing Simrad EK80 Wideband Autonomous Transceiver (WBAT) echosounder deployed on the seabed at ~85 m depth in Holyhead Deep (Wales, UK) were analysed with the associated windspeed and direction measurements, and tide speed and direction model predictions (Whitton *et al*., 2020). The WBAT was programmed to collect data for a continuous 20 min period every hour from the 5th of September to the 10th of October 2019. Echoview software was used to estimate the mean depth of entrained bubbles for each 20 min period using the Threshold Offset algorithm (threshold S_v = −58 dB), on the assumption that the strong near-surface scattering layer was primarily due to air bubbles rather than sediment or density gradients (Figure 2.5).

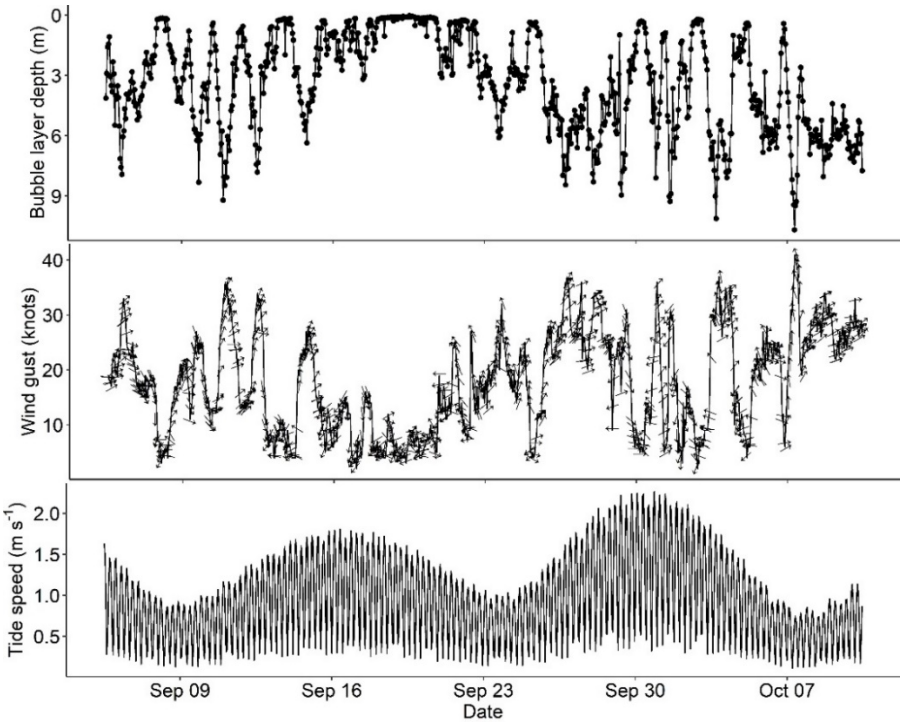

Figure 2.6. A 35-day time-series of measurements in the Holyhead Deep (Wales, UK) in 2019. Upper panel: Mean depth of entrained air bubbles measured over a 20-min period every hour, by a 70-kHz upward-facing Simrad EK80 WBAT echosounder on the seabed at ~ 85 m depth. Middle panel: Mean wind-gust speed measured every hour with an anemometer. Lower panel: Modelled mean tide velocity measured every hour.

The maximum depth of entrained air bubbles for an averaged 20-min period was 10.68 m (mean = 3.32, standard deviation (s.d.) = 2.43; Figure 2.6). Despite the fast tidal currents (> 2 m s^{-1} on occasion), the depth of the bubble layer was more highly correlated with windspeed than with tidal current speed (figures 2.6 and 2.7). The mean hourly wind gust speed (local wind speed maxima) was highly correlated with the mean windspeed (Figure 2.7), and showed a significant positive correlation with bubble depth ($p < 0.001$, $r_s = 0.88$), whereas the mean hourly tidal current speed showed no significant correlation to bubble depth ($p > 0.05$, $r_s = -0.05$). A multiple linear regression model of wind gust direction, wind gust speed, tide current speed, and tidal current direction explained 77% of the variation in bubble depth ($p < 0.001$). Wind-gust speed accounted for 95% of that variation, while wind gust direction and tide velocity accounted for just 5 and 0.3%, respectively (calculated using the LMG R2 estimate of relative importance; Grömping, 2007).

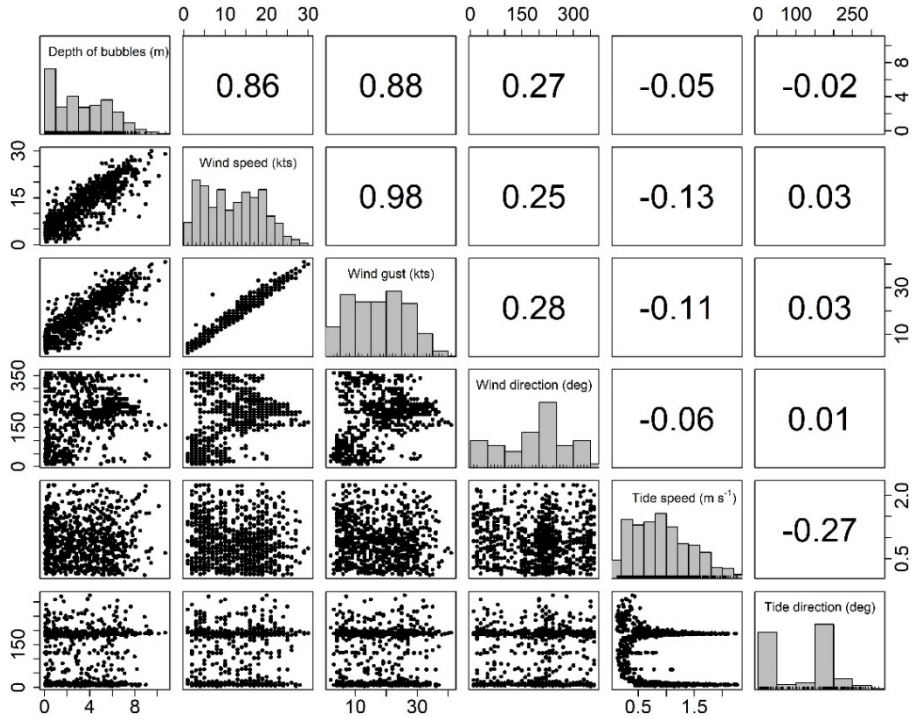

Figure 2.7. Scatterplots and Spearman's rank correlation (r_s) between the various hourly metrics computed for a 35-day period in Holyhead Deep (Wales, UK) in 2019. Numbers show the r_s coefficient. * indicates a significance of the correlation at $p \leq 0.001$, ** at ≤ 0.01, and no symbol indicates $p > 0.05$.**

As a comparison to the findings from the Holyhead Deep, a 14-day acoustic dataset collected from the 27th of October to the 10th of November 2018 in the Minas Passage of the Bay of Fundy (Canada), was also analysed with the associated wind and tidal current measurements [data courtesy of the Fundy Ocean Research Center for Energy (FORCE)]. The acoustic data were collected for 5 min every half hour by an upward-facing 120-kHz Simrad WBAT echosounder, deployed on the seabed at 32–44 m depth (low to high tide, respectively). Average entrained air depth was obtained for each 5 min recording period using methods similar to the Holyhead Deep analysis. Average water column current speed and direction data were obtained from a co-located Nortek Signature 500 ADCP, which measured water velocity for 1 m depth bins every 15 min. Windspeed and direction data were collected by a weather station nearby (FORCE shore station; data available[2]). Unlike at Holyhead Deep, data from the Bay of Fundy (figures 2.8 and 2.9) indicated that the depth of entrained air was most strongly correlated with the tidal current speed (r_s = 0.70), followed by wind and gust speed. A linear model utilizing current speed, wind gust maximum speed, and tide (ebb or flood) as explanatory variables explained 73% of the variance in the data, and indicated that entrained air depth was positively correlated with current and gust speed, and was greater during flood tide than ebb. Other factors, including the absolute and relative directions of wind and current, were examined, but did not noticeably improve the fit of the model. The Bay of Fundy site is shallower and faster than the Holyhead Deep site, with complex bathymetry that affects hydrodynamics depending on the direction of flow. Current speed is greater during the flood tide than the ebb, and local

[2] https://data.oceannetworks.ca/home. Last accessed 2 November 2021.

bathymetry results in large eddies forming at different locations, which likely affects the entrained air depth observed at a given location.

These results indicate that collecting upward-facing echosounder data in an area regularly included in acoustic stock assessment surveys may provide valuable information for survey planning. For a given wind and current forecast, the depth of entrained air bubbles may be reasonably predictable, as seen for the Holyhead Deep and the Bay of Fundy sites. In addition, the characteristics of each survey vessel with respect to transducer depth and bubble sweep-down will uniquely determine the influence of these bubbles on the data.

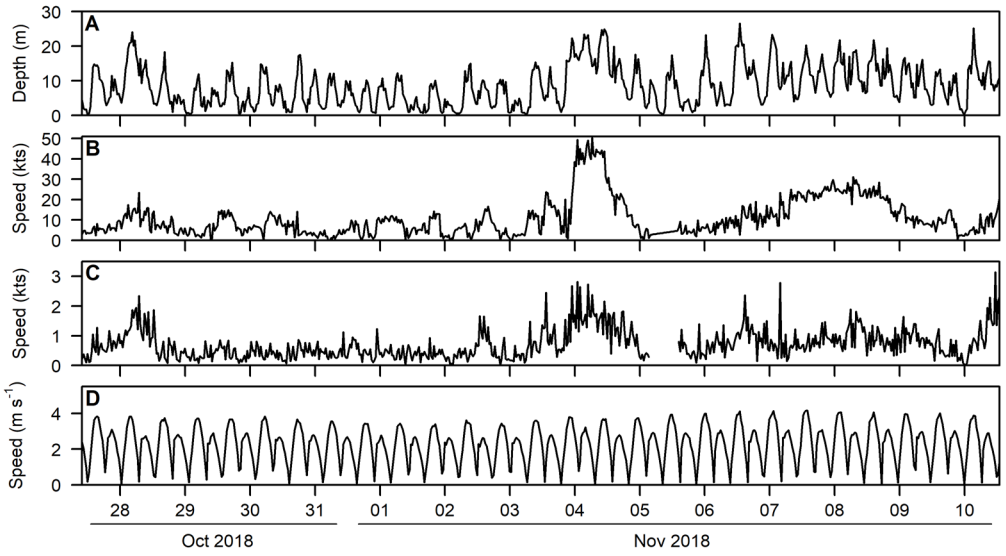

Figure 2.8. A 16-day time-series of acoustic and environmental measurements from the Minas Passage of the Bay of Fundy (Canada) in 2018. (A) Average depth of entrained air bubbles, obtained for each 5-min acoustic recording period, as measured by a 120-kHz upward-facing Simrad EK80 WBAT echosounder on the seabed at ~ 50 m depth. (B) Windspeed at the midpoint of each acoustic recording period. (C) Mean wind gust speed for each acoustic recording period. (D) Mean water column current speed, interpolated at the midpoint of each acoustic recording period, as measured by a Nortek Signature 550 ADCP. Windspeed and wind-gust speed were measured at the FORCE weather station.

2.3.2 Transducer motion

For fisheries acoustic surveys, transducers are mounted on survey platforms in such a way that the acoustic axis is vertical and the sound transmission travels vertically downward through the water column. During inclement weather, the transducer heaves and rotates with the pitch and roll of the platform. Transducer heave only affects the range calculation (time to range using speed of sound) and as such does not affect the magnitude of the backscatter measurements. However, transducer rotation does affect the magnitude of the measurements, since the acoustic axis may not be oriented downward, and, if the rotation is sufficiently severe, the angle at transmission may be different from the angle at reception. Because the acoustic beam does not have equal sensitivity across all beam angles (i.e. beam pattern and directivity), the reception of the S_v signal may be attenuated when the transducer rotates. The amount of signal attenuation depends on the rate of transducer rotation relative to the range of the targets. In general, the level of attenuation increases with range, because the angle of rotation at short ranges is small for the short two-way travel time, while at longer ranges, this rotation can cause significant loss of signal, to the extent that the echo signal can fall below the detection threshold level. This effect of transducer motion on S_v measurements was theoretically studied by Stanton (1982),

and, more recently, Dunford (2005) developed a correction factor based on Stanton's work that could be applied to S_v data (Figure 2.10). It should be mentioned that the effect of transducer motion on S_v measurements has been theoretically studied, and the respective corrections implemented in software, but, to our knowledge, this effect has not been empirically verified *in situ* or *ex situ*.

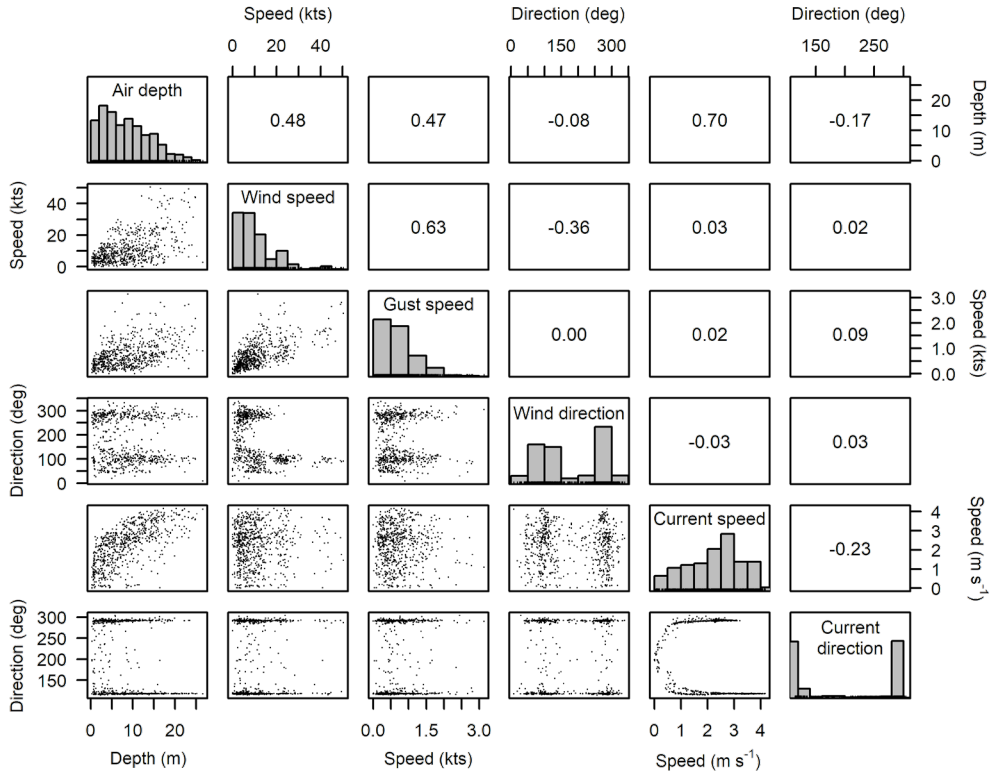

Figure 2.9. Scatterplots and Spearman's rank correlation (r_s) between the air, current, and wind metrics computed for a 14-day period in the Bay of Fundy (Canada) in 2018. Numbers above the diagonal are the r_s coefficients for each variable pair. * indicates a significance of the correlation at $p \leq 0.001$, ** at $p \leq 0.01$, and no symbol indicates $p > 0.05$.**

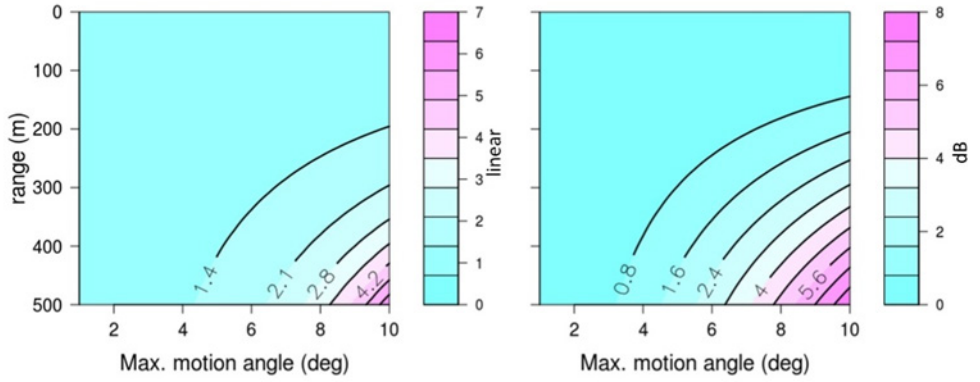

Figure 2.10. Effect of platform motion with a 5-s period on S_v as a function of the angular motion of the platform (0–10°) and range (i.e. depth) of data collection for a transducer with a 7° total angular beam width. The left panel shows the effect in linear units, and the right panel shows the effect in decibels.

The amount of signal reduction due to transducer motion is a non-linear and non-monotonic relationship between the rate and extent of transducer motion, the range of the targets, and the beam width of the transducer. Two examples highlight an intuitive (Figure 2.10) and possibly unexpected (Figure 2.11) set of corrections. The 7° beam width (total angular distance between the half-power points) is a common transducer beam width for many fisheries acoustic surveys. Figure 2.10 shows the effects of transducer motion on received acoustic energy. In the case of a 7° beam width transducer mounted on a platform that is pitching and/or rolling with a 5-s period at a range of 500 m and a 10° maximum angular motion of the platform, corrections to S_v are on the order of 8 dB, or about a factor of 6. This amount of transducer motion is quite severe and will likely result in unusable data.

Figure 2.11 highlights the non-monotonic nature of the corrections. In the case of an 11° beam width transducer (e.g. the Simrad 18 kHz 18–11) mounted on a platform with periodic 2-s motion, and surveying in open ocean waters, the corrections to S_v have a non-monotonic relationship with depth. In this case, at 750 and 1500 m, the motion of the ship is such that the transducer has rotated from centre to side and back to centre in the amount of time the sound has travelled to those depths and back.

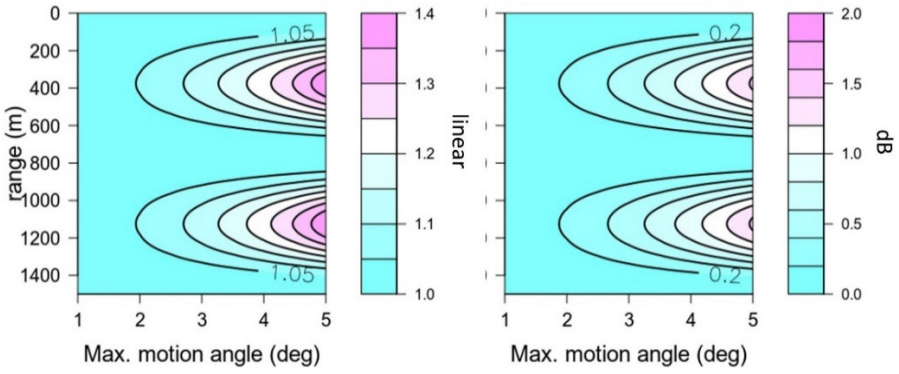

Figure 2.11. Effect of platform motion with a 2-s period on S_v as a function of the angular motion of the platform (0–5°) and range (i.e. depth) of data collection for a transducer with an 11° total angular beam width. The left panel shows the effect in linear units, and the right panel shows the effect in decibels.

The code to generate these graphs is written in R (R-Core-Team, 2020) and is available on Github[3].

2.4 Practical approaches to reduce data degradation

The problem of echosounder data degradation is well recognized, and a range of practical approaches can be taken to reduce the effects. Indeed, considerable effort has gone into the development of specifications for new research vessels to reduce the negative effects of radiated noise on both target animals and acoustic data (Mitson, 1995; De Robertis and Handegard, 2013; Spence and Fischer, 2017).

Practical approaches to reduce data degradation can be grouped into those aimed at reducing the degradation source itself and, should that not be possible, those aimed at isolating the echosounder from the effects of those sources. Despite best efforts with both types of

[3]https://github.com/ices-eg/wg_WGFAST/tree/master/CRR_352. Last accessed 15 November 2021.

approaches, it is likely that S_v will still suffer from some degree of degradation, requiring the subsequent application of appropriate data-processing techniques (see Section 7).

2.4.1 Reduction of degradation sources

Some of the degradation sources themselves can be reduced (prevention rather than cure). Approaches for the reduction of signal degradation sources include:

- power supply conditioning (Benoit-Bird *et al.*, 2018);
- hydrodynamic hull design to reduce bubble sweep-down (Mitson, 1995);
- systems to reduce platform motion, e.g. active ballast, outriggers, gimbal, and hull design;
- positioning transducers away from entrained air bubbles, e.g. retractable keel, or sweet spot on the hull (Mitson, 1995);
- composite ceramic transducers to reduce transducer ringing;
- switching off non-essential acoustic and electric noise sources during survey operations;
- timing surveys to avoid adverse conditions;
- adjusting the transect direction with respect to swell and wave direction to reduce platform motion, engine noise, and bubble sweep-down;
- increasing transmit interval to avoid multi-ping aliasing (Renfree and Demer, 2016); and
- careful choice of transmit-pulse acoustic frequencies to avoid the generation of harmonics at the other echosounder frequencies and, hence, cross-talk.

2.4.2 Isolation from degradation sources

If the degradation source cannot be reduced, then efforts can be made to isolate the echosounder from the effects of that source (cure rather than prevention). The echosounder can be isolated from sources of acoustic noise, electric noise, signal attenuation, motion, and aliasing in space, time, and/or frequency in a number of ways:

- acoustic sound-proofing around noisy machinery (Mitson, 1995);
- synchronization of the transmit pulse across multiple transceivers. If the chosen transmit frequencies generate harmonics within the receive bandwidth of one or more of the other echosounders, rapidly sequential pinging is required (Demer *et al.*, 2017);
- careful choice of transducers with receive bandwidths outside the transmit bandwidth of any of the other synchronized echosounders;
- signal filtering within the receive electronics of the transceiver to remove unwanted frequencies (bandpass filtering);
- deployment of the transceiver and/or transducer on alternative platforms [e.g. towed body, lowered probe, remote-operated vehicle (ROV), AUV, or ASV] to separate them from acoustic noise, electrical noise, wave motion, and entrained air bubbles, and increase the SNR by moving closer to the targets of interest (Benoit-Bird *et al.*, 2017);
- increasing the transmit interval to avoid multi-ping aliasing (Renfree and Demer, 2016; Blackwell *et al.*, 2019);
- appropriate grounding of the transceiver and transducer to either the platform or the sea;

- electrical insulation of transducer cables, including additional shielding in steel conduits (including sand filler at corners to prevent vibration) and sufficient separation from other electrical cables; and
- mounting the transducer on a gimbal to isolate it from the platform motion (De Robertis *et al*., 2019).

3 Metadata

One of the primary causes of acoustic data degradation during survey operation is inclement weather conditions. Data degradation can be caused by numerous other sources, as outlined in previous chapters, but inclement weather can increase the severity of some noise and attenuation. Different vessels respond differently to weather conditions (sections 4 and 5). For example, while signal attenuation due to the presence of bubbles can generally be linked directly to weather conditions and sea state, the effect, frequency, amplitude, and occurrence are highly dependent on the platform. Several metrics and analyses have been developed and assessed to produce indicators of data quality in the following chapters, and data from a number of different platforms were used as examples to generate the indicators. Because different vessels respond differently to inclement weather, it is not possible to provide generic advice that will be directly applicable to all vessels. However, with the appropriate metadata for a platform, it may be possible to compare metrics and indicators among platforms. One goal of providing platform metadata is to allow the comparison between a survey vessel and any of the example platforms provided in this CRR, which will increase understanding on how the platform may react to inclement weather.

An initial list of the appropriate platform metadata is provided in Table 3.1. This list is based on several sources, including the fisheries acoustic metadata convention for processed acoustic data from active acoustic systems (AcMeta) now available as a living document in Github[4].

[4] https://github.com/ices-publications/AcMeta

Table 3.1. Platform metadata outlined in AcMeta to create comparable analyses when determining the impact of inclement weather on acoustic signal.

Category	Metric	Metric definition	Unit	Metadata obligation
Mission attributes [1]	Cruise description	Free text field to describe the cruise. May include list of cruise objectives. E.g. scientific survey, commercial fishing, resupply, or combinations of these		Mandatory if applicable
Ship attributes	Ship name	Name of the ship		Mandatory if applicable
	Ship type	Describe type of ship that is hosting the acoustic instrumentation. (See first three rows in Annex 4, Standard lists)		Mandatory if applicable
	Ship length	Overall length of the ship	m	Strongly recommended
	Ship breadth	The width of the ship at its widest point	m	Strongly recommended
	Ship tonnage	Gross tonnage of the ship	t	Strongly recommended
	Ship engine power	The total power available for ship propulsion	kW	Strongly recommended
	Ship noise design	E.g. ICES 209 compliant (Mitson, 1995); or a description of ship noise performance		Strongly recommended
Instrument attributes	Instrument frequency	Frequency of the transceiver/transducer combination. Some systems such as broadband and multibeam will have a range of frequencies. If so, specify the minimum, maximum and centre frequency	kHz	Mandatory
	Instrument transducer location	Location on the ship, e.g. hull, drop keel, or gondola		Mandatory
	Instrument transducer manufacturer	Transducer manufacturer		Mandatory
	Instrument transducer model	Transducer model		Mandatory
	Instrument transducer beam type	E.g. single-beam or split-aperture		Mandatory
	Instrument transducer depth	Mean depth of transducer face beneath the water surface.		Optional
	Instrument transducer orientation	Orientation of the transducer face, e.g. downward-facing, side-facing		Mandatory

[1] **Indicator: Background information for qualitative data quality assessment**

4 Quantifying signal attenuation using only echosounder data

In this section, we consider ways to quantify echosounder data degradation using only echosounder data. We focus exclusively on signal attenuation (Section 2.3), because this is typically the most influential manifestation of inclement weather with respect to echosounder data quality. It is generally assumed that entrained air bubbles are the dominant cause of signal attenuation, although this is hard to prove, and the influence of transducer motion cannot be discounted. Because the identification of attenuated pings forms such an important component of the analyses presented here, we consider the potential sources of error associated with this metric in Section 7.4.

4.1 Seabed backscatter

When seabed backscatter is present in echosounder data, it is typically many orders of magnitude stronger than the backscatter from biological targets in the water column. As with any acoustic target, the magnitude of seabed backscatter is a complex function of the magnitude and spatial arrangement of acoustic impedance gradients with respect to the direction, amplitude, volume, and frequency (or frequencies) of the transmitted pulse (ICES, 2007). If inclement weather is causing signal attenuation due to entrained air bubbles, it can potentially be quantified through changes in the seabed backscatter, if variability due to all other factors can be dismissed or accounted for.

Some of the transmitted sound energy can reflect or scatter from the seawater-seabed interface, and some energy can penetrate the substrate and scatter from the various impedance boundaries within. The relative contributions of surface reflection and scattering and volume scattering will vary depending on the nature of the seabed and the transmitted pulse. Despite this, surface reflection and surface scattering are assumed to be the dominant mechanisms by which a transmitted sound pulse is scattered by the seabed (e.g. Cutter and Demer, 2014). This has led to the use of surface backscattering strength, S_s (dB re 1 m^2 m^{-2}) as a common metric for seabed backscatter (Demer *et al*., 2015).

Throughout this document, S_v or s_a (m^2 m^{-2} re dr) is used for seabed backscatter. This is not because volume backscattering has been identified as the dominant mechanism for seabed backscatter in the data, but rather because echosounder data processing software is used that is designed primarily for water column analysis. The primary metrics calculated by these software packages are TS, which is appropriate for point targets in the water column, and S_v, which is appropriate for volume scattering. The area backscattering coefficient (ABC or s_a) is simply the integral of S_v over a defined range extent, dr (m) (i.e. distance between a minimum and maximum range). The use of s_a as a metric of seabed backscatter is consistent within the individual analyses presented here, and should not impact the interpretation of the results. However, it cannot be considered as an absolute measurement of the seabed backscatter and cannot be directly compared to measurements of S_s presented elsewhere (e.g. Manik *et al*., 2006).

4.1.1 Fishing-vessel data from the Bounty Platform

Annual acoustic surveys of southern blue whiting (*Micromesistius australis*) have been carried out in late summer to early autumn (August/September) over the Bounty Platform (southeast of New Zealand), from fishing vessels, since 2004 (O'Driscoll *et al*., 2016). Calibrated measurements of S_v at 38 kHz were obtained from the hull-mounted Simrad ES60/ES70

echosounder on the FV Tomi Maru 87, which undertook 283 night-time acoustic transects between 2004 and 2013. These transects, which varied in length from 1 to 14 km (mean 5.9 km), were repeated in opposite directions and under varying conditions, with up to 13 m s^{-1} (25 knots) windspeed and 2 m swell.

ESP3 software (Ladroit *et al.*, 2020) was used to calculate seabed s_a and the proportion of attenuated pings for each transect (Figure 4.1). Seabed s_a was calculated by integrating the sample S_v values from the detected start of the seabed echo over a range extent of dr = 10 m. Attenuated pings were identified by applying an automated algorithm and verifying the results by eye. A generalized additive model (GAM) was fitted to the 283 estimates of seabed s_a vs. proportion of attenuated pings (Figure 4.2). For each transect, the proportion of attenuated pings ranged from ~2 to 40%, with a noticeable reduction in seabed s_a over the range of ~10 to 25% attenuated pings. The results suggest that data quality was minimally affected from 0 to 10% attenuated pings, and maximally affected when the proportion of attenuated pings exceeded ~25%. The transect direction did not appear to affect the relationship between seabed s_a and the proportion of attenuated pings.

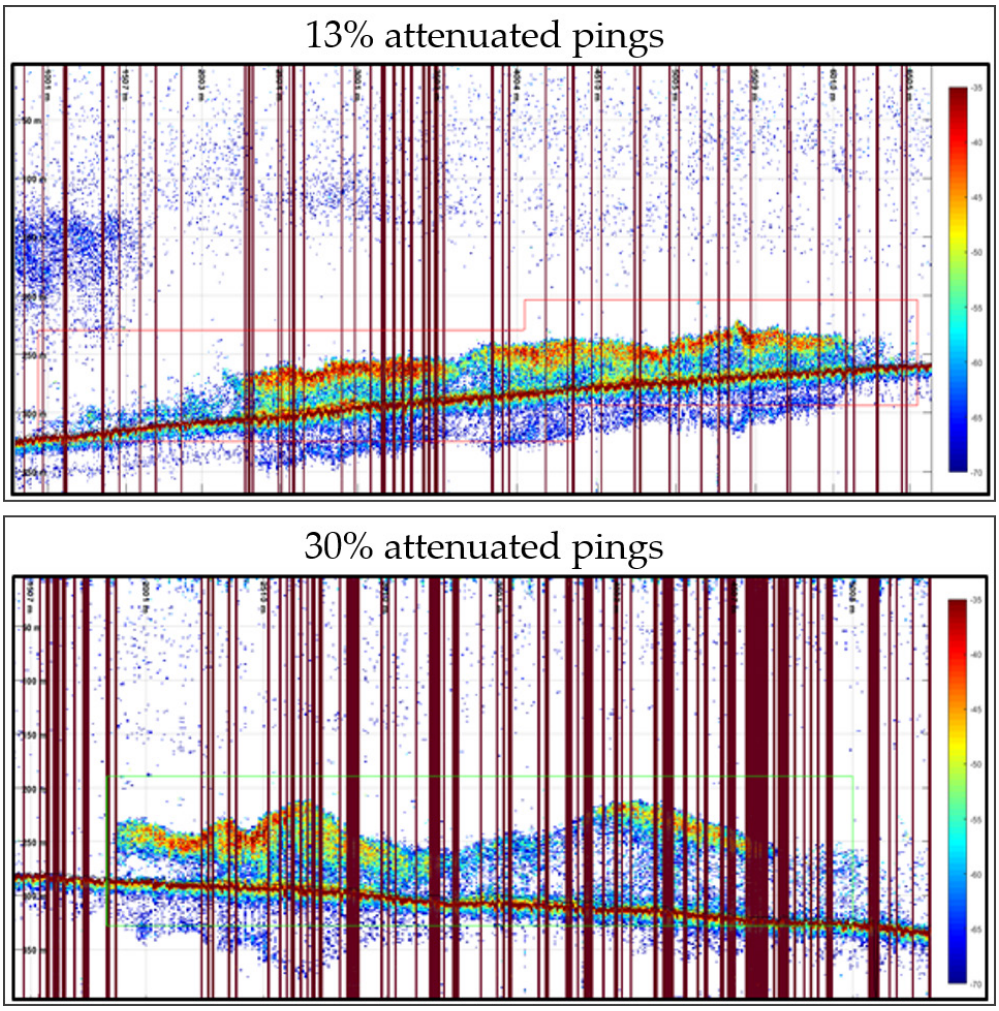

Figure 4.1. Two example transects showing S_v at 38 kHz from the Simrad ES60/ES70 echosounder on the FV Tomi Maru 87 over the Bounty Platform. The S_v colour scale extends from –35 to –70 dB. The water depth was ~ 300 m. The dark vertical bars show the pings that were identified as attenuated (see text for details). Data provided by the National Institute of Water and Atmospheric Research (NIWA; New Zealand).

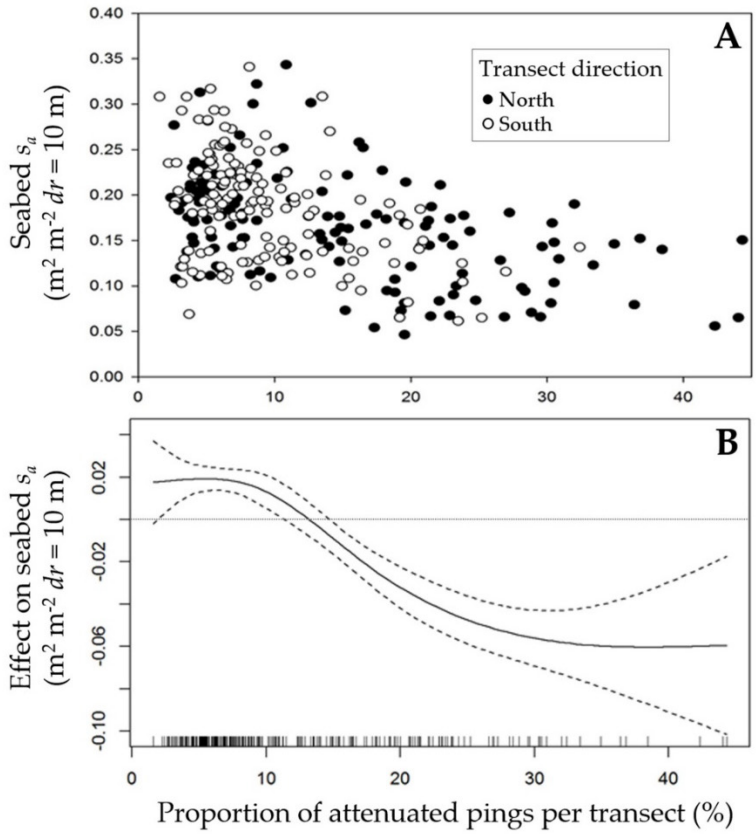

Figure 4.2. (A) Seabed s_a at 38 kHz as a function of the proportion of attenuated pings for 283 transects carried out by the FV Tomi Maru 87 over the Bounty Platform between 2004 and 2013. (B) A GAM fitted to the data. Data provided by NIWA. The attenuated pings were removed for these analyses. For panel B, the magnitude of the GAM is relative, and positive values do not imply a positive effect on seabed backscatter. In this case, the trend of the GAM is a useful indicator of the effect of ping attenuation, where the transition from a flat response to a negative slope (i.e. the shoulder) can be used to indicate effect on data quality.

4.1.2 Fishing-vessel data from Chatham Rise

Acoustic surveys of orange roughy (*Hoplostethus atlanticus*) have been carried out at various times of the year off the coasts of Tasmania and New Zealand from both research and fishing vessels since 1987 (Kloser *et al.*, 2015; Ryan and Kloser, 2016). Calibrated measurements of S_v at 38 kHz were obtained from the hull-mounted Simrad ES60 echosounder on the FV Amaltal Explorer during a 24 h survey over Chatham Rise east of New Zealand in June 2016. During this survey, 25 parallel transects were completed within a 5 × 8 km survey area.

Echoview software was used to calculate seabed s_a, and the proportion of attenuated pings every 30 min, in a similar manner to the analysis described in Section 4.1.1. In this instance, seabed s_a was calculated by integrating the sample S_v values from ~2 m above the detected start of the seabed echo over a range extent of dr = 80 m. Figure 4.3 shows a high variability of seabed s_a (over an order of magnitude) in calm weather conditions, when the proportion of attenuated pings was < 10%. As weather conditions deteriorated, the proportion of attenuated pings increased from 10 to 30%, and the variability of seabed s_a decreased significantly. These results are consistent with those from the FV Tomi Maru 87 (Figure 4.2), although it should be noted that there are only a small number of measurements from the FV Amaltal Explorer where the proportion of attenuated pings was > 10%.

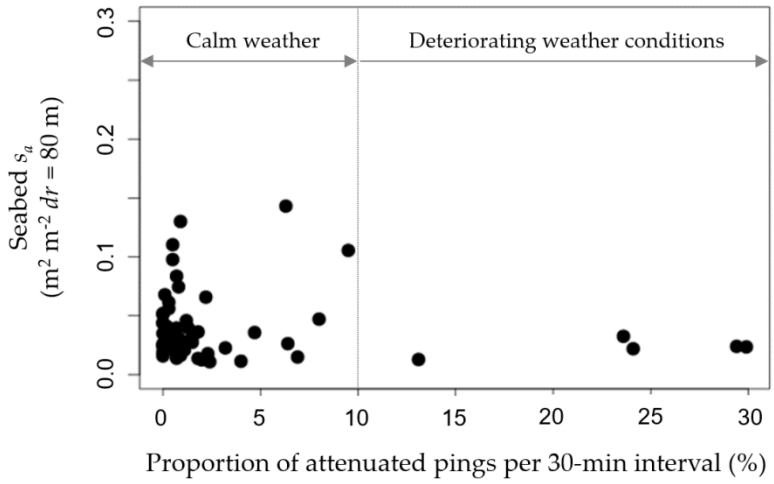

Figure 4.3. Seabed s_a at 38 kHz as a function of the proportion of attenuated pings for 30-min intervals during a 24-h survey carried out by the FV Amaltal Explorer over Chatham Rise in June 2016.

4.1.3 Saildrone data from the west coast of North America

Annual, biennial, and triennial acoustic surveys of Pacific hake (*Merluccius productus*) have been carried out in summer (June–August) off the west coast of North America from US and Canadian research vessels since 1977 (e.g. Fleischer *et al.*, 2005). In 2018, these surveys were supplemented with echosounder data collected from five Saildrones deployed by the National Oceanographic and Atmospheric Administration (NOAA, US) Northwest Fisheries Science Center (NWFSC) and Southwest Fisheries Science Center (SWFSC) to explore the effectiveness of Unoccupied Surface Vessels (USVs) as survey and research platforms (Chu *et al.*, 2019). Calibrated measurements of S_v at 38 kHz were obtained from the hull-mounted, gimbaled Simrad EK80 WBT-Mini echosounders on all five Saildrones, which together undertook 126 transects orthogonal to the coastline, totalling ~5403 nautical miles, over a period of 90 days.

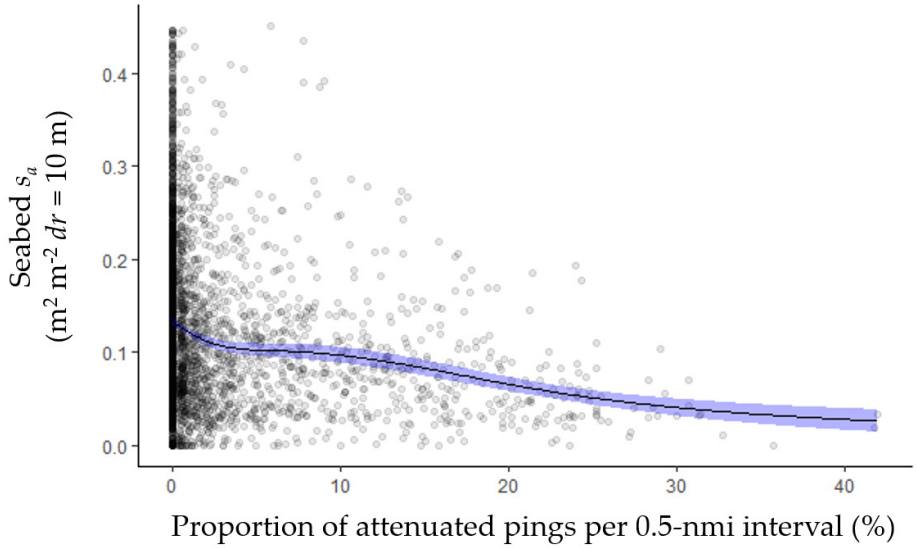

Figure 4.4. Seabed s_a at 38 kHz as a function of the proportion of attenuated pings for 3847 0.5-nautical mile intervals during a 90-day survey carried out by five Saildrones off the west coast of North America in summer 2018. Also shown is a GAM fitted to the data (solid line). The shaded area shows the model prediction uncertainty.

Echoview software was used to calculate seabed s_a and the proportion of attenuated pings every 0.5 nautical miles along each track, in a similar manner to the analysis described in Section 4.1.1. A GAM was fitted to the 3847 estimates of seabed s_a vs. the proportion of attenuated pings (Figure 4.4). As seabed s_a is always positive, a gamma family was used for the model. Seabed s_a was found to be significantly related to the proportion of attenuated pings ($p < 0.01$). Overall, there was a steady decline in seabed s_a as the proportion of attenuated pings increased, with marginally increased declines around 1–3% and 10–20%. The variability of seabed s_a decreased as the proportion of attenuated pings increased, consistent with the observations from the FV Tomi Maru 87 (Section 4.1.1) and the FV Amaltal Explorer (Section 4.1.2).

4.2 Transducer ringing

A subset of the Saildrone dataset described in Section 4.1.3 (Saildrone SD1024, ~67 nautical miles, ~23 000 pings) was analysed to investigate the relationship between signal attenuation (Section 2.3) and transducer ringing (Section 2.2.5). Echoview software was used to identify attenuated pings (as described in Section 4.1.3) and to quantify the S_v value of each of the first six samples in each ping (Figure 4.5).

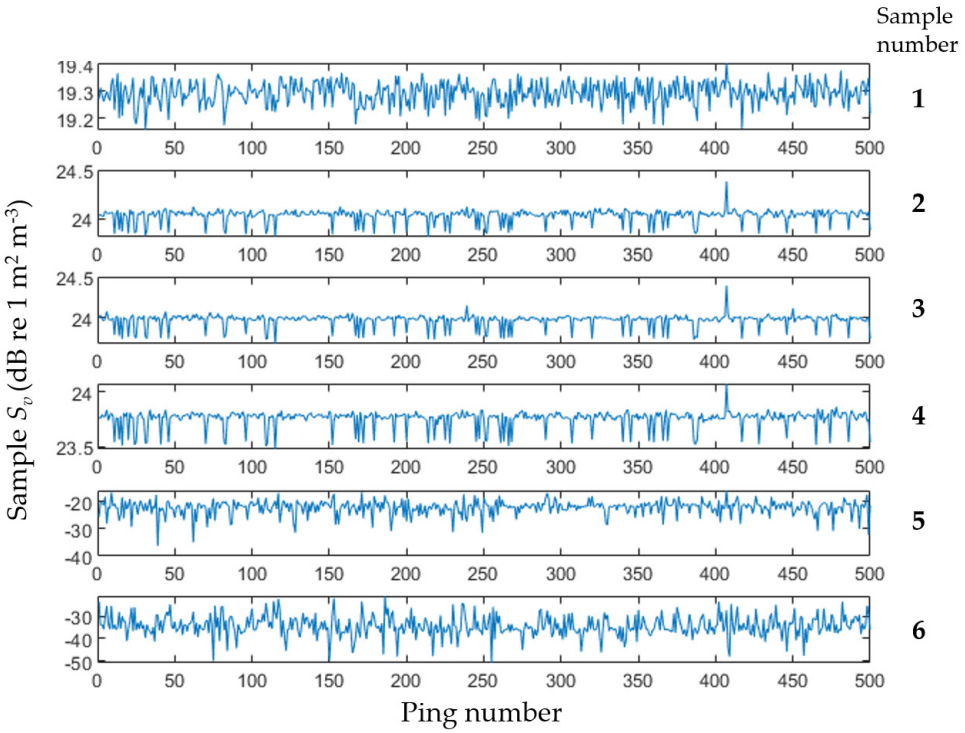

Figure 4.5. A 500-ping subset of the survey carried out by Saildrone SD1024 off the west coast of North America in 2018 showing the S_v value at 38 kHz for each of the first six samples in each ping. The range extent of each sample was 0.2 m. Note the different y-axis scales.

The S_v value of each of the first six samples in each ping was cross-correlated with the timing of attenuated pings, showing a strong correlation between the timing of attenuated pings and changes in the S_v value of samples 5 and 6 (Figure 4.6). The distribution of S_v values for sample 5 was compared between attenuated and non-attenuated pings, showing considerable overlap

across the 25–75th percentiles (Figure 4.7). This means that variation rather than the absolute S_v value of sample 5 could be used as a predictor of attenuated signal in this dataset.

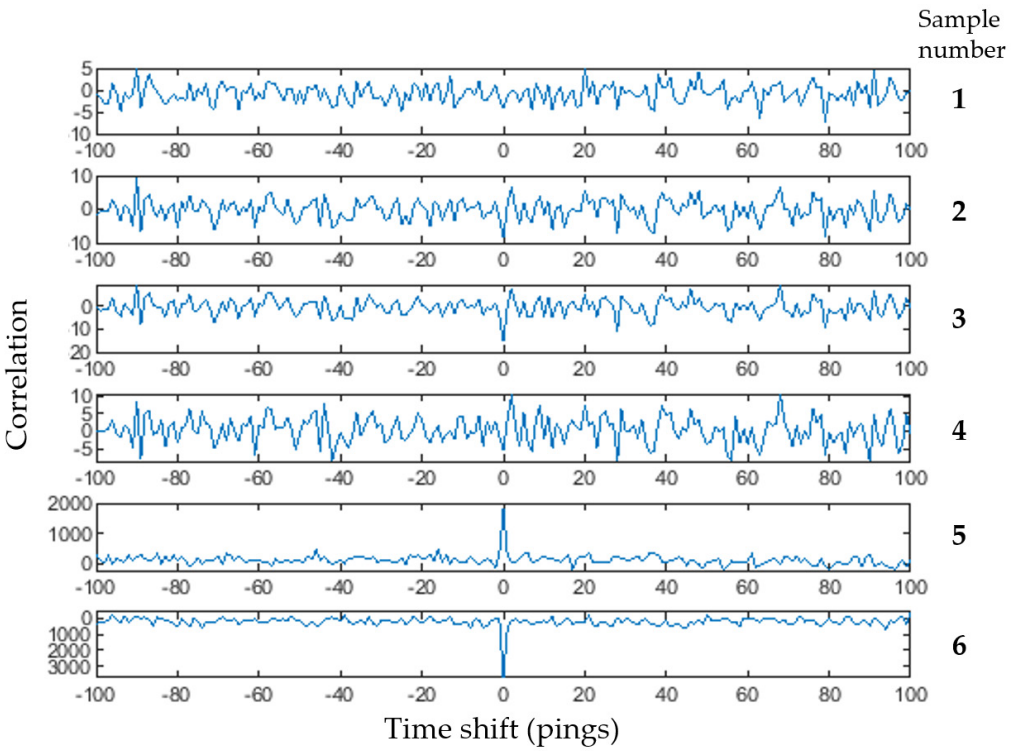

Figure 4.6. Cross-correlation of the timing of an attenuated ping with the S_v value, at 38 kHz, for each of the first six samples in each ping, for the survey carried out by Saildrone SD1024 in 2018. The cross-correlations displayed here are centred at 0-pings offset and extend for 100 pings before and after, since there is unlikely to be a relationship beyond this time period.

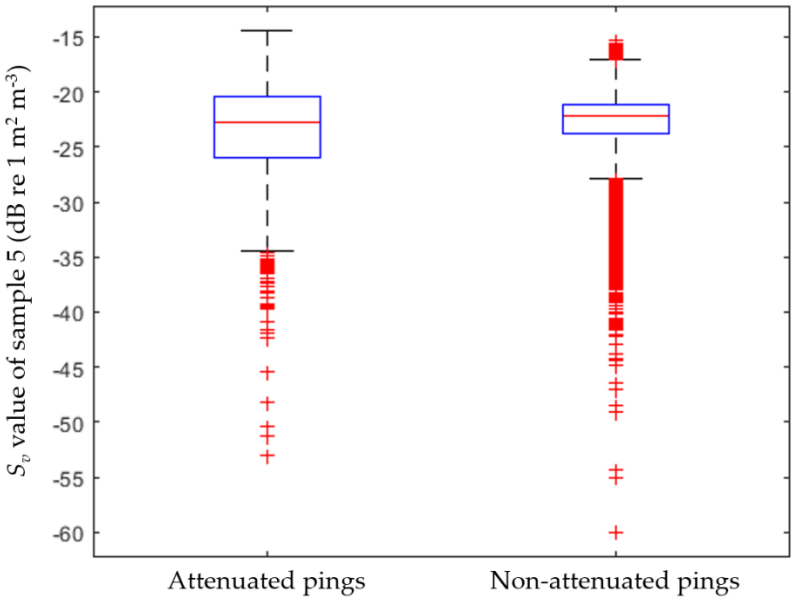

Figure 4.7. The distribution of S_v values at 38 kHz for the fifth sample in attenuated and non-attenuated pings from the survey carried out by Saildrone SD1024 in 2018.

4.3 Transducer impedance

When the ceramic elements in a transducer vibrate, they experience mechanical resistance from the medium in front of the transducer. In theory, this resistance (acoustic impedance) should be reflected in the electrical impedance of the circuits within the transducer. Since the acoustic impedance of air and water is different, it is possible that transducer impedance could be used to identify the presence of air bubbles near the transducer and, hence, the probability of signal attenuation.

A common echosounder, the Simrad EK80, measures voltage and current during the transmit cycle. These values can be used to calculate the transducer impedance according to Ohm's law (impedance = voltage / current). LSSS software was used to conduct a preliminary analysis from data collected with a Simrad EK80 WBT-Mini operating in CW mode on a Saildrone in the North Sea during June 2019, by comparing the impedance from one sector of the 38-kHz transducer with the proportion of pings identified as attenuated (Figure 4.8). The results indicate that the variation in transducer impedance increased in line with the proportion of attenuated pings, suggesting that this is a fruitful area for further research.

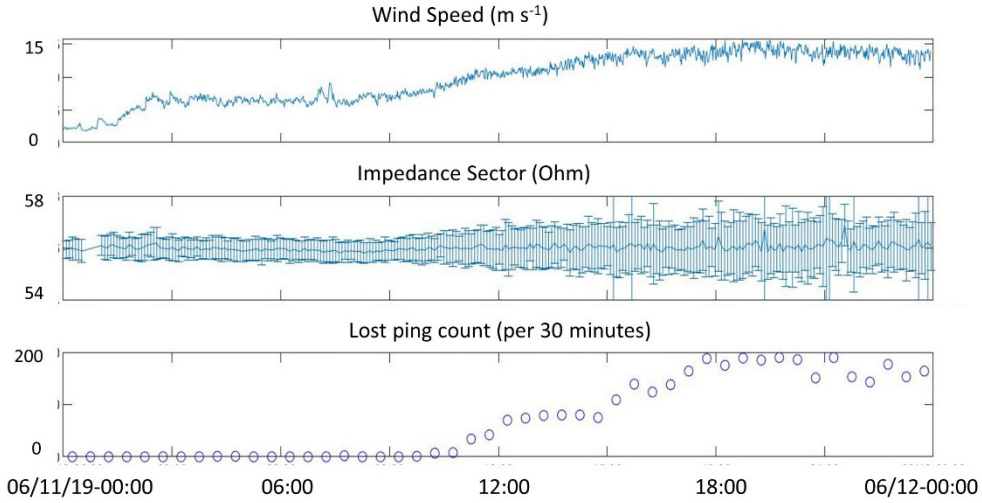

Figure 4.8. Relationship between electrical impedance of a 38-kHz transducer, windspeed, and the number of attenuated pings, for data collected with a Simrad EK80 WBT-Mini (operating in CW mode) from a Saildrone in the North Sea during June 2019.

4.4 Comparisons

4.4.1 Hull-mounted vs. towed transducers

Towing a transducer behind a surface vessel can place the transducer below the entrained bubble layer, isolate it from the vessel motion, and reduce the range to the targets of interest, all of which can improve the data quality (e.g. Kloser, 1996). The magnitude of this improvement can be estimated by comparing surface-vessel data with concurrent towed data.

Calibrated measurements of S_v at 38 kHz were obtained in poor weather from the hull-mounted Simrad ES60 echosounder on the FV Amaltal Explorer during a 24 h survey of orange roughy over Chatham Rise (east of New Zealand) in July 2016. The survey consisted of nine parallel transects, with five transects running into the swell and four transects running with the swell.

Concurrent measurements of S_v at 38 kHz were also obtained from a downward-facing Simrad ES60 echosounder towed behind the vessel on the headline of a deep-water demersal trawlnet (Ryan *et al*., 2009). The transducer was towed at a depth of ~600 m and a distance of ~1500 m behind the vessel. The water flow tensioned the net to provide exceptional stability, and transducer motion was negligible. Both the vessel and towed transducers had similar half-power beam angles of ~7°.

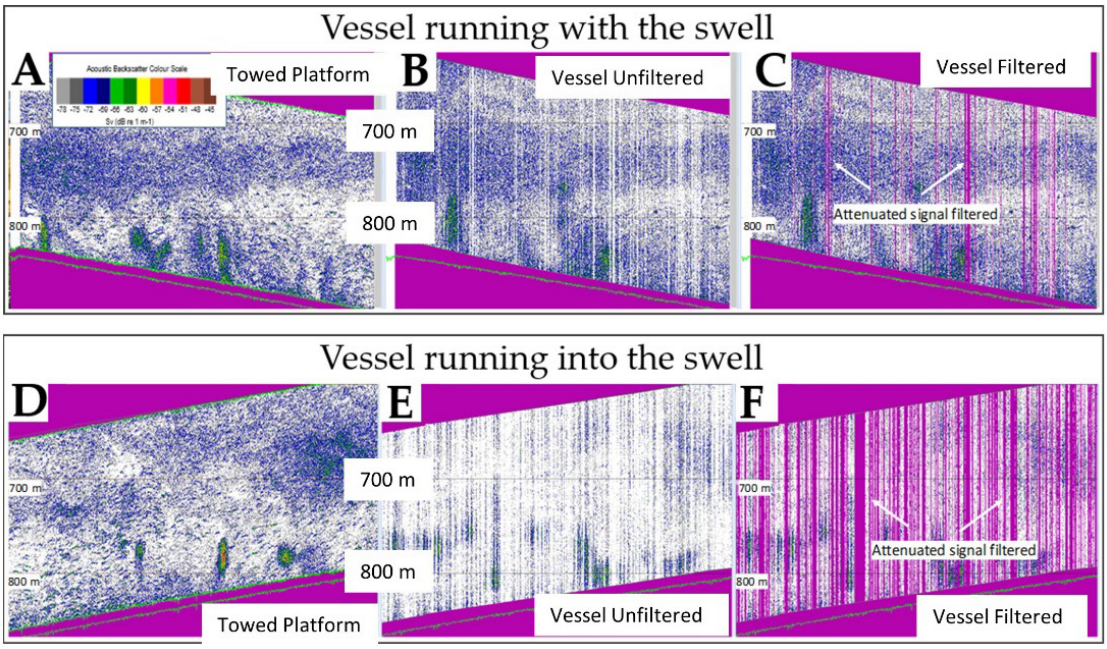

Figure 4.9. Example echograms of water column S_v (colour scale ranges from −45 to −78 dB) at 38 kHz over Chatham Rise in July 2016, from a downward-facing, towed Simrad ES60 echosounder at ~ 600 m depth (A and D), and a hull-mounted Simrad ES60 echosounder on a surface vessel before (B and E) and after (C and F) data filtering (vertical purple lines indicate attenuated pings detected by software). The towed echosounder was part of an Acoustic Optical System (AOS) attached to the headline of a deep-water demersal trawlnet, and the vessel echosounder was installed on the FV Amaltal Explorer. The echograms were aligned to consider approximately the same 200 m layer of water above the seabed. (A–C) shows an example of running with the swell. (D–F) shows an example of running into the swell.

Echoview software was used to process the data from both echosounders (Figure 4.9). The layer of water from just above the seabed to 200 m above in the water column was isolated in both datasets. A time offset of 10.5 min was applied to the vessel data to account for the approximate distance offset between vessel and net. This was based on the mean vessel speed and did not account for any horizontal offset of the net from the vessel track. The different range-dependent sampling volumes of each echosounder for a given depth interval were accounted for by the use of S_v, which is a volume-normalized metric of backscatter. The implicit assumption with S_v is that the targets are acting as volume targets. This assumption was robust for the vessel data, which was at > 600 m range, and was also reasonable for the towed data, which was at > 100 m range. The vessel data were also processed (filtered) to account for impulse noise, attenuated signal, and background noise, as described by Ryan *et al*. (2015). Ping and transect S_v statistics were calculated for the same 200 m layer for the unfiltered vessel data, the filtered vessel data, and the towed data. Although the matching of sampled water volumes and the measured backscatter between each dataset was approximate, it was hypothesized that (1) any significant differences between the S_v statistics of each dataset would be due to signal attenuation in the

vessel data, and (2) even after filtering, the vessel S_v statistics would still be biased low due to attenuation.

The sample S_v statistics for each transect showed a consistent decrease in the median S_v and an increase in the S_v variance of the vessel data compared to the towed data when running into the swell, but not when running with the swell (Figure 4.10). The data cleaning algorithms reduced the variance in the vessel data, in part because the impulse noise and attenuated signal algorithms are designed to remove samples where the S_v value is noticeably different from those in adjacent pings. However, they did not increase the median S_v relative to the unfiltered data (Figure 4.11), demonstrating that significant bias may remain in degraded data even after filtering.

For each transect, the ratio of the filtered vessel s_a to the towed s_a was plotted against the proportion of attenuated pings identified in the vessel data (Figure 4.12). If the towed s_a represents an unbiased measurement, and the other sources of error discussed above are minimized, a close correspondence between vessel and towed s_a might be expected when no attenuated pings are identified in the vessel data. Noting the small sample size, this correspondence was observed from both linear and cubic fits to the data. These regressions show > 30% reduction in filtered vessel backscatter when the proportion of attenuated pings exceeds 30%, and suggest that the bias in degraded data increases as more attenuated pings are identified, even after the application of data cleaning algorithms.

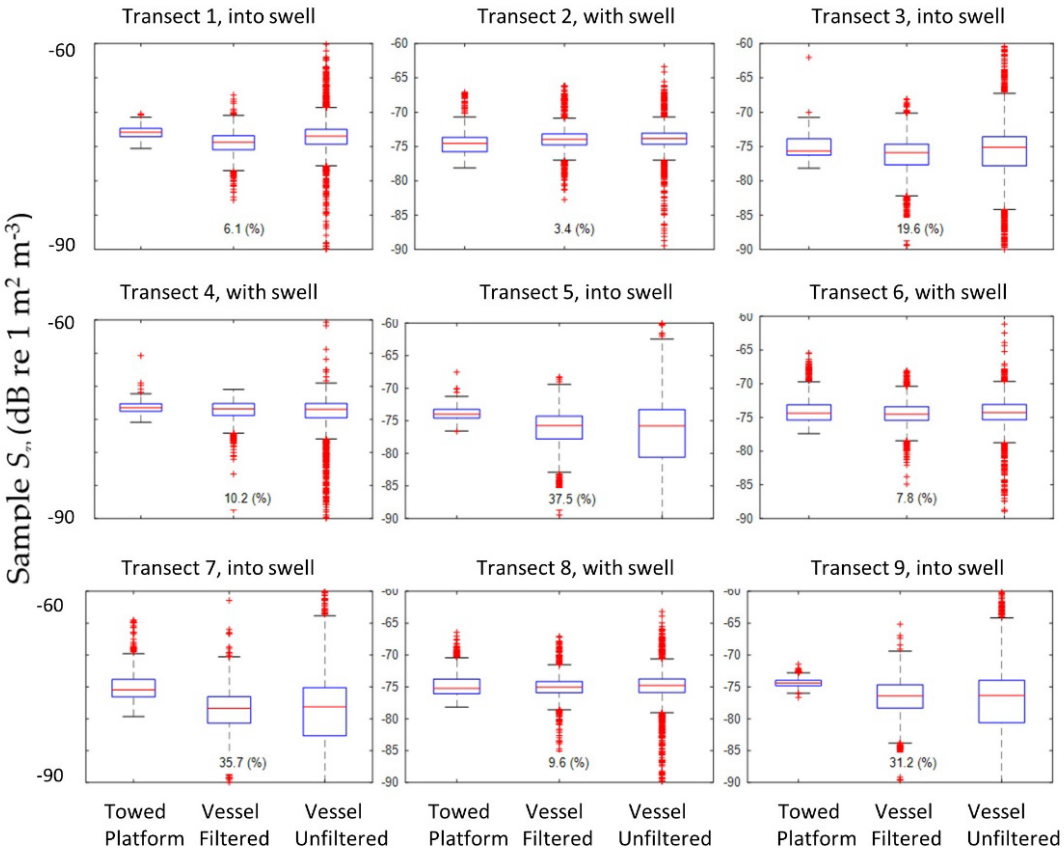

Figure 4.10. The distribution of sample S_v values at 38 kHz for the towed and vessel data from each transect carried out by the FV Amaltal Explorer over Chatham Rise in July 2016. The proportion of attenuated pings is indicated below the filtered vessel data. See text for details. Data provided by CSIRO.

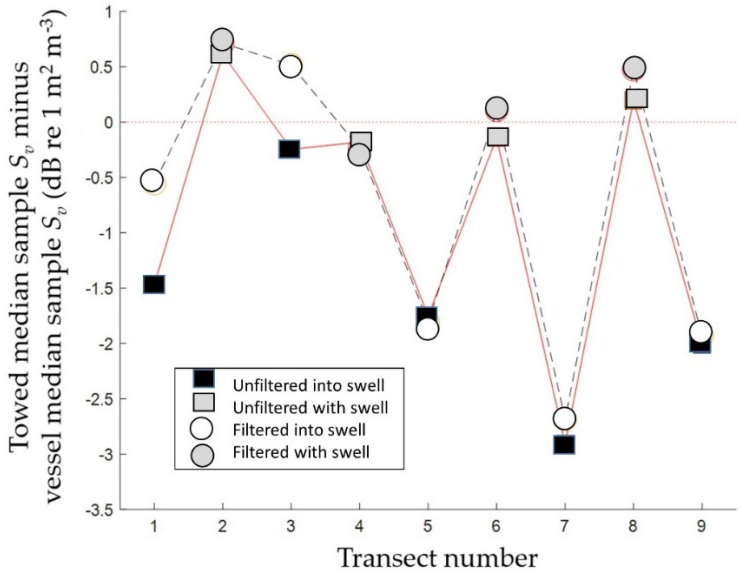

Figure 4.11. The ratio of towed median sample S_v to unfiltered vessel median sample S_v (squares) and filtered vessel median sample S_v (circles) for each transect. Also indicated is the direction of the transect relative to the swell. Data provided by CSIRO.

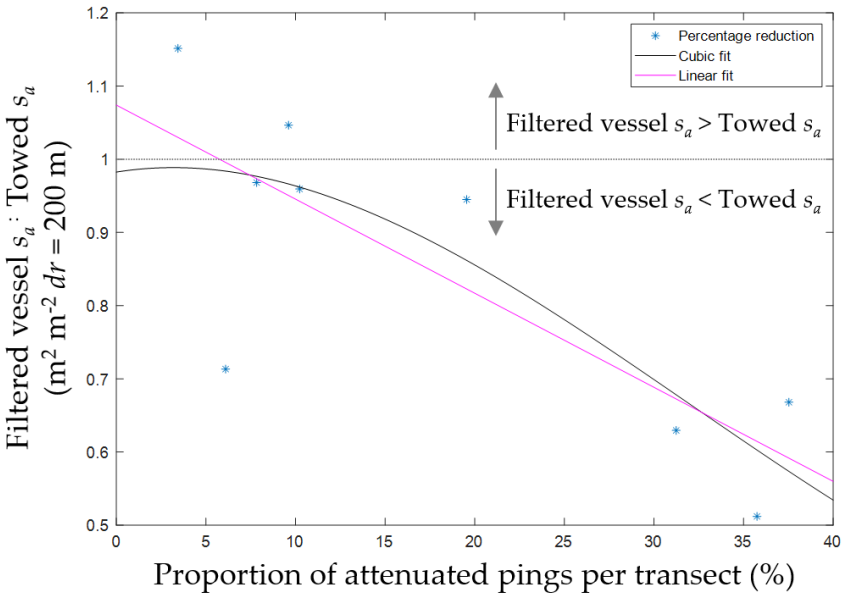

Figure 4.12. The ratio of filtered vessel water column s_a to towed water column s_a for each transect as a function of the proportion of attenuated pings in the vessel data, along with linear and cubic regression fits.

4.4.2 Seabed vs. water column backscatter

Seabed backscatter is generally more directive than the backscatter from targets in the water column. This means that transducer motion during inclement weather may affect seabed and water column measurements differently. What does this mean when using seabed backscatter as a metric of water column data degradation (Section 4.1)?

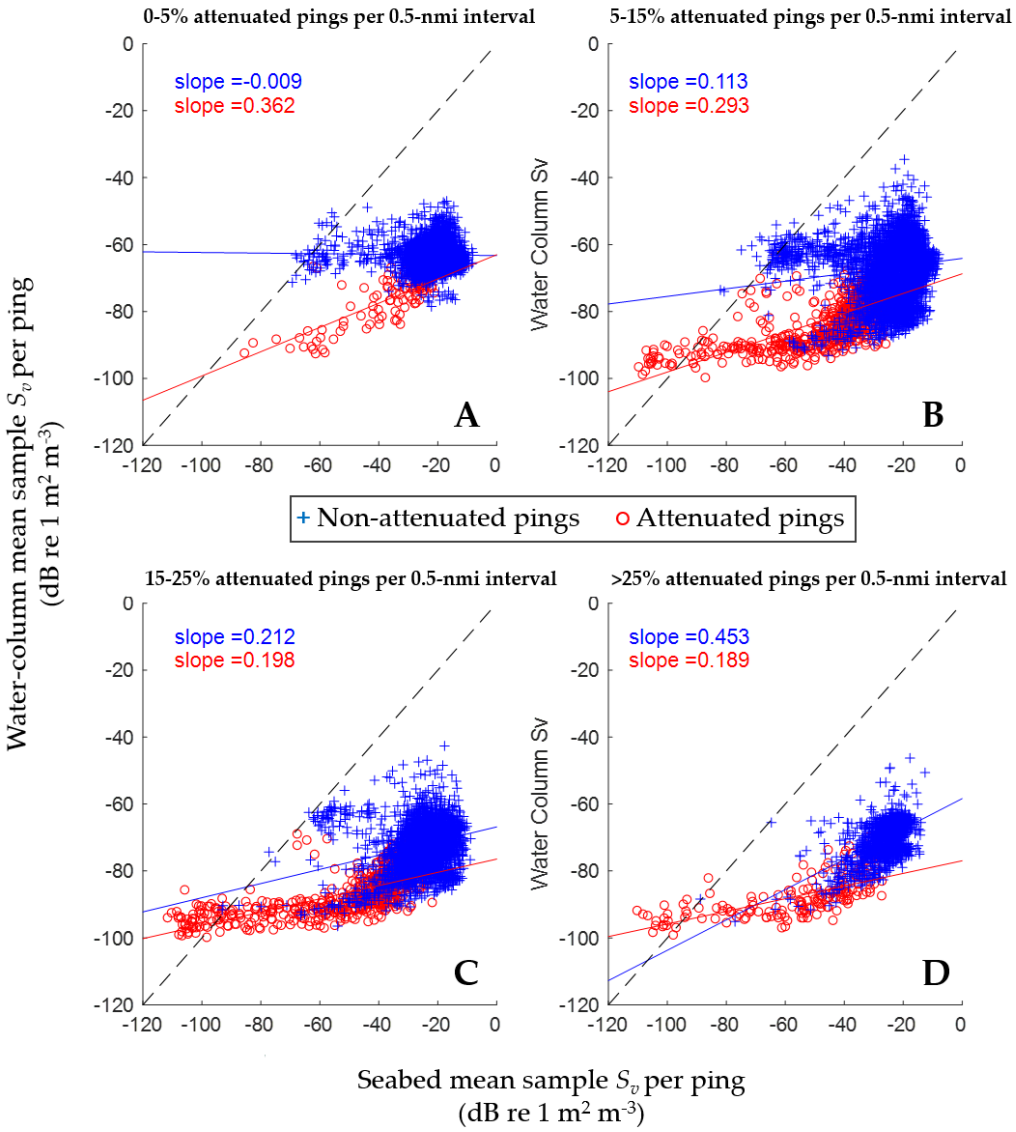

Figure 4.13. The relationship between seabed mean S_v and water column mean S_v at 38 kHz for each ping of the Saildrone dataset. The dashed black line shows the 1:1 slope of equal S_v. The blue and red lines show linear-regression fits to the data.

Using the Saildrone dataset described in Section 4.1.3, Figure 4.13 shows that, as expected, for each ping, water column S_v was generally lower and less variable than seabed S_v. Exceptions occurred when seabed S_v decreased below −100 dB in attenuated pings, and below −60 dB in non-attenuated pings. Furthermore, the slope was less than 1 in all cases, suggesting that seabed backscatter was more sensitive to attenuation than water column backscatter. This relative sensitivity decreased as the proportion of attenuated pings per 0.5-nautical mile interval increased, suggesting that as the data quality deteriorates, the water column and seabed backscatter become more similarly affected, and seabed backscatter can indeed be used as an indicator of water column signal attenuation. The slopes for attenuated and non-attenuated pings were different, particularly when the proportion of attenuated pings was low, presenting the possibility of using the relationship itself as an indicator of signal attenuation. Overlap between attenuated and non-attenuated pings in these plots is indicative of the continuous rather than binary nature of signal attenuation (Section 7.4). The increasing similarity between

slopes as the proportion of attenuated pings increased is consistent with the findings from the FV Amaltal Explorer (Section 4.4.1), which indicate that more and more of the data are likely to be degraded as conditions deteriorate.

4.4.3 Hull-mounted vs. keel-mounted transducers

A transducer mounted on the retractable keel of a surface vessel can be lowered below the entrained bubble layer and hence reduce signal attenuation (Section 2.3.1). The magnitude of this reduction can be estimated by comparing keel-mounted measurements with concurrent hull-mounted measurements.

Calibrated S_v measurements at 38 kHz were obtained in poor weather (~15 m s^{-1}, 29 knots windspeed) from the keel-mounted Simrad EK60 echosounder on the RV Johan Hjort during a two-day oceanographic survey in the Barents Sea (north of Norway) in February 2009 (Shabangu *et al.*, 2014). Concurrent measurements of S_v at 38 kHz were also obtained from a hull-mounted transducer connected via a multiplexer to the same echosounder. The multiplexer allowed the two transducers to ping sequentially and avoid interference while effectively measuring the same volume of water. The nominal depths of the hull- and keel-mounted transducers were 5.5 and 8 m, respectively.

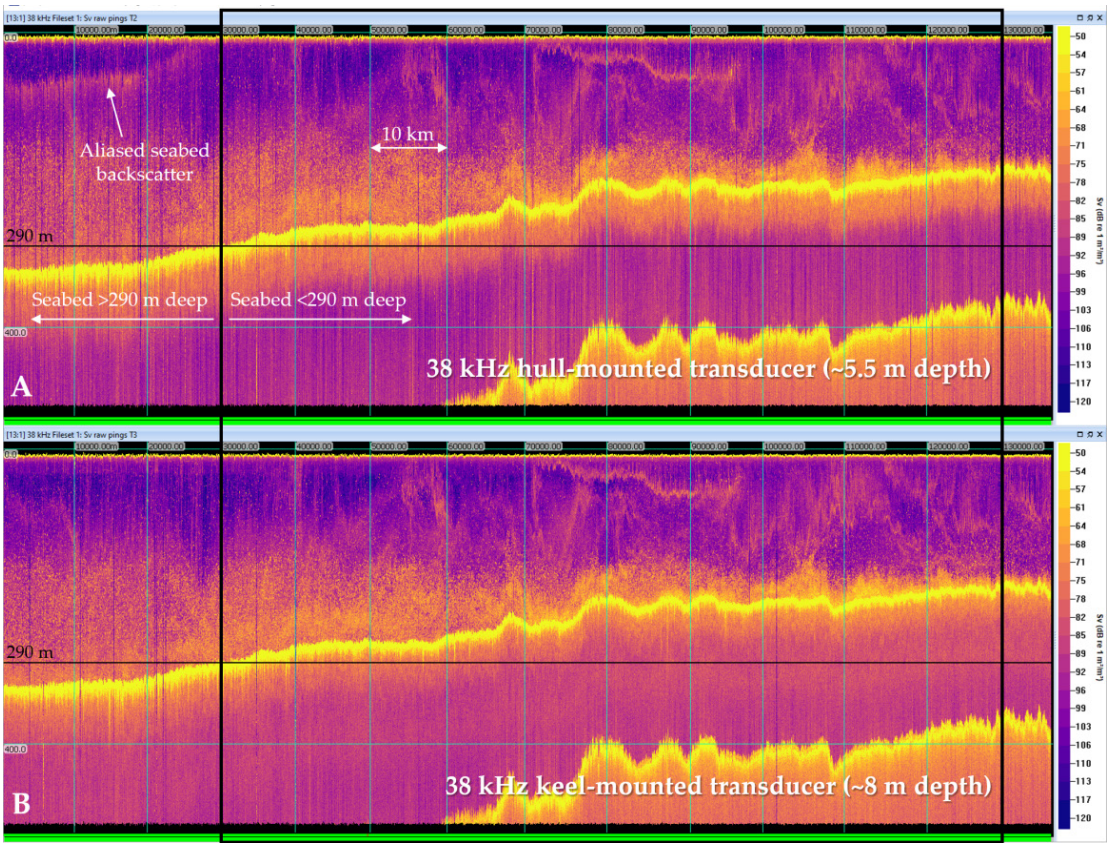

Figure 4.14. Calibrated and heave-corrected S_v from two 38-kHz transducers multiplexed to a single Simrad EK60 transceiver on the RV Johan Hjort in the Barents Sea in February 2009. (A) S_v from the hull-mounted transducer (~ 5.5 m depth). (B) S_v from the keel-mounted transducer (~ 8 m depth). The black box shows the ~ 8-h, 100-km, ~15 000-ping subset of data chosen for analysis. Every 13th ping is shown in this overview. The colour scale represents S_v from −50 to −120 dB. Data provided by the Institute of Marine Research (IMR; Norway) and the Republic of South Africa Department of Forestry, Fisheries and the Environment (DFFE; Republic of South Africa).

Echoview software was used to process an ~ 8-h, 100-km, ~ 15 000-ping subset of data for each transducer as the vessel steamed at ~ 3.5 m s^{-1} (7 knots) into the wind and swell (Figure 4.14). Data were chosen when the water depth was < 290 m to avoid the presence of an aliased seabed echo in the hull-mounted transducer measurements (see Figure 2.2). The nominal transducer depths were corrected for vessel heave, as measured by the vessel's motion reference unit. Pings affected by attenuation, transient noise, and impulse noise were manually identified from the S_v echograms and removed. A conservative approach was taken for this subjective identification process, i.e. if in doubt, the ping was removed. Background noise (Section 2.2.1) was not deemed to be significant at this frequency and over this range extent. Water column s_a (20 m depth to 10 m above the detected seabed) was calculated every 10 km for the raw and filtered data for each transducer.

Both transducers were affected by signal attenuation, with the hull-mounted transducer much more noticeably affected (Figure 4.15). On average, the raw hull s_a was 12% less than the raw keel s_a (min = 6%, max = 27%, n = 10). After filtering (Figure 4.16), the hull s_a was still, on average, 5% less than the filtered keel s_a (min = 0%, max = 22%). This is consistent with the findings from the FV Amaltal Explorer (Section 4.4.1) and Saildrones (Section 4.4.2), which indicate that even filtered data may be biased if the raw data are sufficiently degraded.

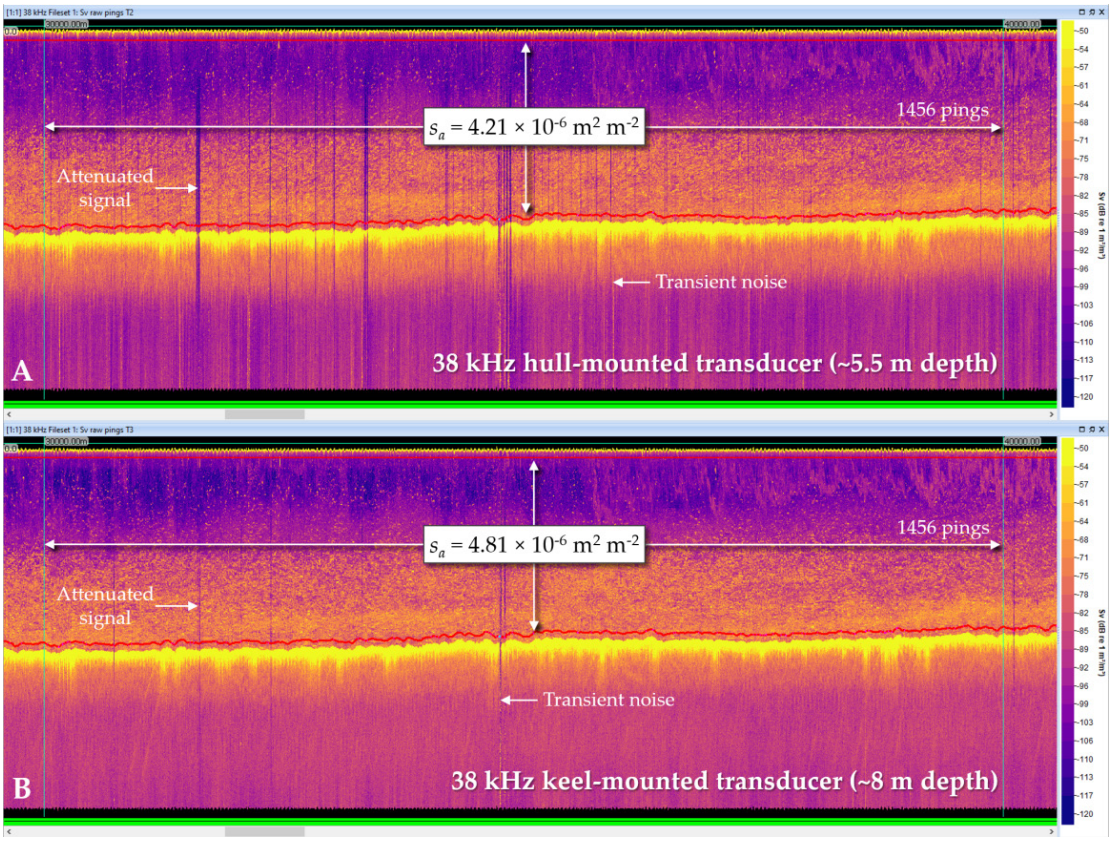

Figure 4.15. The first 10-km interval of the data subset shown in Figure 4.14. For this interval, the water column s_a was ~ 15% less for the hull-mounted data. The colour scale represents S_v from −50 to −120 dB. Data provided by the Institute of Marine Research (IMR; Norway) and the Republic of South Africa Department of Forestry, Fisheries and the Environment (DFFE; Republic of South Africa).

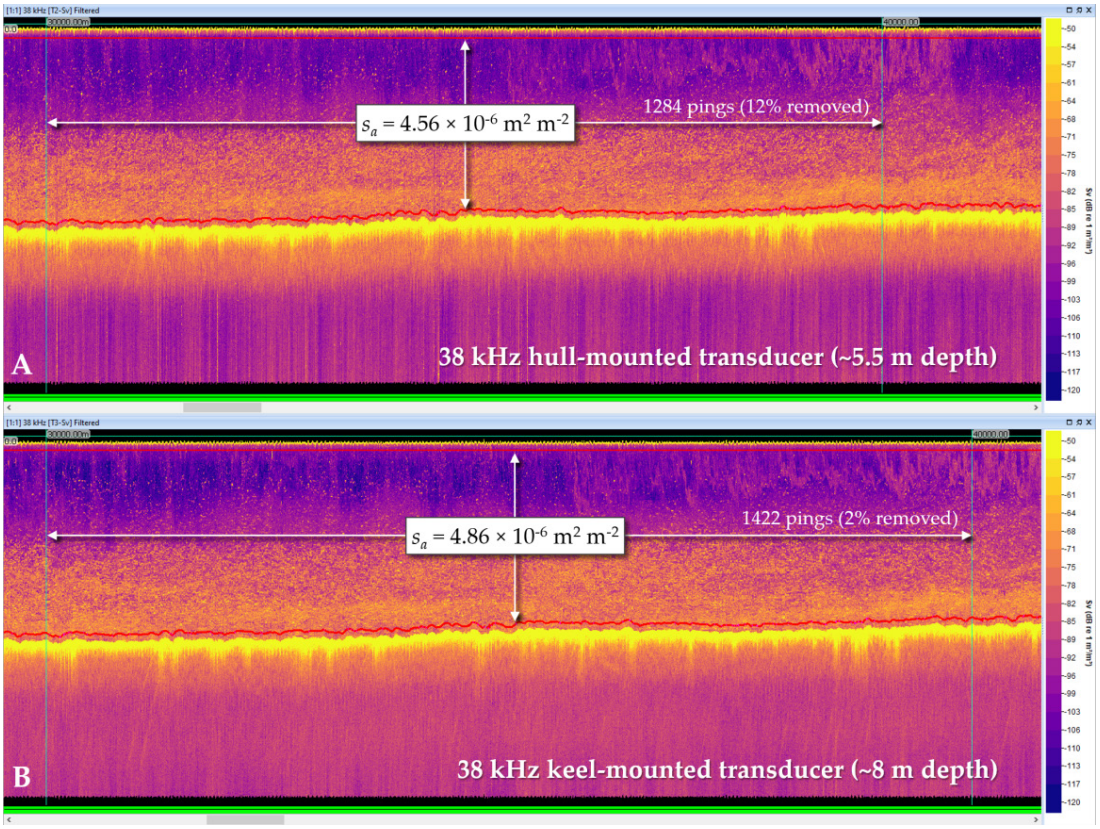

Figure 4.16. The same 10-km interval of data presented in Figure 4.15 after data processing to remove pings affected by attenuation, transient noise, and impulse noise. Twelve percent of the raw pings were removed from the hull data, and 2% from the keel data. Even after filtering, the water column s_a from the hull-mounted transducer was still ~5% less than both the processed and the raw keel-mounted s_a. The colour scale represents S_v from −50 to −120 dB. Data provided by the Institute of Marine Research (IMR; Norway) and the Republic of South Africa Department of Forestry, Fisheries and the Environment (DFFE; Republic of South Africa).

5 Quantifying signal attenuation from echosounder data in conjunction with other data

Section 4 focused on metrics involving only acoustic data. In many situations, other types of data are also available that may help in quantifying or mitigating signal degradation. Additional datasets may include meteorological data (e.g. windspeed and direction) and vessel motion data, namely pitch (the up-and-down motion of the bow and stern) and roll (side-to-side rotation of the vessel). This section will examine case studies for which these additional datasets were useful for quantifying or mitigating signal degradation.

The data available for the examples presented here were appropriate for investigating attenuation effects on echosounder data. The response variables of seabed s_a and attenuated pings were used to analyse effects of windspeed and direction as well as platform motion on data quality.

5.1 Windspeed

5.1.1 Seabed backscatter

Backscatter from the seabed (e.g. s_a) is a complicated convolution of seabed type (e.g. mud, sand, or gravel) and slope, transducer characteristics (beam width and acoustic frequency), and acoustic pulse (duration and bandwidth; ICES, 2007). However, as seen in Section 4, seabed s_a can be a useful metric of data quality.

5.1.1.1 Saildrone data

Seabed s_a collected during the NWFSC/SWFSC 2018 Saildrone survey off the west coast of North America, was calculated at 0.5-nautical mile intervals for a seabed region defined as the seabed detection to 10 m below that detection. The maximum depth for seabed detection was set to 400 m, i.e. the maximum depth recorded was 400 m although the true seabed was deeper. Attenuated pings were removed before calculating the final seabed s_a. The model was sensitive to large seabed s_a outliers at low windspeeds. To remove these outliers in an objective fashion, the top 1% of seabed s_a values were removed. Windspeed was measured once per minute by a Gill 1590-PK120 Windmaster three-dimensional sonic anemometer. GAMs were applied to the data to examine the effects of windspeed on seabed s_a. As the seabed s_a is always positive, a gamma family was used for the model. Model uncertainty is shown in the GAM figures as ± 2 times the standard error of the prediction fit.

The seabed s_a declined only incrementally until a windspeed of about 9–10 m s^{-1} (17–19 knots). At higher windspeeds, the seabed s_a decreased more rapidly (Figure 5.1). The GAM predicted that at about 10 m s^{-1} (19 knots), the seabed s_a would have decreased to 80% of the s_a at low windspeeds (averaged over 0–5 m s^{-1}, or 0–10 knots).

The relationship between seabed s_a and windspeed will be platform-dependent. The Saildrone is a small platform (7 m in length), and shows an increased sensitivity to wind at lower windspeeds when compared to larger research vessels such as the NOAA Ship Bell M. Shimada (hereafter FSV Shimada; 63.4 m in length; Figure 5.2). The source of the apparent bimodality in the GAM in Figure 5.2 is unclear. A potential explanation is a storm that the ship weathered during a large portion of data collection, and which resulted in fewer data being collected at

intermediate windspeeds. There could also be an effect of the transect direction, if the calculation from apparent windspeed to true windspeed was imperfect.

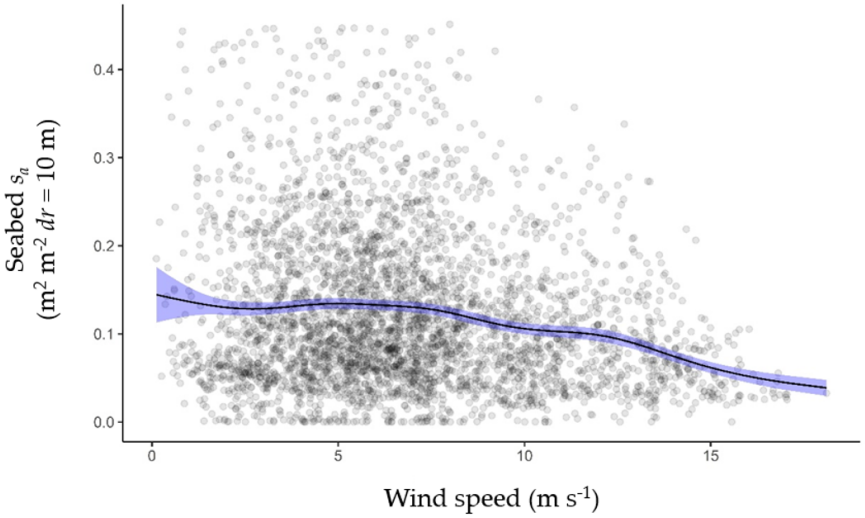

Figure 5.1. Saildrone seabed s_a with respect to windspeed. Data were from NWFSC/SWFSC 2018 Saildrone survey off the west coast of North America. The predicted seabed s_a from the GAM (solid line) and model prediction uncertainty (shaded area) are also shown.

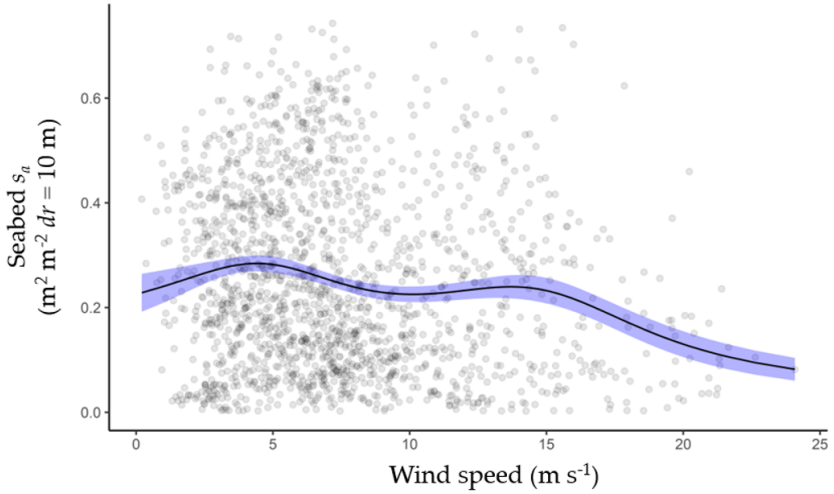

Figure 5.2. Seabed s_a measured by the 38-kHz ship-borne EK60 on the FSV Shimada, as a function of windspeed. Data were obtained from the NWFSC 2016 winter hake (*Merluccius productus*) survey off the coasts of Oregon and California, US. The predicted seabed s_a from the GAM (solid line) and model prediction uncertainty (shaded area) are shown.

5.1.1.2 International Ecosystem Survey in Nordic Sea (IESNS) data

Data were collected on the RV Dana (Denmark) during the IESNS in April/May 2017. The survey covered the distribution of the Norwegian spring-spawning herring (*Clupea harengus*) to estimate herring biomass, using the simultaneous efforts of five different vessels with 38-kHz echosounders. The RV Dana used a towed body for the 38-kHz transducer, and hull-mounted transducers at the 18- and 120-kHz frequencies. Echosounders were calibrated with a standard

sphere calibration prior to the survey. Wind speed and direction were recorded throughout the survey at a 1-Hz sampling rate.

During the survey, approximately 6.2×10^5 pings were recorded from 0 to 500 m, but only 2×10^5 pings corresponded to transects shallower than 500 m. To isolate seabed echoes, the Echoview best-bottom-candidate algorithm was used with a 5-m backstep, and gaps in the detected seabed echo were corrected manually. Another line was created with an offset of 35 m below the seabed echo, and data between these two lines were integrated for each ping. The remaining 60% of the survey data corresponded to regions where the seabed was below the recorded range. In order to identify the attenuated signals in these regions, 50 m of the water column were isolated, by manually drawing polygons with ~50 m vertical range, at a depth of around 400 m. At this depth, there was generally a consistent, homogeneous backscatter layer.

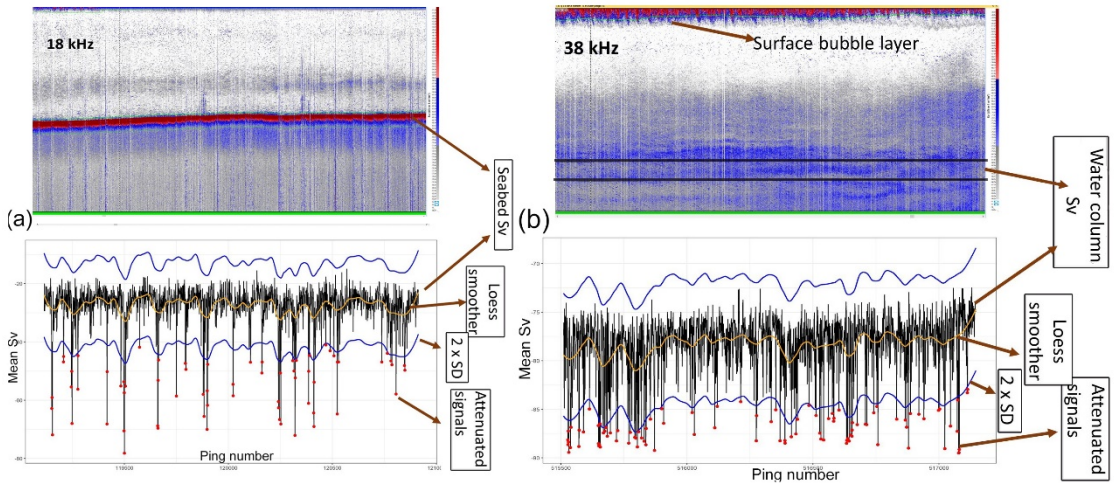

Figure 5.3. Example echograms and mean S_v for 30-min sections of 18- and 38-kHz data. The upper-left panel shows the 18-kHz echogram section, and the lower-left panel shows the time series of mean S_v for each integrated section of the ping. The yellow line at the centre of the time-series shows the local regression fit (loess), the blue lines show the two-standard-deviations from the loess curve. The red dots show the points where the mean S_v is below the threshold, and which have been identified as an attenuated signal. The right panels show an example for the 38-kHz (towed body) data. In this section, the seabed is deeper than the recorded data. The highlighted section on the echogram indicates the water column region used for the integration. This corresponds to a section when the vessel was heading into the wind (towards the west), with relatively strong wind (15 m s^{-1}, 29 knots) coming from the port bow side. A thick layer of the bubbles is visible at the surface extending down to 30 m.

The integrated data from both the seabed and the water column were averaged into 30-min bins (ca. 1800 pings). Local regression smoothers (loess) were fitted to the mean S_v data separately for each 30-min section with a 10% span (Figure 5.3). The standard deviation of the mean S_v in each 30-min section was calculated. The two-standard-deviation distance from the loess prediction was used as a threshold for determining the attenuated signal. After detection, the total number of attenuated pings were calculated for each interval.

The surface bubble layer was initially detected using the Echoview threshold offset algorithm, then corrected manually throughout the echogram. The bubble-layer detection was performed only for the 38-kHz data. The wind velocity and bubble-layer thickness were averaged over 30-min intervals and merged with the count of the attenuated signals. Figure 5.4 shows the relationship between mean seabed S_v and windspeed.

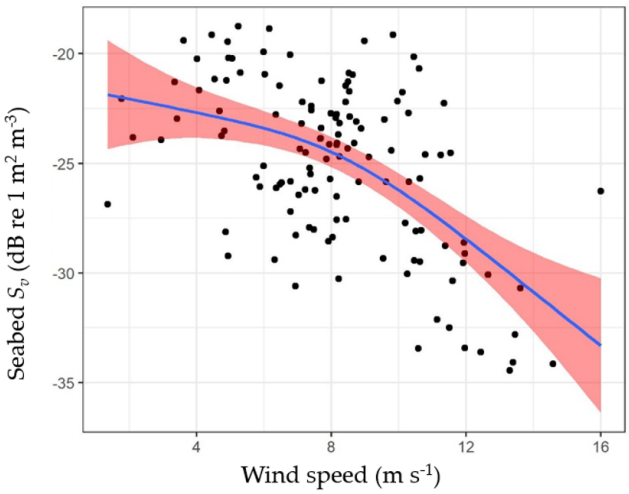

Figure 5.4. Relationship between windspeed and seabed backscatter. The blue line is the results of a GAM with 95% confidence interval (shaded area). Data obtained from the 2017 IESNS survey.

5.1.2 Attenuated pings

In this section, the effects of windspeed on the percentage of dropped pings and bubble-layer characteristics are examined for two datasets.

5.1.2.1 Saildrone data

Using the NWFSC/SWFSC 2018 Saildrone survey data, the percentage of attenuated pings was calculated at 0.5-nautical mile intervals using an attenuated signal algorithm (Toby Jarvis; Echoview). Results from a GAM indicated that windspeed had a significant effect on the percentage of ping dropouts ($p < 0.01$; Figure 5.5). Further, the percentage of ping dropouts appeared to increase sharply at about 9–10 m s^{-1} (17–19 knots), with 10% of pings attenuated at windspeeds of 12.5 m s^{-1} (24 knots).

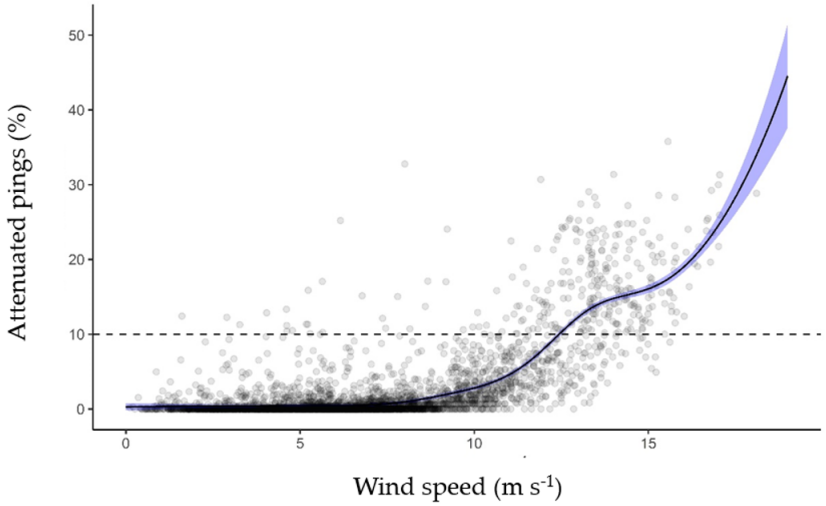

Figure 5.5. Percentage of attenuated pings (ping dropouts) as a function of windspeed for the NWFSC/SWFSC 2018 Saildrone survey off the west coast of North America. The predicted percentage attenuated pings from the GAM (solid line) and model prediction uncertainty (shaded area) are shown. The horizontal dashed line indicates 10% ping dropouts.

These results were roughly consistent with a separate seabed s_a vs. ping dropouts GAM (Figure 4.4) that predicted that at 2.7% ping dropouts the seabed s_a will have dropped to 82.8% of its initial value (considering the seabed s_a at < 0.5% ping dropouts as a reference), and by 10% ping dropouts, the seabed s_a will have dropped to 74.5% of the initial values.

5.1.2.2 IESNS data

Figure 5.6 shows the relationship between ping attenuation and windspeed for data collected during the IESNS. In accordance to the other results presented in this report, 10 m s^{-1} (19 knots) seems to be the critical windspeed where the ping attenuation starts to increase sharply. In Figure 5.6, there is a noticeable reduction in ping attenuation at very high windspeeds, which is an artefact due to the significant reduction in data quality. Assessing ping attenuation becomes problematic when most pings are greatly attenuated. Ping attenuation also co-varies with the surface bubble-layer thickness (Figure 5.7), although the relationship is not as strong as with windspeed, potentially due to the effect of this latter variable on ping attenuation. However, windspeed also seems to be a good predictor of bubble-layer thickness (Figure 5.8).

The results obtained indicate that wind velocity, number of attenuated pings, and surface bubble-layer thickness co-vary highly with each other. Based on the strength of the relationships, wind velocity seems to be the best predictor for ping attenuation. For this reason, a GAM was constructed taking the interaction between windspeed and direction into account, and also adding the bubble-layer thickness as an additional explanatory variable, using the formula:

Attenuated Pings ~ te(dirdiff, windSpCor, k = 10) + s(bubble)

where *dirdiff* is wind direction relative to the vessel, *windSpCor* is windspeed corrected relative to the vessel's speed, *te* and *s* are smoothing functions, and *bubble* is the surface bubble-layer thickness.

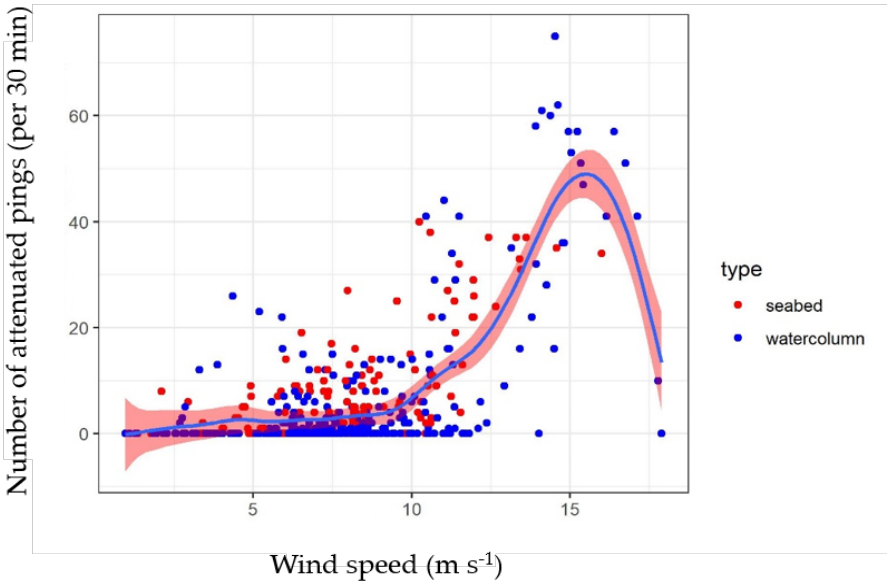

Figure 5.6. The relationship between windspeed and number of attenuated pings. The blue line shows a GAM with 95% confidence interval (shaded area), the red and blue dots indicate the number of attenuated pings detected from the sections with and without seabed, respectively. Data obtained from the 2017 IESNS survey.

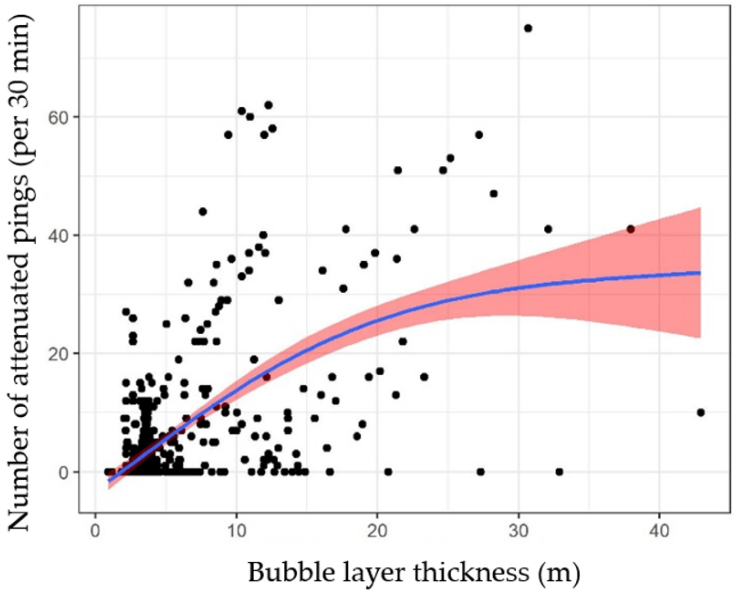

Figure 5.7. The relationship between bubble layer thickness and number of attenuated pings. The blue line shows a GAM with 95% confidence interval (shaded area). Data obtained from the 2017 IESNS survey.

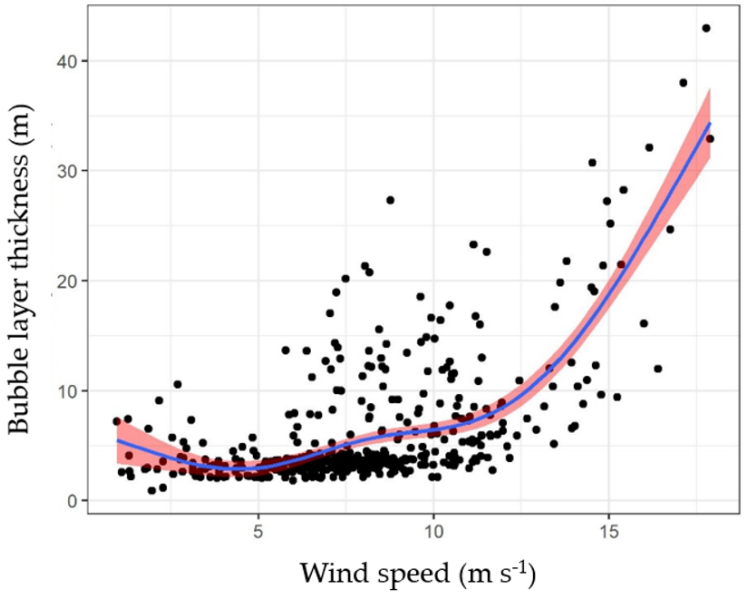

Figure 5.8. The relationship between windspeed and surface bubble layer thickness. The blue line shows a GAM with 95% confidence interval (shaded area). Data obtained from the 2017 IESNS survey.

The model was fitted using the mgcv package in R, with the method REML. Since the interaction between wind direction and speed has a variable effect on signal attenuation, a tensor spline smoother was used to model its effects. The total deviance explained by this model is 74%. Although both wind velocity and bubble layer appear to have significant effects on ping attenuation, 66% of the variance is explained by wind velocity alone (Figure 5.9). The weak relationship between bubble layer thickness and ping attenuation could be due to the bubble layer going undetected when the signal is severely degraded.

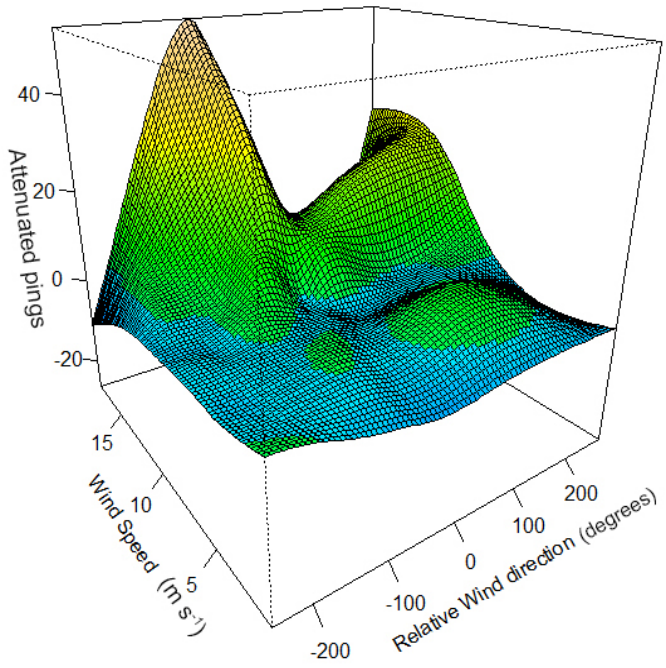

Figure 5.9. Effect of the interaction between windspeed and wind direction on ping attenuation. The effect seems to be strongest when the wind comes from the port bow, and lower when it comes directly from the bow. Data obtained from the 2017 IESNS survey.

5.1.3 Reference target

Ideally, a standard reference target (e.g. a calibration sphere; Foote *et al*., 1987) would be positioned within the acoustic beams during a survey so that any imperfections in signal transmission or reception could be compared directly to a standard. In practice, this is not possible, so echosounders are calibrated in conjunction with a survey and those calibrations are assumed to be valid for the entire dataset. If a calibration is conducted in inclement weather or the weather becomes a factor during a calibration, the deleterious effects of noise or attenuation may cascade throughout the data. Additionally, seabed backscatter can be highly variant, while the backscatter of a standard target is effectively invariant across a wide range of environmental conditions. Therefore, using a standard target to study the effects of inclement weather should provide higher confidence in the interpretation of noise or attenuation on backscatter than using seabed backscatter. Here, we provide data from a calibration exercise to evaluate potential effects of inclement weather on calibration results.

A Simrad EK60 calibration process (Andersen, 2001) on the NOAA ship Henry B. Bigelow (hereafter FSV Bigelow) was conducted on 5 March 2019 as part of the preparation for the NEFSC annual spring bottom-trawl survey. The FSV Bigelow's 18-, 38-, 120-, and 200-kHz EK60 echosounders with split-beam transducers (11° for the 18-kHz echosounder, and 7° for all others) were mounted on a retractable centre board positioned flush with the keel. The calibration was conducted using the wireless calibration system (EchoCal) developed at the NEFSC and the Simrad EK60 Lobe program. A 38.1-mm diameter tungsten carbide with 6% cobalt binder (WC) sphere was used for all frequencies. The FSV Bigelow was anchored (single-point anchor) at a location with a water depth of approximately 30 m of water in Narragansett Bay, US.

At the start of the calibrations process, the wind was light, the sea calm, and no surface bubbles were detected (Figure 5.10), but by the end of the calibration exercise, the wind had picked up and the wave height was 0.1–0.5 m (Figure 5.11). There was enough wind that bubbles were injected under the transducers (bubble sweep-down) and were detected by each echosounder frequency (Figure 5.12).

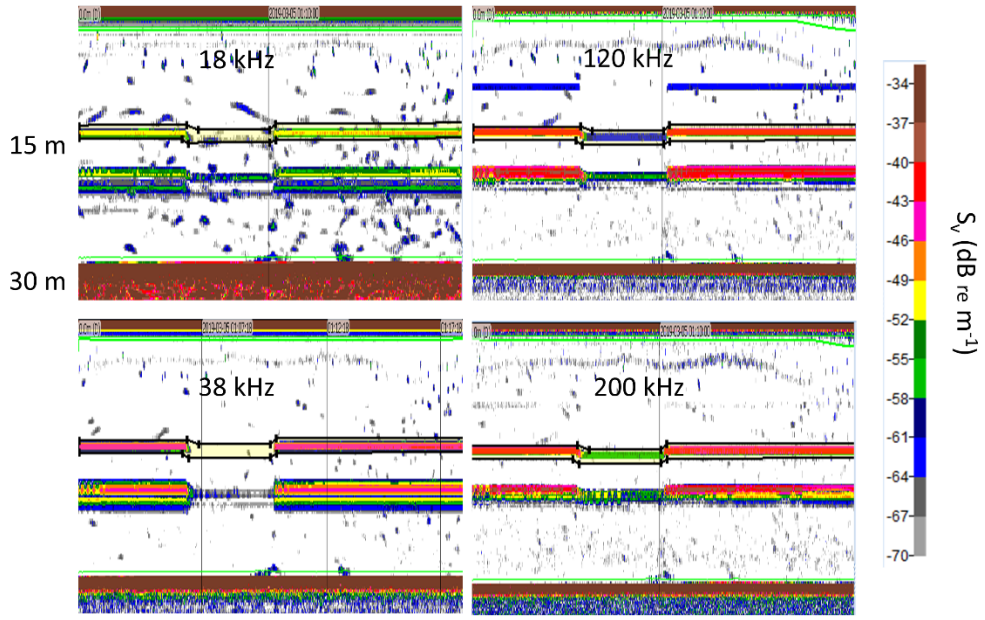

Figure 5.10. 18-kHz (upper left panel), 38-kHz (lower left panel), 120-kHz (upper right panel), and 200-kHz (lower right panel) S_v echograms obtained during the echosounder calibration process on the FSV Bigelow in March 2019. The S_v threshold was set to −70 dB. The echo from the sphere (upper echo at about 13.5 m) and weights (lower echo at about 17.5 m) are visible above the seabed echo. The green lines denote analysis regions. No surface bubbles are visible just below the transmit pulses. The section where the sphere echo is missing or has a lower intensity is due to the sphere moving outside the acoustic beams, and these values were not included in the analyses.

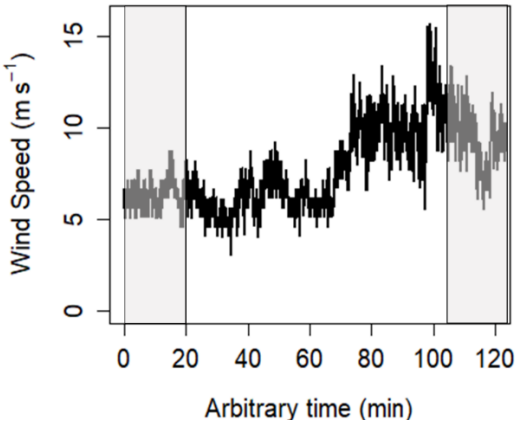

Figure 5.11. Windspeed over the course of the EK60 echosounder calibration process on the FSV Bigelow in March 2019. The left-shaded time-band corresponds to the time period in Figure 5.10, and the right-shaded time-band corresponds to the time period in Figure 5.12.

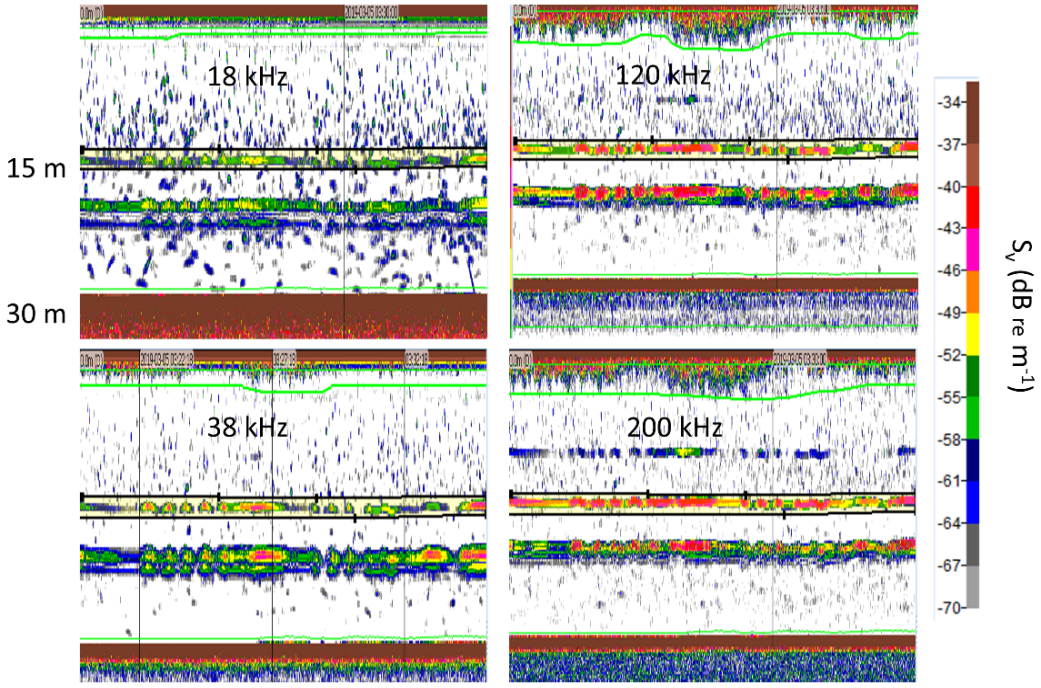

Figure 5.12. 18-kHz (upper left panel), 38-kHz (lower left panel), 120-kHz (upper right panel), and 200-kHz (lower right panel) S_v echograms during the calibration process on the FSV Bigelow in March 2019. The S_v threshold was set to −70 dB. The echo from the sphere (upper echo at about 13.5 m) and weights (lower echo at about 17.5 m) are visible above the seabed echo. The green lines denote analysis regions. Surface bubbles are visible just below the transmit pulses, especially in the 120- and 200-kHz echograms.

Analysis regions were manually drawn on the echograms in Echoview, delimiting the bubble layer to encompass surface bubbles (excluding the transducer ringdown and biological backscatter), the seabed layer to encompass the seabed echo [0.5 m above the peak seabed echo to 10 m (18-kHz echosounder) or 5 m (38-, 120-, and 200-kHz echosounders) below the seabed echo], and the calibration sphere echo. The bubble and seabed S_v and s_a values within each layer, and the TS values for the sphere were analysed for each echosounder frequency.

Visually, more surface bubbles were seen in the 120- and 200-kHz frequencies (Figure 5.13), which corresponded to higher mean S_v of the bubble layer, when compared to the 18- and 38−kHz frequencies (Figure 5.14). Seabed backscatter was lower during periods with surface bubbles than during periods without for all frequencies, but the 38-kHz echosounder was affected the most and the 200-kHz system the least. The TS of the sphere was affected by less than 1 dB (linear factor of about 1.26) for all frequencies. The differences in TS were −0.6, −0.4, −0.4, and +0.1 dB for the 18-, 38-, 120-, and 200−kHz systems, respectively (linear factors of 0.87, 0.92, 0.92, and 1.02, respectively; Figure 5.15). Interestingly, the mean TS at 200 kHz was slightly larger when surface bubbles were present compared to when they were absent. The magnitudes of these differences approach the threshold criterion of calibration precision (e.g. 0.5 dB; Foote *et al.*, 1987), so it is useful to understand the cause(s) of the apparent change. The visual evidence of surface bubbles suggests that the effect is due to bubble intrusion, but vessel motion (Section 5.3.1.3) or transducer transmit power could also be the culprits.

The transmit power should remain constant regardless of weather conditions or presence of surface bubbles for quantitative fisheries monitoring and research. To check whether the transmit power was the cause of the observed changes in measured TS, the transmit echo was

compared between periods with and without surface bubbles (data not shown). A 0.3-m range bin beginning at the 0-m range of the S_v echogram was selected to monitor the transmit pulse. The S_v of the transmit echo varied by at most 0.2 dB (linear factor of 1.05; 0.2, 0.1, 0.0, 0.1 dB for the 18-, 38-, 70-, and 200-kHz echosounders, respectively) over the course of the calibration. Only the 18-kHz echosounder had a weaker transmit echo between periods with bubbles (11.3 dB, linear factor of 13.5) and without (11.4 dB, linear factor of 13.8), with no difference in transmit echo among all other frequencies. These results suggest that transmit power was not responsible for the change in measured TS during the calibration exercise.

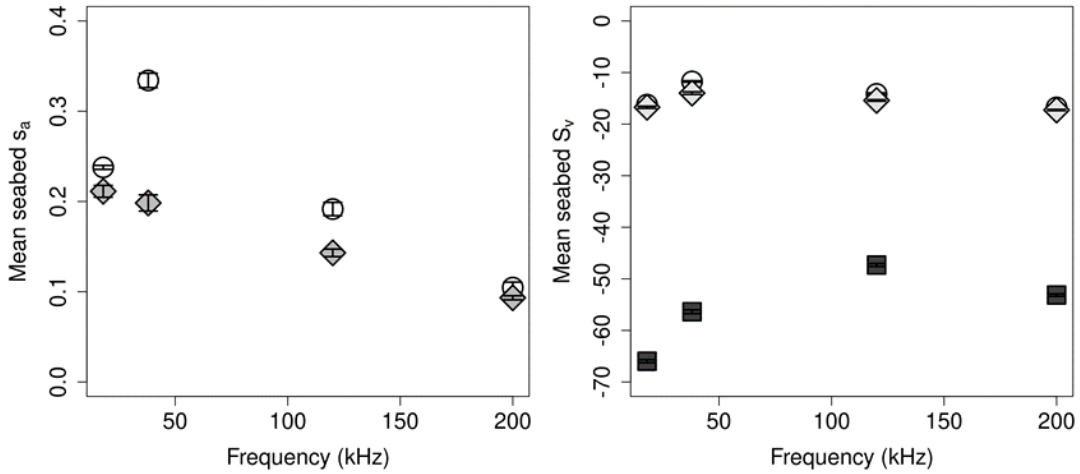

Figure 5.13. Left panel: mean s_a of the seabed backscatter as a function of acoustic frequency during no bubble periods (open circles) and during periods with bubbles (grey diamonds). Right panel: mean S_v of the seabed backscatter as a function of acoustic frequency during periods with no bubbles (open circles) and periods with bubbles (light grey diamonds). The dark grey squares are the mean S_v of the bubble layer during periods with bubbles. Error bars on both graphs represent the 95% confidence intervals.

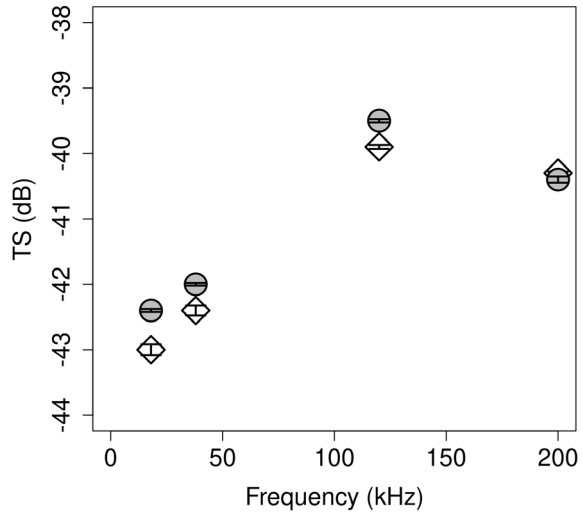

Figure 5.14. Effect of surface bubbles on the mean TS of a 38.1-mm WC sphere as a function of frequency. Grey circles represent the mean TS without surface bubbles, while open diamonds are the mean TS with surface bubbles present, and the error bars are the 95% confidence intervals.

5.2 Relative wind heading

5.2.1 Seabed backscatter

The direction of a platform (i.e. heading) relative to wind direction affects how the platform rides in inclement weather. As a consequence, the relationship of seabed s_a to wind direction may be dependent on the direction of the wind relative to the platform heading. In this report, wind direction is defined as the direction the wind was coming from, and platform heading as the direction the platform is heading.

Relative wind direction is especially important for the Saildrone, as it is a sailing platform. Wind-relative heading was calculated as wind direction minus Saildrone heading. The wind-relative heading was formatted to range from 0 to 360°, with 0° defined as the Saildrone heading in the same direction as the wind, and 180° defined as the Saildrone heading directly away from the direction of the wind. As the Saildrone is a sailing vessel that moves using only wind power, the following definitions of points of sail were used:

- into the wind: heading within 45° of the wind direction;
- close reach: heading 45–67.5° from the wind (wind on the bow, but not directly);
- beam reach: heading 67.5–112.5° from the wind (wind on the beam);
- broad reach: heading 112.5–157.5° from the wind (wind from the stern, but not directly); and
- running: heading 157.5–180° from the wind (wind directly on the stern).

These points of sail were symmetric about 180°, so port and starboard wind-relative headings were not distinguished. The Saildrone infrequently ran into the wind or with the wind.

A generalized linear model (GLM; gamma family) was constructed relating seabed s_a to windspeed and direction. Beam reach was used as the reference relative wind direction in the model. Both windspeed ($p < 0.001$) and wind-relative heading (depending on wind direction) significantly affected seabed s_a. Therefore, considering the wind-relative heading in addition to windspeed may be useful when designing or analysing data from surveys meant to be run in inclement weather, especially from a sailing vessel.

Seabed s_a was significantly different when the Saildrone was on a broad reach (relative to a beam reach; $p < 0.01$), but not for other sailing directions [close reach ($p < 0.61$), into the wind ($p < 0.14$), or running ($p < 0.58$); Figure 5.15].

5.2.2 Attenuated pings

A GLM relating the percentage of ping dropouts to the windspeed and wind-relative heading (Figure 5.16) was applied to the NWFSC/SWFSC 2018 Saildrone survey data. Wind-relative heading was defined as in Section 5.2.1, with the beam reach as the reference heading.

The results obtained were similar to those of the GLM for seabed s_a and windspeed and wind-relative heading (Section 5.2.1). The percent of attenuated pings was significantly affected by both windspeed ($p < 0.01$) as well as wind-relative heading, with significant effects of being on a broad reach ($p < 0.01$) relative to a beam reach. There were also significant effects of heading into the wind ($p < 0.02$) or running with the wind ($p < 0.01$), as opposed to sailing on a beam reach (Table 5.1). However, the sample sizes were relatively low, and these orientations may be difficult for the Saildrone to sail, given transect design and prevailing winds. The effects of being on a close reach were not significant ($p < 0.13$).

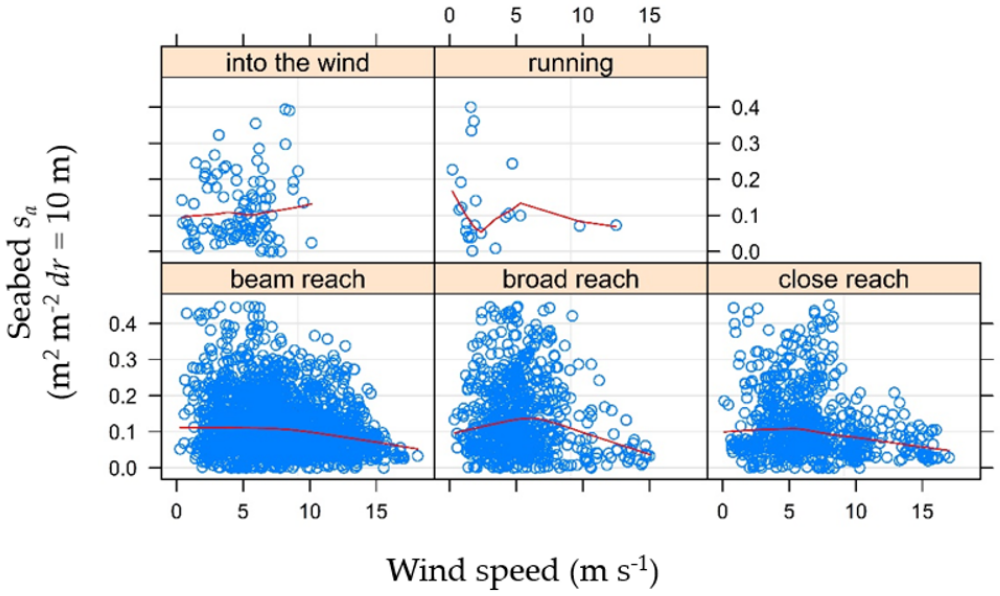

Figure 5.15. Seabed s_a with respect to windspeed under five different points of sail during the NWFSC/SWFSC 2018 Saildrone survey off the west coast of North America. A loess curve (red line) was fitted to the data for each point of sail.

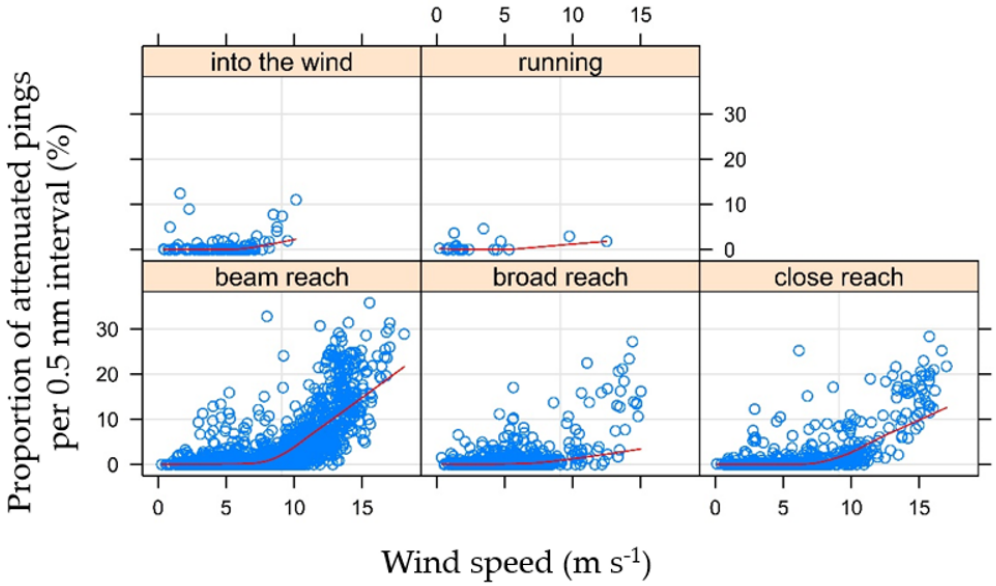

Figure 5.16. Percentage attenuated pings (ping dropouts) as a function of windspeed under five different points of sail during the NWFSC/SWFSC 2018 Saildrone survey of the west coast of North America. A loess curve (red line) was fitted to the data for each point of sail.

The model did not find a statistical difference between being on a beam reach and a close reach, although it did find a difference between being on a beam reach and a broad reach. When looking at the plots of attenuated pings vs. windspeed and wind-relative heading (Figure 5.17),

increasing windspeed when on a beam reach resulted in the most attenuated pings, with a (non-significant) improvement when on a close reach, and a (significant) improvement when on a broad reach. It is difficult to interpret the effect of running into or with the wind as there are few sample points at high windspeeds.

These results suggest that when possible, the Saildrone should avoid sailing on a beam reach, with a broad reach preferred over a close reach. This could be interpreted intuitively as the Saildrone is less stable when it is perpendicular (beam reach) to the wind and seas, and is more stable traversing the same direction as the wind and seas (broad reach). In this survey case study, wind direction is relatively consistent (Figure 5.17), so wind-relative heading will have implications for survey design and execution using a Saildrone. These considerations will likely be different in areas without consistent wind directions or for non-sailing vessels. For these platforms, understanding how pitch and roll affect the acoustic results may be more useful.

Table 5.1. The *t* and *p* values for the GLM relating percentage of attenuated pings to windspeed and wind-relative heading (beam reach as reference heading). * denotes significance at the $p < 0.05$ level.

Model inputs	Pr (>|t|)	*t*-value
Windspeed	<.001*	53.72
Wind-relative heading factors:		
Broad reach	<.001*	4.68
Close reach	0.13	1.52
Into the wind	0.02*	2.42
Running	<.001*	3.50

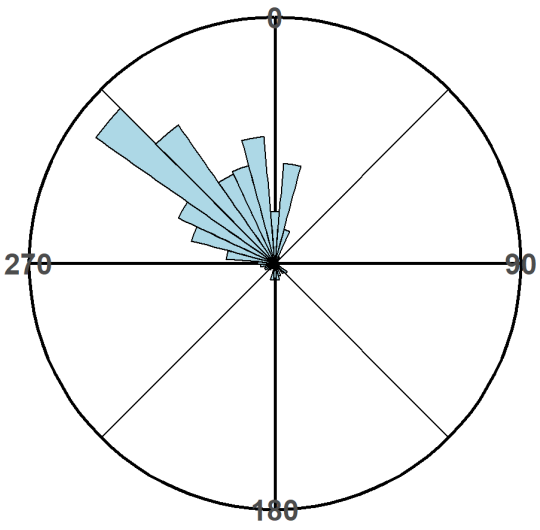

Figure 5.17. Polar histogram of wind direction over the 2018 Saildrone survey, where north is 0° and east is 90°.

5.3 Platform motion

Vessel or platform motion data can be used to develop predictive models of data quality that can be used during surveys to make decisions about when to halt operations, change course, take other action, or potentially correct lower-quality data that have been collected. The availability of vessel motion data does not preclude analysing and evaluating the data as developed in Section 5.2, but does add another layer of analysis.

5.3.1 Seabed backscatter

5.3.1.1 Saildrone data

The Saildrone is a small, sail-driven platform, for which motion, such as pitch and roll, will change relatively quickly. In many cases, the variability, or rate of change of pitch and roll, may be a more useful diagnostic for vessel motion than mean pitch and roll (see Section 5.3.1.2). However, the NWFSC/SWFSC 2018 Saildrone survey data had a relatively low sampling rate of acoustic data and motion (> 8 s). In this scenario, with rapidly changing platform motion but slow sampling rate, the rate of change of pitch and roll did not prove useful, so the absolute pitch and roll were examined instead.

Seabed s_a with respect to pitch and roll were plotted in Figure 5.18 and fitted to GAM models. Seabed s_a was found to be significantly affected by roll ($p < 0.01$), but not by pitch ($p < 0.1$). However, not all platforms will be more sensitive to roll than to pitch in inclement weather, and the wind-powered Saildrone may react differently than platforms powered by other means.

5.3.1.2 NIWA data

Survey vessels are usually trimmed, and the transducers are mounted accordingly so that the acoustic axes are oriented vertically downward. As a consequence, the mean pitch and roll of a vessel should be 0° over time, and, accordingly, mean pitch and roll are not useful diagnostics for vessel motion. However, as sea state deteriorates, the variability (e.g. standard deviation and variance) in pitch and roll will increase. Thus, variability in pitch and roll may be a useful diagnostic of data quality.

An analysis was carried out on EK60 38-kHz acoustic data and vessel motion data collected by NIWA during a demersal trawl survey south of New Zealand in 2016 on the RV Tangaroa (O'Driscoll *et al.*, 2014, 2016). The mean of the standard deviation of roll, the mean of the standard deviation of pitch, the mean of the absolute value of the rate of change (^{o} s^{-1}) of roll, and the mean of the absolute value of the rate of change of pitch were investigated as indicators of data quality. Each recording corresponded to the 3-nautical mile duration of the trawl (n = 56 tows). The time-averaged mean of the rate of change of roll and pitch over the tow interval was calculated (Figure 5.19).

These data were used to investigate correlations between the pitch and roll rates of change and data quality, as measured by the percent of attenuated pings. The rate of change of pitch had the highest linear correlation to the percent attenuated pings, with correlation coefficients of 0.91 and 0.85 for the rate of change of pitch and standard deviation vs. percent of attenuated pings, respectively (Figure 5.20). Correlation coefficients were much lower using roll, with coefficients of 0.48 and 0.32 for standard deviation of roll and absolute value of the rate of change of roll vs. percent of attenuated pings, respectively. It should be noted that the data were collected during the trawl, and, consequently, the variation in roll may be limited.

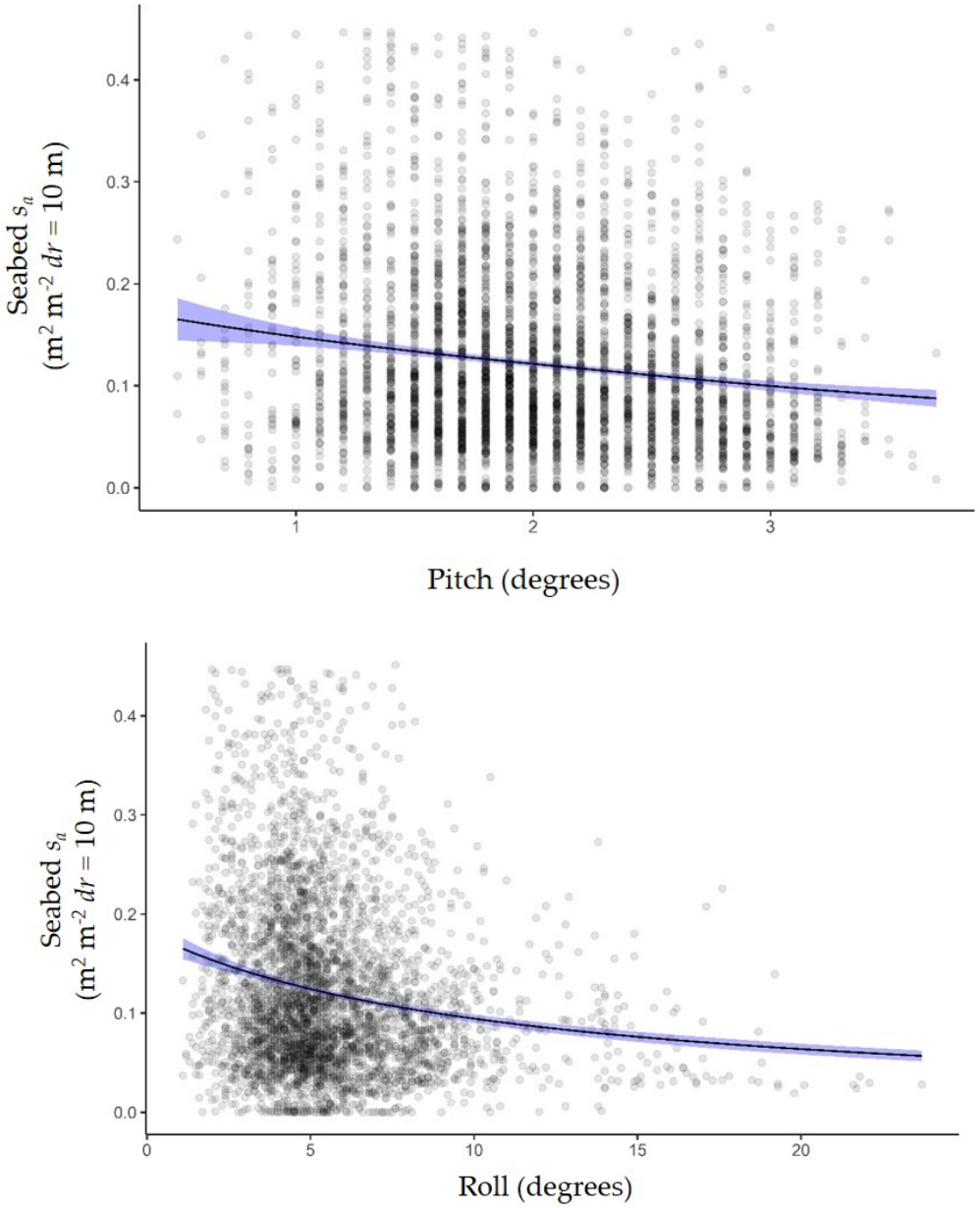

Figure 5.18. Saildrone seabed s_a as a function of Saildrone pitch (upper panel) and roll (lower panel) from the NWFSC/SWFSC 2018 Saildrone survey off the west coast of North America. Predicted seabed s_a from the GAM (solid line) and model prediction uncertainty (shaded area) are shown.

Not all vessels react in the same way to inclement weather. As an example, the relationship observed in the NIWA data (collected on the FV Tangaroa) between percent attenuated (bad) pings and vessel pitch rate (deg s^{-1}), was not observed for the CSIRO data (collected on the FV Amaltal Explorer; see Section 4.1.2), despite having corresponding vessel-motion data at an appropriate sampling rate. The absolute values of pitch rate of change were averaged over 30-s intervals, and the corresponding percent of attenuated pings were plotted (Figure 5.21). For the FV Amaltal Explorer data, the range of vessel pitch rates was much lower than for roll, and there was almost no correspondence between pitch rate and the percent of attenuated pings.

However, roll rates of change indicated an increase in the percentage of attenuated pings with increasing roll rates, and a stronger relationship with roll, which was not linear. This is contrary to the NIWA dataset, which indicated that the pitch rate of change was more highly correlated with the percent attenuated pings than the roll rate of change. Thus, these results highlight that diagnostics can be vessel-specific, which is perhaps an unsurprising outcome given the highly variable nature of vessel design and their motion characteristics. In this case, it appears the Amaltal Explorer is considerably more susceptible to roll than to pitch, suggesting that the dynamic range of pitch and roll should be evaluated in addition to the rates of change.

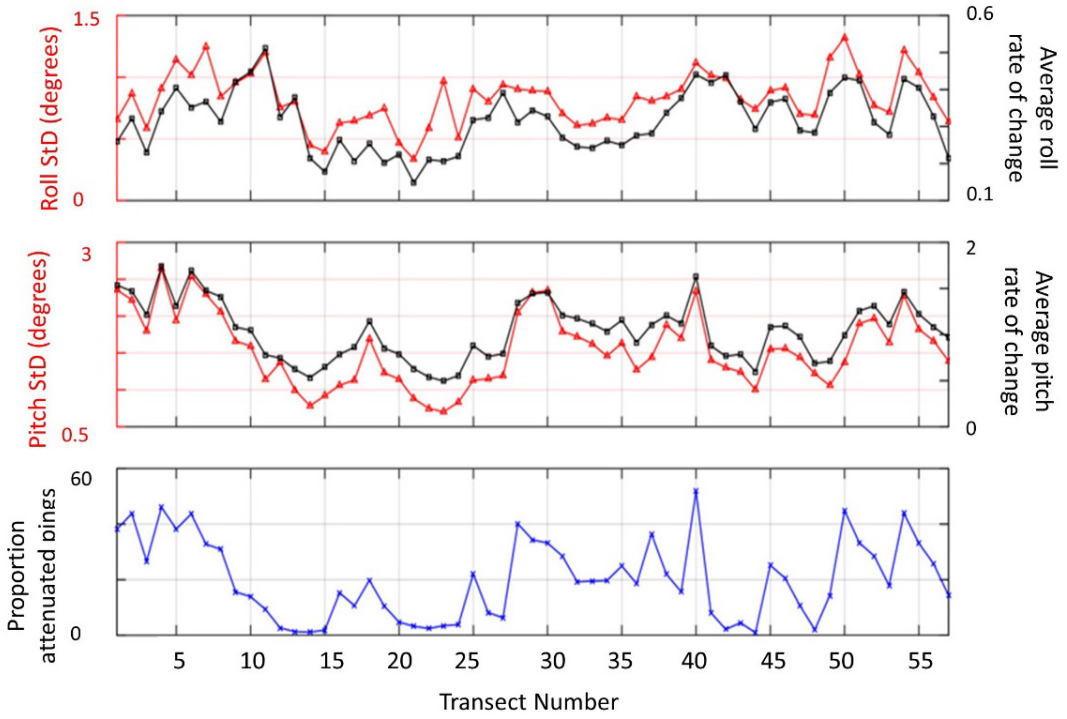

Figure 5.19. Mean standard deviation (red line) and mean absolute value of the rate of change (° s⁻¹; black line) of roll (top panel) and pitch (middle panel). Lower panel: Percent of attenuated pings (or bad ping percentage).

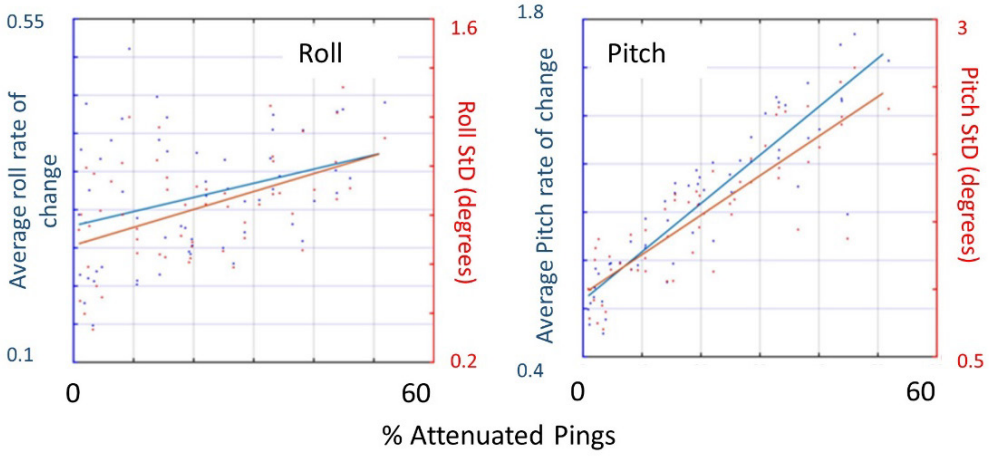

Figure 5.20. Plots of mean absolute value of rate of change (° s⁻¹; blue line) and standard deviation (red line) for roll (left) and pitch (right) vs. percent attenuated pings (ping dropouts).

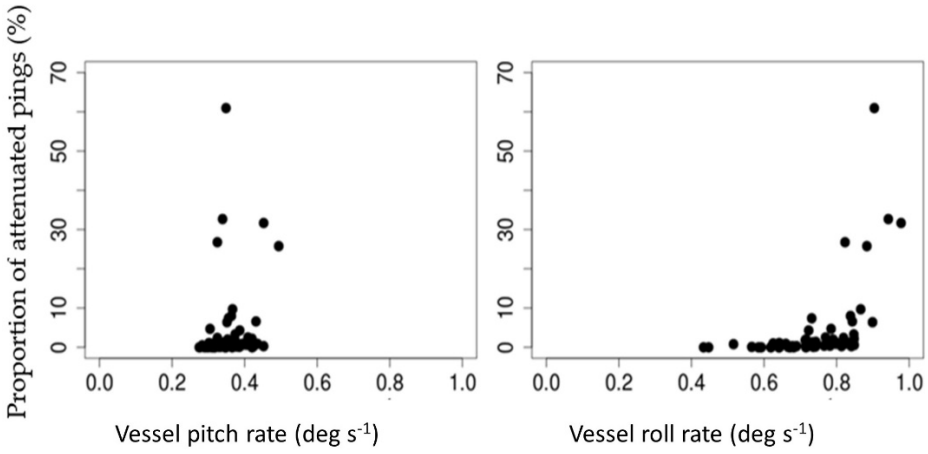

Figure 5.21. Percent attenuated pings (ping dropouts) as a function of the mean absolute value of rate of change (deg s^{-1}) of pitch (left) and roll (right). Data from the FV Amaltal Explorer, obtained courtesy of CSIRO.

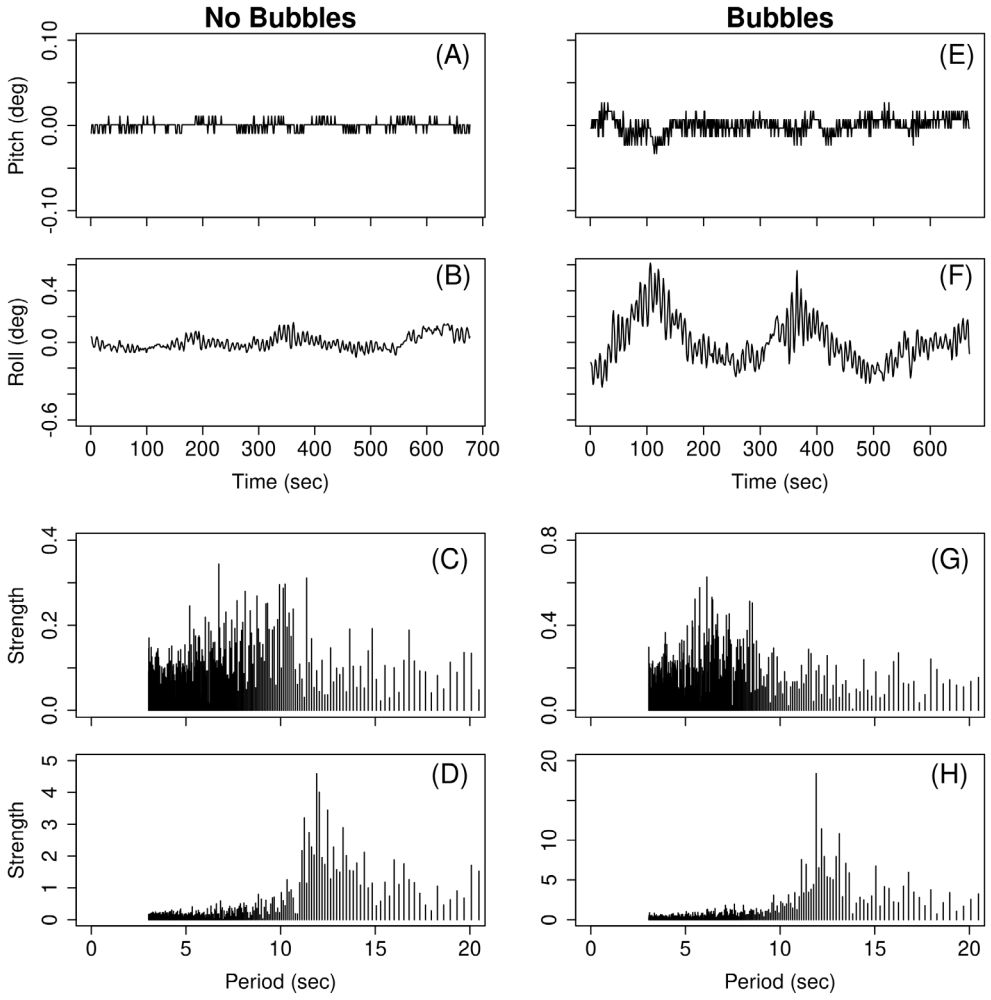

Figure 5.22. Pitch (panels A and E) and roll (panels B and F) motion data for periods during the EK60 calibration process on the FSV Bigelow when surface bubbles were absent (left column) and surface bubbles were present (right column). The motion data were collected at nominally 1 Hz. Results of a Fast Fourier Transform (FFT) applied to the pitch (panels C and G) and roll (panels D and H) motion data. Note the difference in ordinate scale for the FFT results to highlight differences in spectral energy.

5.3.1.3 Reference target

The effect of transducer motion was evaluated to determine the magnitude of the possible error introduced by vessel motion. During periods of no surface bubbles, the pitch and roll ranged from 0.1 to 0.2°, and from 0.1 to 0.4°, respectively, with dominant periods of 7 and 12° in pitch and roll, respectively (Figure 5.22). As windspeed increased (Figure 5.11), pitch remained stable, whereas roll increased from 0.1 to 1.1° and the periodicity remained constant (Figure 5.22). The Dunford corrections based on vessel motion and periodicity ranged from 0 to 0.02 dB (linear factors of 0 to 0.005; Figure 5.23). These corrections are nearly an order of magnitude smaller than the apparent effect on mean TS, suggesting that vessel motion is not a factor in the TS change observed during the calibration exercise (Section 5.1.3).

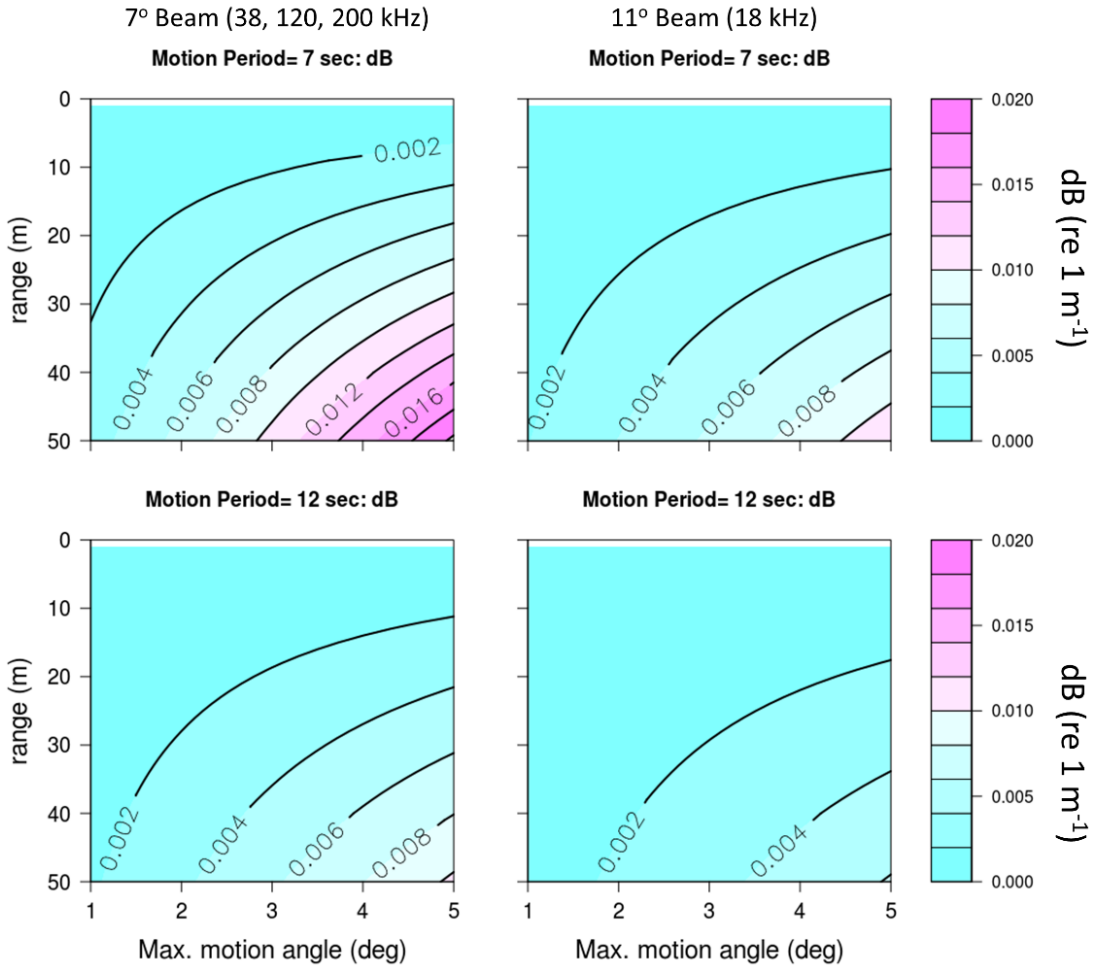

Figure 5.23. Dunford correction for the 38-, 120-, and 200-kHz transducers (7° beam width, left panels) and the 18-kHz transducer (11° beam width, right panels) at 7-s period (upper panels) and 12-s period (lower panels). The periodicity is based on the FFT of the motion data during the EK60 calibration on the FSV Bigelow in March 2019.

6 Synthesis of metric evaluations

Methods used to evaluate data quality in this report are grouped into two categories: acoustic data with and without ancillary information. Ancillary information includes meteorology, sea state, or data that monitor the platform status. This report only analyses platform motion data (pitch, roll, and heading) and meteorological data (windspeed and direction). In both cases, methods and metrics used to evaluate and diagnose data quality are not exhaustive. Instead, they are a starting point to evaluate whether survey data should be included or excluded from data analyses, and they provide an objective approach to decide when to continue or suspend data acquisition.

6.1 Acoustic data without ancillary information

Evaluation and diagnostic criteria need to be developed using only acoustic data in cases where ancillary information and data are not collected in conjunction with water column backscatter data, are not collected appropriately, or are not readily available. In these cases, the dependent variable is ideally the echo intensity of a target that is invariant over a wide range of conditions. The TS of a calibration sphere is an example of an ideal dependent variable (Section 5.1.3). Unfortunately, having a calibration sphere suspended below the transducer during a survey is not possible. Instead the seabed echo intensity can be used as an alternative. The seabed echo is very nearly an ubiquitous feature of acoustic data collected during vessel-based, fisheries surveys. Under certain conditions, the seabed echo may provide a useful variable to monitor data quality (Section 4.1), although variability of seabed scattering is well known (e.g. ICES, 2007),

Indicators and metrics of data quality should be simple to calculate, sensitive to changing meteorological conditions, and robust over a wide range of conditions and surveys. The terms simple and robust suggest using backscatter features that are easily detectable, quantifiable, and representative of data quality and/or changing conditions. The use of attenuated pings, transducer ringing, and transducer impedance as independent variables to monitor data quality were investigated during different survey and deployment situations (Section 4).

The proportion of attenuated pings was shown to be a useful indicator of data quality (Table 6.1), but the use of seabed s_a as an indicator of data quality was variable and inconsistent. In some cases, the proportion of attenuated pings was a useful indicator of data quality, where an attenuated ping rate below ~10% indicated good-to-reasonable data quality and an attenuated ping rate above ~25% indicated unusable data (Section 4.1.1). For attenuated ping rates between 10 and 25%, data quality decreased monotonically, potentially providing an index to define a criterion to accept or reject data. However, because the range of seabed s_a is quite large even under calm conditions, seabed s_a may be an insensitive indicator of data quality. In datasets from a survey vessel and a Saildrone (Section 4.1.3), there was a decrease in seabed s_a with an increase in ping attenuation rate, but the decrease was slow, with no obvious inflection points that could be used to define thresholds.

Transducer ringing was not a consistent indicator of data quality (Table 6.1). The intensity of the transducer ringing (i.e. S_v within 0.8–1 m from the end of the transmit pulse) was not indicative of data quality as measured by the number of attenuated pings (Section 4.2). However, there appeared to be a strong relationship between attenuated pings and timing and

variation in S_v in the latter portion of the ringdown. This relationship could be used as an index and/or predictor of attenuated signal.

Table 6.1. Acoustic, platform motion, and meteorological variables, metrics of those variables, and qualitative ranking of the metric usefulness as an indicator of data quality. deg s^{-1}: angular degrees per s (used as a unit of time).

Variable	Metrics	Usefulness
Acoustic - dependent		
Seabed echo intensity	S_v, s_a	Moderate
Calibration sphere TS	TS	High
Acoustic - independent		
Attenuated pings	Proportion of pings	Moderate
Transducer ringdown	S_v @ 0.8 or 1 m	Variable
Transducer impedance	Ohm	Variable
Surface bubble layer	S_v	Moderate
Platform		
Pitch	Angle (°)	Moderate
	Rate of change (deg s^{-1})	Moderate
Roll	Angle (°)	Moderate
	Rate of change (deg s^{-1})	Moderate
Heading	Angle (°)	High/moderate
Meteorology		
Windspeed	Velocity (m s^{-1} or knots)	Moderate
Relative wind heading	Angle (°)	Moderate

Measures of transducer impedance are beginning to be standard output from echosounder manufacturers, but there is much work to be done to understand relationships between impedance measures and data quality. In preliminary analyses of Saildrone data, increased variation in transducer impedance corresponded to an increased number of attenuated pings (Section 4.3), suggesting a possible use for transducer impedance as a metric of data quality.

Comparisons of data collected from surface-platform-mounted transducers and data collected from towed vehicles, nets, or modified hull mounting (e.g. retractable keel), provided insights into how data collected from different platforms are affected by inclement weather as well as potential ways to diagnose and maybe correct degraded data. Mounting transducers to platforms that are isolated from bubbles and surface conditions (sea state and winds) can dramatically improve data quality (Section 4.4), but at the cost of requiring additional resources to deploy (hardware/gear, instrumentation, software, and personnel). These comparisons also strongly suggest that data quality is degraded even before signs of degradation become visible or prominent in the data (e.g. attenuated pings, or reduced seabed backscatter).

6.2 Acoustic data with ancillary information

Monitoring data quality using only acoustic data is useful, but it has limitations when relating data quality to other indicators such as inclement weather (e.g. windspeed, sea state, or vessel

motion), and when deriving predictive relationships that can be used at sea or during data processing. The effect of platform motion and windspeed on measured data quality were investigated using seabed backscatter, number of attenuated pings, and the target strength of a calibration sphere (Section 5).

The case studies showed that the different platforms responded differently to meteorological and ocean conditions. The Saildrone is a small (7 m long) autonomous vehicle that, due to its size and sailing preferences (i.e. cannot sail directly into the wind), responds differently to ambient conditions than much larger (> 10 m) research and fishing vessels. When using seabed backscatter as an indicator for data quality, it was observed that the quality of data obtained on the Saildrone and RV Dana decreased when windspeeds rose above about 7–8 m s^{-1} (14–16 knots), whereas the FSV Shimada data quality was consistent up to about 14 m s^{-1} (28 knots; Section 5.1.1).

Platform motion also affected data quality. Measurements of pitch, roll, and heading relative to sea and swell direction were identified as the best indicators of data quality, although the effects observed were inconsistent. For the RV Tangaroa, the rate of change in pitch correlated with data quality measured using attenuated ping attenuation rate, but roll did not. In contrast, for data from the RV Amaltal Explorer and the Saildrone, roll was linked to changes in data quality as measured by ping attenuation rate (Section 5.3) and changes in seabed s_a, respectively. Saildrone heading relative to the direction of seas (i.e. tacking into or sailing with following seas) also affected the attenuated-ping dropout rate, with the rate of increase of attenuated pings (i.e. the slope of the regression) being greater when the Saildrone tacked into the wind than when it sailed with the seas (Section 5.2).

Despite differences in size, shape, and draft, the Saildrone and the RV Dana interestingly shared a transition point from minimal attenuated pings to an increase in attenuated pings (i.e. the inflection point of the regression curve) at a windspeed of about 10 m s^{-1} (~20 knots; Section 5.1). For the Saildrone, relative heading did not appear to modulate the inflection point, with the transition from minimal attenuated pings to an increase in attenuated pings remaining constant at about 10 m s^{-1} (19 knots), but it did affect the slope of the attenuated ping rate. Heading with the wind (i.e. following seas) had a reduced slope up to wind speeds of 15 m s^{-1} (~30 knots) compared to that at a slower wind speed (~12 m s^{-1}; ~24 knots) when tacking into the wind.

Comparing results from the GAMs for seabed s_a vs. windspeed, and seabed s_a vs. attenuated pings, indicates that data quality may be compromised at windspeeds above 10 m s^{-1} (19 knots). Seabed s_a dropped by 71.1% at 12.5 m s^{-1} (24 knots) windspeed, compared to seabed s_a at very low windspeeds (0–5 m s^{-1}; 0–10 knots). For comparison, a 2.7% attenuated ping rate is predicted at this windspeed (Section 5.1.1). The ability to visualize trends in plots of attenuated pings compared to measurements from seabed s_a also highlights the utility of the attenuated ping as a data quality metric, despite the increased lag when calculating attenuated pings compared to instantaneous measures of seabed s_a.

Meteorological data, such as windspeed and wind direction, can be used to understand and quantify signal degradation. However, the specific effects will likely vary between different platforms. For instance, while signal degradation in acoustic data from the Saildrone occurred at windspeeds above 9–10 m s^{-1} (17–19 knots; exacerbated by wind on the beam), data from a larger vessel, such as the FSV Shimada, might not undergo signal degradation until higher windspeeds. Therefore, the use of a threshold for any particular metric should be vetted for the platform of interest.

A comparison of backscatter from the seabed and a calibration sphere conducted during a calibration exercise throughout which windspeed increased, suggest that both variables are reasonable indicators of data quality (Section 5.1.3). Changes in backscatter intensity were observed for sphere TS and seabed S_v between calm conditions with no surface bubbles, and periods with strong wind and surface bubbles. The effects were frequency-dependent. Backscatter effects were ≤ −0.6 dB (linear factor of < 13%) for both the seabed and sphere. Seabed backscatter was affected most at 38 kHz and least at 200 kHz, while the calibration sphere TS values were affected most by surface bubbles at 18 kHz and least at 200 kHz. These effects are close to the acceptance criteria for calibration results of ± 0.5 dB, so attention to reductions in data quality due to weather conditions is critical during calibration exercises.

The variability of the case study results presented above highlights the fact that despite applying consistent methods to analyse echosounder data quality, it is difficult to recommend one particular criterion and absolute threshold value across all platforms. Acoustic data quality can be evaluated using many variables to determine how the transducer and platform are affected by inclement weather. Therefore, we recommend collecting as much platform motion and meteorological data as possible, and to use seabed echo intensity, calibration sphere TS, and/or rate of attenuated ping dropouts to determine data quality. While this is a large list of variables to consider, platform-motion analysis may also help rule out causes of data degradation. Such an analysis was conducted for the calibration case study on the FSV Bigelow, and demonstrated that surface bubbles were the most likely culprit impacting backscatter measurement quality. Ideally, platform motion will be recorded at a sufficiently high rate to allow full characterization of the platforms movement (i.e. above Nyquist sampling rate, see Section 7.5). When platform-motion measurements are not available (e.g. small vessels, or some UxVs), meteorological data may serve as a proxy for vessel motion. However, it can be expected that relationships between meteorological variables and motion parameters will be platform-dependent and probably not linear.

6.3 Error due to inclement weather relative to the total error budget

There are a series of steps when converting acoustic energy to abundance/biomass of the resource being surveyed. Errors in measurements, equation and regression parameters, and methodologies can accumulate throughout the estimation process, so it is important to understand the sources and inputs of error relative to the cumulative estimation error (i.e. the error budget). The components of the abundance/biomass error budget for a fisheries survey using echosounders (i.e. echo integration survey) can be separated into two broad categories: (i) random, which affects the precision (i.e. data variability), and (ii) systematic, which affects the mean (i.e. data bias; Tesler, 1989; MacLennan and Simmonds, 1992; Demer, 2004). Demer (2004; cf. Table 2) provides a convenient comparison of the Tesler (1989) and MacLennan and Simmonds (1992) component estimates. Among the common sources of error, such as those due to instrument (e.g. calibration, TVG, attenuation coefficient, and equivalent beam angle), environment (e.g. temperature and salinity), sampling (e.g. random or systematic design), and target specie(s) (e.g. target strength, behaviour, and identification/classification), two sources that result from inclement weather are transducer motion and bubble attenuation. MacLennan and Simmonds (1992) attribute 0 to 30% (< 1 dB) of error due to transducer motion and 0 to 90% (< 3 dB) due to bubble attenuation. These errors are larger than those related to instrument and environmental conditions, but are comparable to errors associated with the target species. With respect to transducer motion, it has been shown that for deep-water species, error induced by

ansducer motion can be several decibels (i.e. > 1 dB), but for surveys conducted on continental shelves, the error is usually < 1 dB (Section 2.3.2).

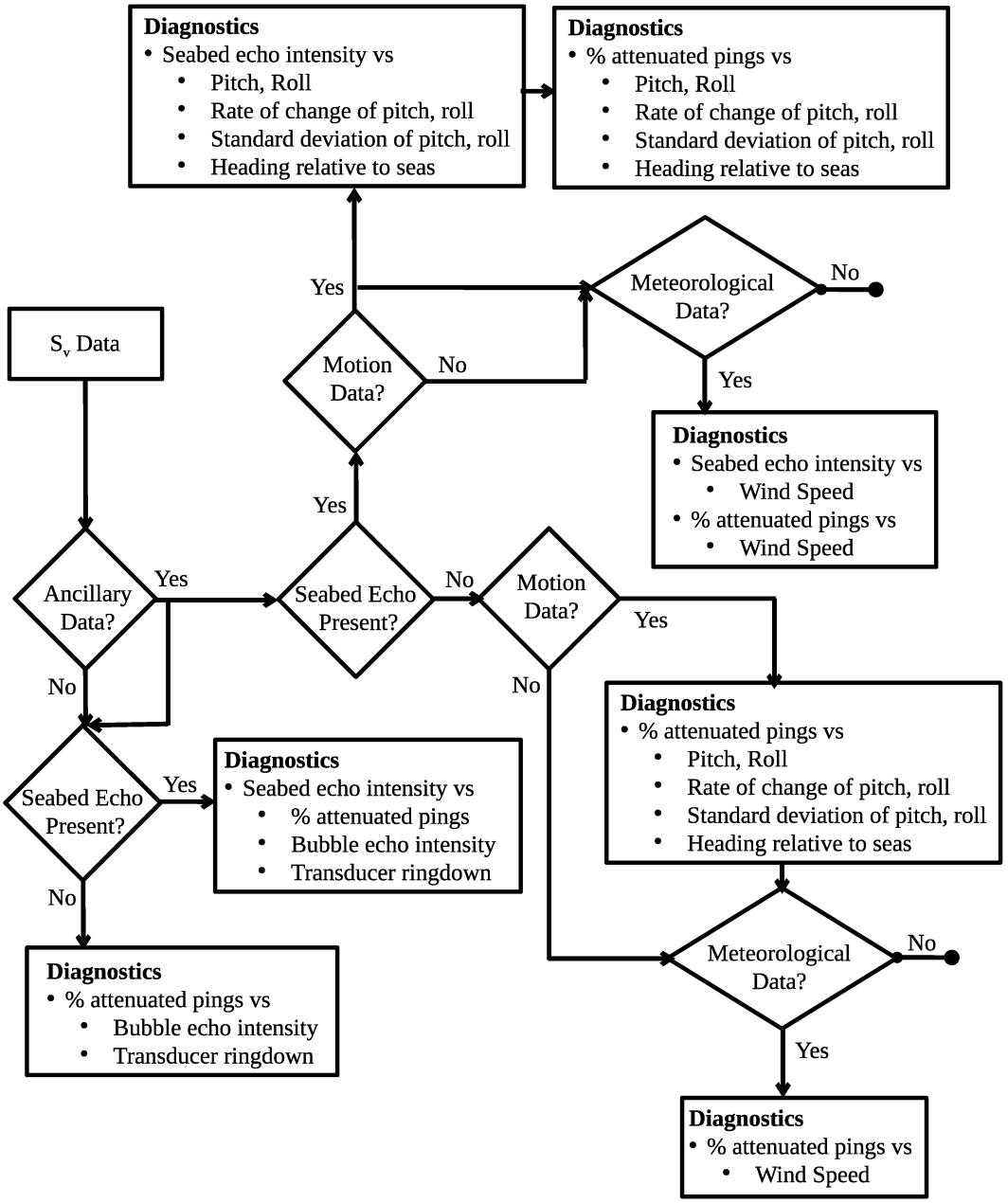

Figure 6.1. Schematic flowchart for diagnosing data quality effects of inclement weather. The input is S_v data, and the diagnostics are based on the analyses presented in this report.

While attenuation of the received echo energy can easily be up to 90% of the acoustic energy, this often results in the removal of the ping data, as the S_v value will be below the data processing threshold. There are a number of factors that can minimize the effects of lost or reduced amounts of data. Levine and De Robertis (2019) suggest that under certain conditions, a reduction in the number of pings (up to 95%) does not result in a commensurate loss of information. Depending on the survey design (i.e. transect layout relative to the spatial distribution of the target species), diversity and composition of the scattering community, and

the desired degree of precision, acceptable abundance/biomass estimates can be generated using a portion of the dataset (with what constitutes acceptable being defined by the analyst; Levine and De Robertis, 2019). However, in the case of inclement weather, attenuated pings are often the manifestation of degraded data (see Section 4.4), with transducer motion, excess attenuation, and other noise contributing to a decrease in S_v data quality. In this latter case, it is not possible to simply remove pings in an effort to increase processing efficiency, because the remaining data are most likely compromised.

The overall goal of this report is not to estimate an error budget for an abundance or biomass estimate, but to measure or derive metrics of data degradation. Metric uncertainty is used to determine if the backscatter measurement quality is compromised. Once metric thresholds are determined, then a strategy needs to be developed to facilitate decisions on whether to accept data as collected and processed, "correct" backscatter values (e.g. Dunford correction; Dunford, 2005), or exclude pings used in analyses (see Section 8.4).

6.4 Workflow

A generalized workflow provides a guide to evaluate the effects of inclement weather on acoustic data quality (Figure 6.1). The diagnostics in the figure are based on analyses and results presented in this report, and are not intended as an exhaustive list. Starting with S_v or s_a data, the first decision is whether ancillary data (platform motion and/or meteorological data) are available. If they are not, then the diagnostics are limited to features of the acoustic data (lower left portion of the schematic). If ancillary data are available, then both sets of diagnostics (with or without ancillary data) can be used in data quality evaluations. In most cases, the maximum range of data recording will include the seabed. However, when surveying pelagic species, or when in the open ocean, the seabed echo may not be present, and the diagnostics will be limited to using attenuated pings as the indicator of data quality.

7 Data processing to reduce the effects of signal degradation

Section 2 describes common sources of noise and signal attenuation and gives practical guidelines on how these might be reduced (Section 2.4). In the case of fisheries acoustics, prevention is better than the cure. However, despite best efforts, datasets with compromised quality are an all-too-common reality, and will bias results if not addressed. To reiterate, noise will positively bias data, and attenuation will negatively bias data. Post-processing (also referred to as data cleaning or filtering) is a bias-reducing exercise where backscatter that has a significant noise component, or that is attenuated, is identified and removed from the dataset. Figure 7.1 shows a conceptual drawing of error as a function of data quality. The larger triangle (white background) shows how the bias in raw data can be either positive (noise) or negative (signal attenuation) and can quickly increase in magnitude as data quality degrades. The coloured insets show how data cleaning will reduce bias and increase the utility of the data over a range of signal qualities. The three colours (green, orange, and red) indicate the notional utility of the cleaned data. Biomass estimates would typically require the lowest degree of bias (green), while other studies may tolerate a higher degree of bias in the signal (yellow or red). For example, metrics of deep scattering layers (depth, migration rise/lower time) or location of frontal systems observed in the echograms, might tolerate a higher degree of bias without the results being affected. An important point is that residual bias will likely remain in cleaned data due to persistent false positive and negative S_v values in the various filtering processes, and that this residual bias will increase with signal degradation. No matter how effective the cleaning process is, cleaned low quality data will have a larger degree of bias than high quality data that required no cleaning.

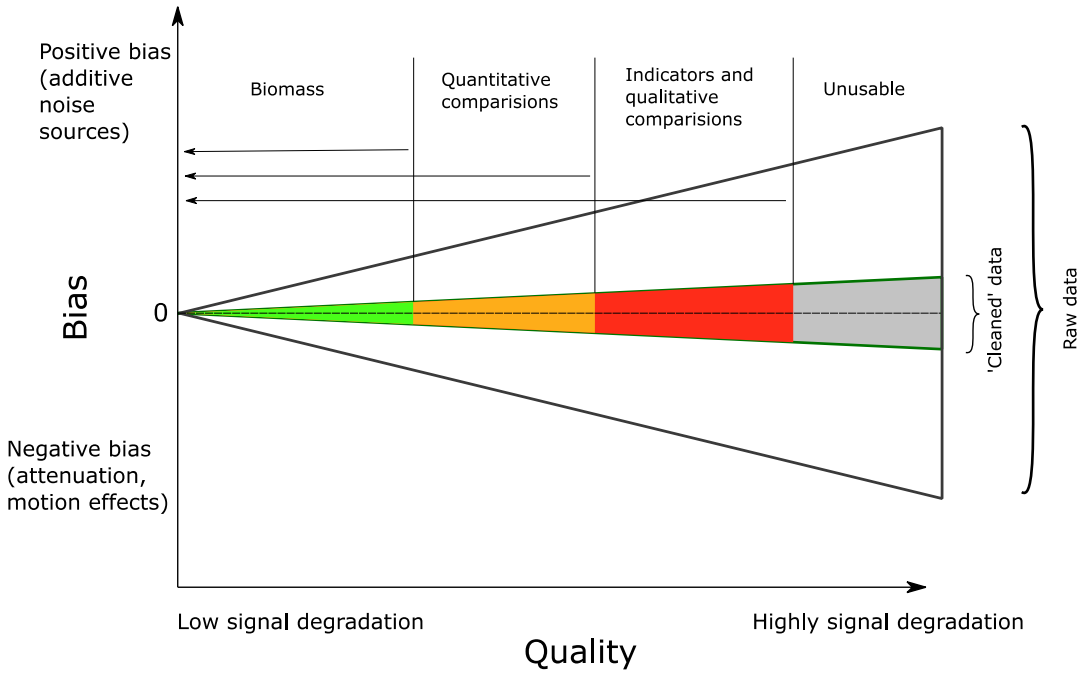

Figure 7.1. Conceptual drawing of error and bias for processed and unprocessed acoustic data.

This chapter summarizes the most commonly employed data-cleaning algorithms in fisheries acoustics. Data cleaning is carried out as part of a workflow, where a series of processing steps are applied to produce quality-controlled data products from raw acoustic data (Figure 7.2). In the case of weather-related signal degradation, various types of noise and attenuation are present, often increasing in number and magnitude as the weather degrades. Therefore, it is common to apply a suite of data-cleaning algorithms, each of which is designed to address a specific class of noise or attenuation. Algorithms may be applied sequentially, in such a way that a particular type of degradation is addressed, and the resulting echogram passed through to the next algorithm (Ryan *et al.*, 2015). Commonly used data-cleaning algorithms for various forms of signal degradation are outlined in Table 7.1.

Table 7.1. Summary of the commonly used data-cleaning algorithms for various forms of signal degradation.

Degradation type	Cause	Algorithms	Requirements
Background noise	Weather-related and/or non-weather related effects, for example electrical noise interference	Kornelliussen (2000) De Robertis and Higginbottom (2007) Peña (2016)	Noise must dominate the signal Below seabed data
Impulse noise	Interference from other instruments and electrical noise	Anderson *et al.* (2005) Ryan *et al.* (2015) Wang *et al.* (2016)	
Transient noise	High-energy wave interactions with the vessel	Ryan *et al.* (2015)	
Signal attenuation due to bubbles	Bad weather, bubbles	Ryan *et al.* (2015) Echoview[1] ESP3 (Ladroit *et al.*, 2020)	Continuous reference layer (e.g. deep scattering layer or seabed)
Signal attenuation due to transducer motion	Bad weather, vessel design	Stanton (1982) Dunford (2005)	Motion data
Speckle noise	Stochasticity	Kovesi (1999) Peña (2016)	
Transducer ringdown	Transducer still vibrating while already listening	ESP3 (Ladroit *et al.*, 2020)	
Seabed aliases	Bottom signal from previous ping	Renfree and Demer (2016) Blackwell *et al.* (2019)	Bathymetry data Phase angle data

[1] **https://echoview.com/**

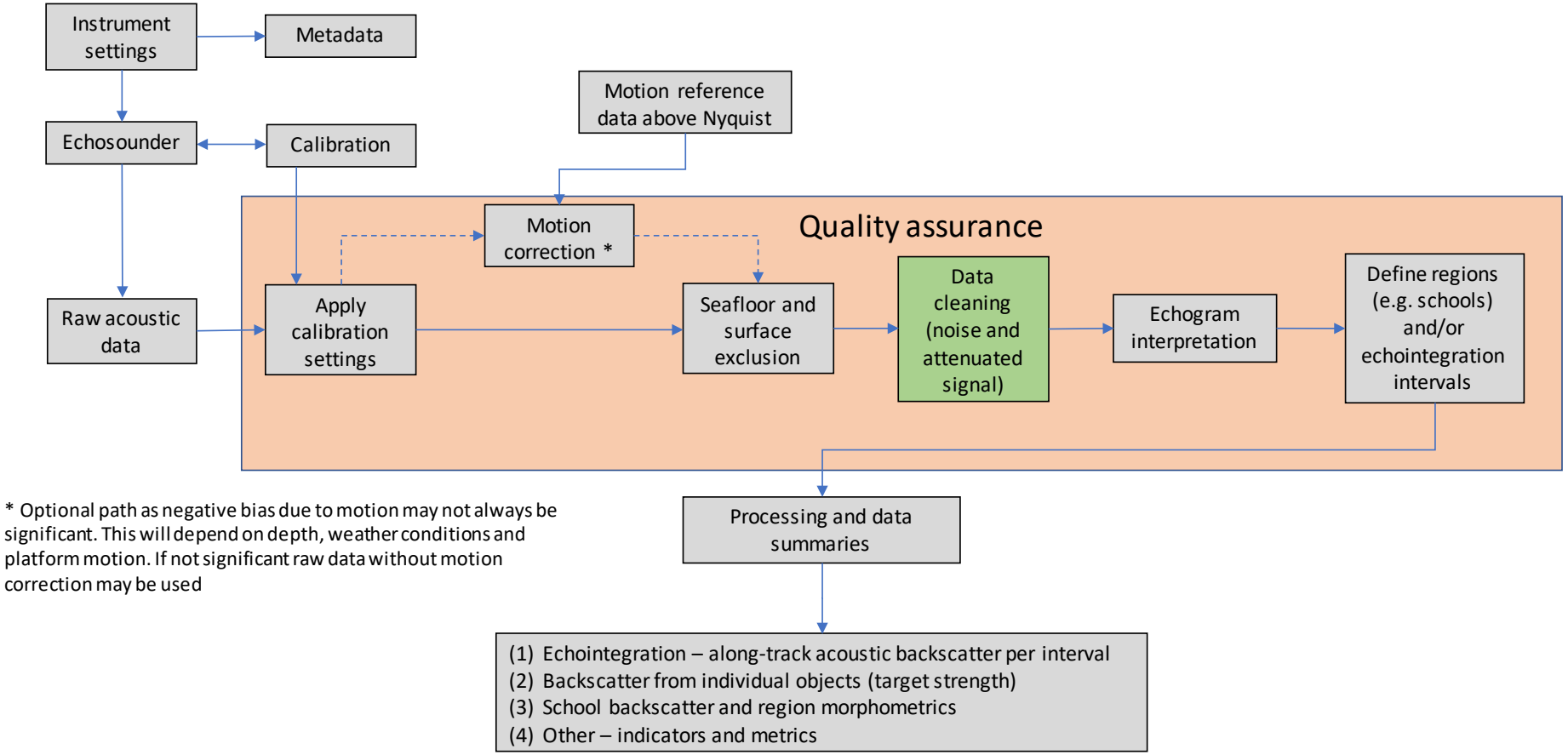

Figure 7.2. Flowchart showing a typical workflow from data acquisition through to production of quality assured outputs.

7.1 Background noise

Algorithms to remove background noise are widely employed as they can visually improve echograms. Further, by quantifying and then removing the contribution of background noise to the total signal, the effective range of an echogram can be extended. The background noise level can be affected by the performance and the settings of the instrument taking the measurements. The susceptibility to noise of the instrument used is determined by the amount of power transmitted, the gain of the transducer, and the pulse frequency and duration (and consequently the bandwidth, which increases with decreasing pulse duration). Radiated electrical or mechanical noise from the vessel and wind- and sea-generated noise are also key factors (Spence and Fischer, 2017). The most direct way to quantify background noise is to record data in passive mode (Nunnallee, 1990). Passive mode is a setting where the echosounder does not transmit an acoustic pulse and the electronics are set to only receive signal. Although passive recordings can be a useful diagnostic, continuous characterization is needed to account for variation in noise levels while operating the echosounder in active mode. Active mode is a setting where the echosounder transmits an acoustic pulse and the electronics are set to synchronize listening with the transmitted pulse. Therefore, methods to estimate the background noise level when data are collected in active mode have been developed.

Watkins and Brierley (1996) estimated background noise from the minimum volume backscattering coefficient S_v for each depth (it should be noted that no evaluation was conducted on how representative results were for the entire dataset). De Robertis and Higginbottom (2007) developed this idea further, estimating background noise for the Simrad EK60 power echogram smoothed in bins of N pings by M samples (the digitized data without any gains applied). The noise was calculated as the minimum value of those homogenized bins. Noise estimates using this algorithm from the data collected in active mode were close to the noise levels measured in passive data. A key assumption of the De Robertis and Higginbottom (2007) algorithm is that the echogram must have samples where noise dominates the signal. This can be ensured by setting a suitably high acquisition range, which permits that at the furthest ranges noise is dominant. This requirement may mean compromising on a faster ping repetition rate to achieve the necessary range. In some situations, noise can dominate signal at lesser ranges if the sampling volume is devoid of sources of backscatter. In those situations, a lower acquisition range could be used to allow a faster ping rate.

The algorithm proposed in Peña (2016) is an extension of the De Robertis and Higginbottom (2007) algorithm. It also homogenizes echotraces (removes speckle noise, see Section 7.6) while retaining the edges of scattering features, by applying a local smoothing kernel with an intensity that is inverse to its variance. By removing speckle noise and applying a threshold to the echogram based on signal-to-noise ratio (SNR), the TVG-amplified background noise is also removed. These algorithms can be applied to any multibeam or single-beam data. An example is shown in Figure 7.3.

7.2 Impulse noise

Impulse noise is a short duration artefact that typically occurs when two acoustic instruments of similar frequency operate without synchronization. It appears in echograms as high intensity vertical, horizontal, or diagonal lines that cover several samples and have duration of less than one ping. Vertical lines can be removed by employing a two-dimensional median filter of 3 x 3, 5 x 5, or other sizes samples by pings (e.g. Klevjer *et al.*, 2012; Figure 7.4). Anderson *et al.* (2005) developed an algorithm where a group of S_v samples in each ping are compared with the

corresponding samples in the previous and following pings. They consider ping-to-ping differences greater than 10 dB as impulse noise. Ryan *et al.* (2015) compared an S_v sample with the median S_v values of a selected number of samples around it. Both these algorithms require an empirically derived S_v threshold to separate interference from signal, and thus require some expertise to set appropriate threshold values. They also assume a low percentage of interference samples. A more refined algorithm was developed by Wang *et al*. (2016) for very poor-quality data. The algorithm includes a series of steps: (a) remove weak and strong interference with a lower and upper threshold, (b) apply an erosion filter to remove interference within those thresholds, (c) apply a dilation algorithm to refill the holes created within layers or aggregations, and (d) correct S_v variations using the original values or the mean values of surrounding samples.

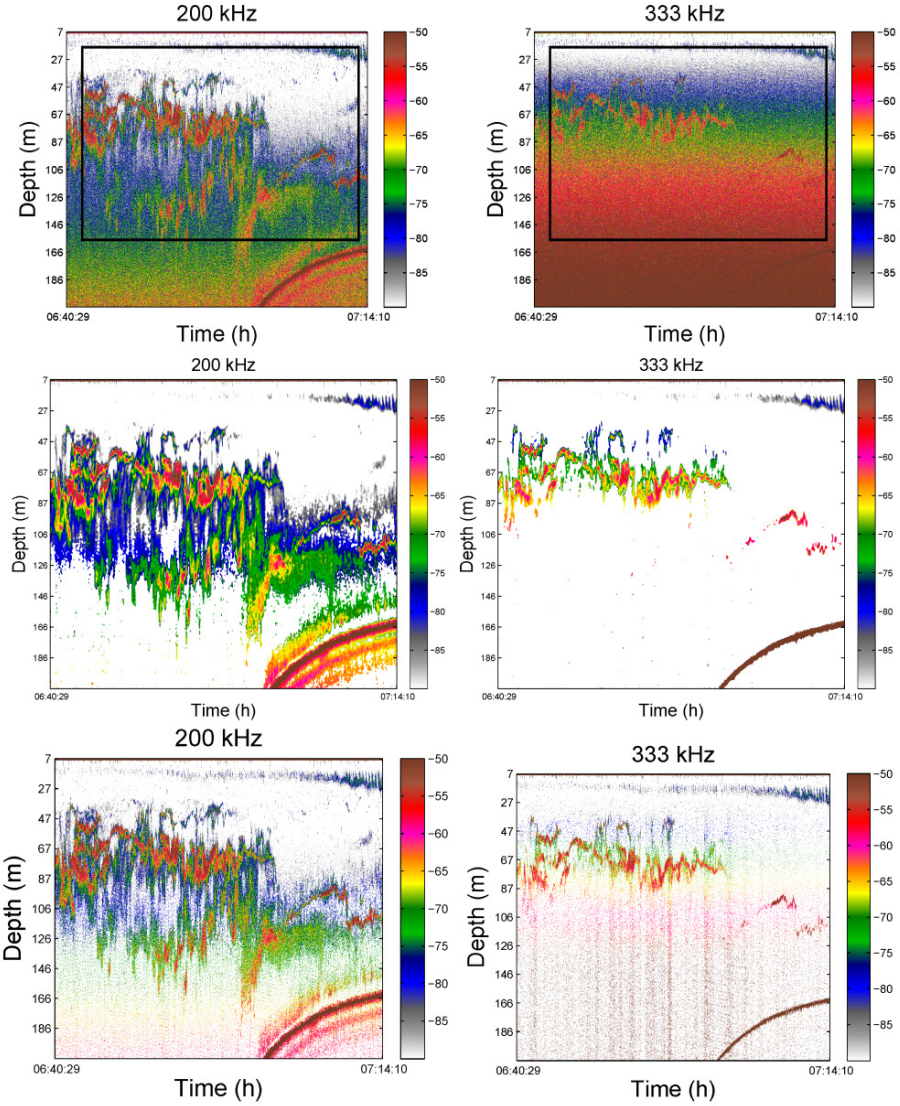

Figure 7.3. Denoising of 200-kHz (left panels) and 333-kHz (right panels) echograms (upper panels), the Adaptive Wiener Filter (AWF) denoising algorithm-processed echograms (middle panels), and the De Robertis and Higginbottom (2007) algorithm-processed echogram (lower panels). The colour bar (S_v range of −90 to −50 dB) and depth scale apply to all echograms. The black boxes in the original echograms were used to calculate noise estimates in Peña (2016). Reproduced with permission from Peña (2016).

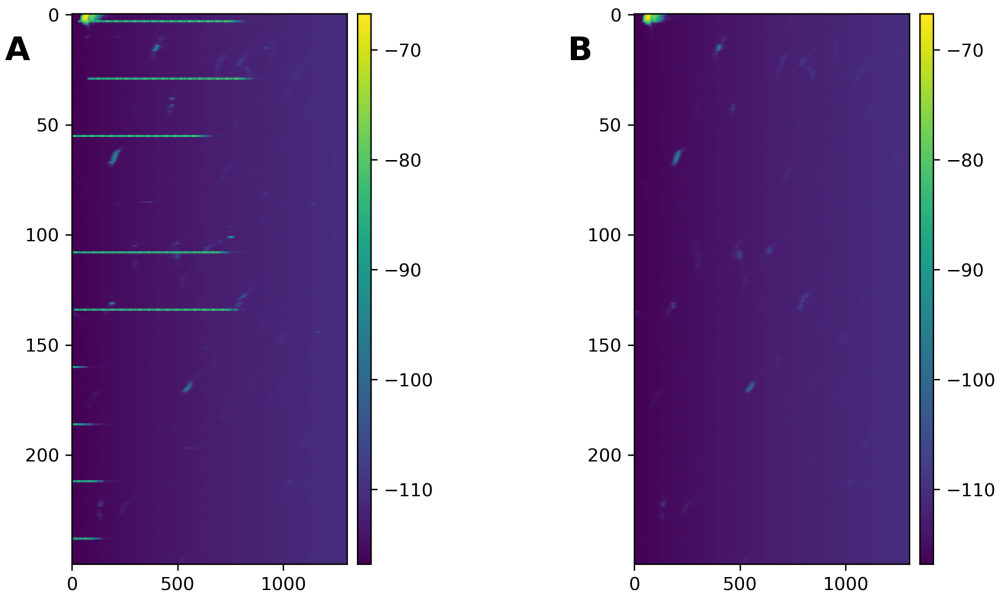

Figure 7.4. Example of echogram with impulse noise in the form of horizontal lines (A) and the same echogram after processing with a median filter with a 3 x 3 kernel.

7.3 Transient noise

Transient noise (Section 2.2.3) can be a source of significant bias, particularly at longer ranges, due to TVG gain being applied (Figure 7.5).

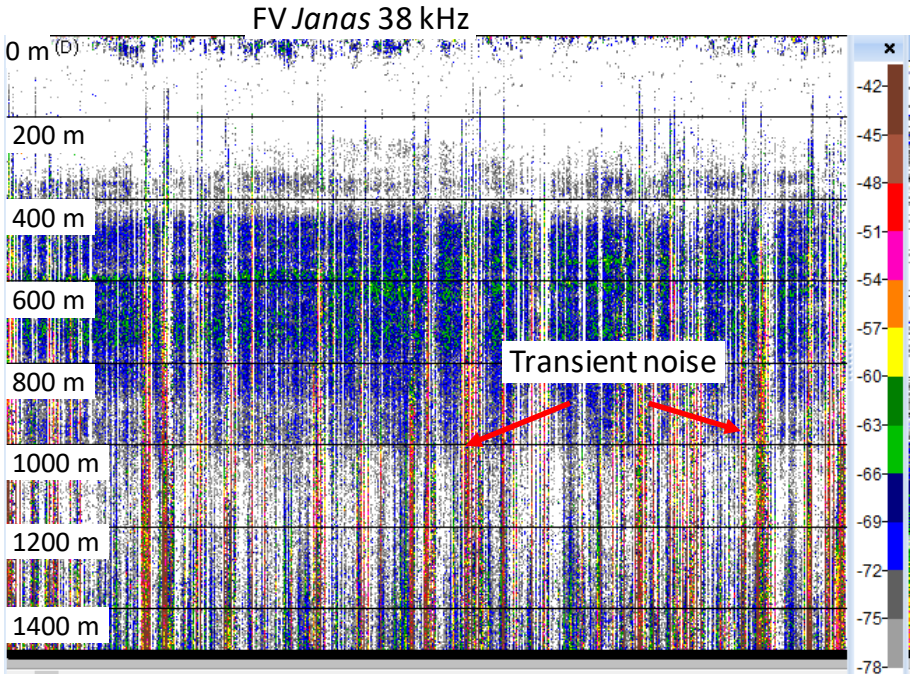

Figure 7.5. Example of a 38-kHz echogram from the FV Janas affected significantly by transient noise.

Unlike impulse noise, which has a characteristically short duration, transient noise persists for multiple pings as a noise source that exists over and above the general background noise. The number of pings that are affected by transient noise is usually greater than pulses of impulse

noise, which can make it particularly challenging to characterize and remove. The algorithm described by Ryan *et al.* (2015) compares each sample with the median value in a surrounding regions of *M* pings by *N* meters. A deviation from a user-defined threshold above this localized median is assumed to be noise. Typically, transient noise only becomes significant at greater depths (> 250 m) due to amplification by the TVG function. At shallow depths, transient-noise algorithms can misidentify fish schools or shoals as noise. To mitigate this effect, approaches include applying the transient noise algorithm to depths below the shallow schools, and masking the schools prior to applying the transient noise algorithms.

7.4 Signal attenuation due to entrained air bubbles

Ryan *et al.* (2015) classify pings as attenuated by comparing samples within a stable reference layer, such as a deep scattering layer, with the median of the surrounding block of S_v values from the same reference layer (e.g. Figure 7.6). The premise is that if the reference layer has an expected degree of homogeneity, pings are likely to be attenuated if they deviate from the surrounding region by being lower than a user-defined threshold. The width (number of pings) of the median window can be defined by the user, guided by an inspection of the echogram to assess how long the attenuated signal exists. The S_v values in attenuated pings can be set to zero or classified as missing data. Setting S_v values to 0 in the linear domain (i.e. −999 dB) will have a different influence on the statistical treatment of the data vs. removing those data from the analysis (i.e. no data/empty water vs. missing data). One approach has been to classify S_v values that have been determined to be attenuated as missing data, so that they are excluded from analysis while retaining the sample count. This practice allows the percentage of rejected data to be calculated as a metric, which can be a useful guide to data quality and provide a threshold for acceptance of data.

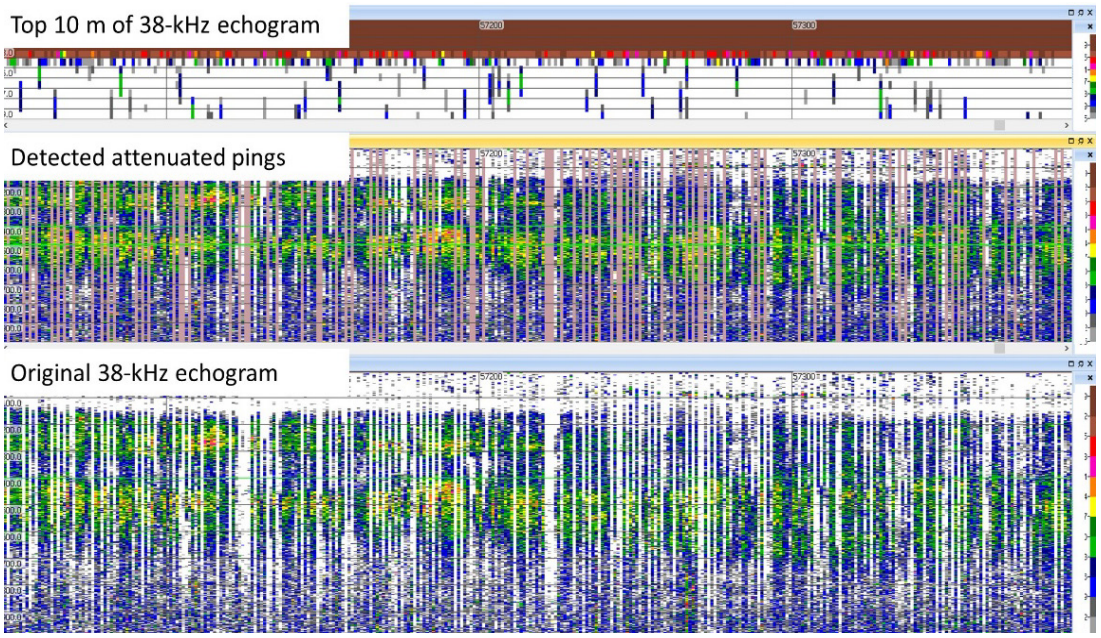

Figure 7.6. Example 38-kHz echogram with extreme signal attenuation (dropouts) but where no bubble layer is apparent (data from the Antarctic resupply icebreaker MV L'Astrolabe). The top panel shows the first 10 m of the echogram, with no obvious bubble layer backscatter. The middle panel is the echogram with vertical red lines denoting ping dropouts. The lower panel shows the 38-kHz original echogram. The colour scale represents S_v from −49 to −85 dB.

7.4.1 Variation in the identification of attenuated pings

In sections 4 and 5, the number of attenuated pings is used as the response variable in many of the analyses. Given that signal attenuation is a continuous, rather than a binary, variable, this requires that a threshold level of attenuation be determined, beyond which a ping is unacceptably attenuated and should be removed from analysis. Variation in the threshold, and the exact way this is quantified, will lead to variation in which pings are identified as attenuated, and, hence, is a potential source of error in these analyses.

To investigate this variation, we identified a 1000-ping subset of echosounder data collected in bad weather (Figure 7.7) and asked 11 experts to determine subjectively (i.e. without recourse to a computer algorithm) how many of those pings were unacceptably attenuated and should be removed from analysis. No further instructions or suggestions were provided, leaving how they wished to explore the data up to the individual. Everyone reported visualizing either the S_v or TS echogram and nothing else (e.g. split-aperture angles, vessel pitch and roll, etc., which were also available in the datafile). There was considerable range in the results (min = 84, max = 208, median = 139, mean = 140, CV = 30%), with the comments received indicating two potential reasons: (1) differences in the chosen colour scheme and display range of the echogram, and (2) differences in the level of attenuation that was considered acceptable.

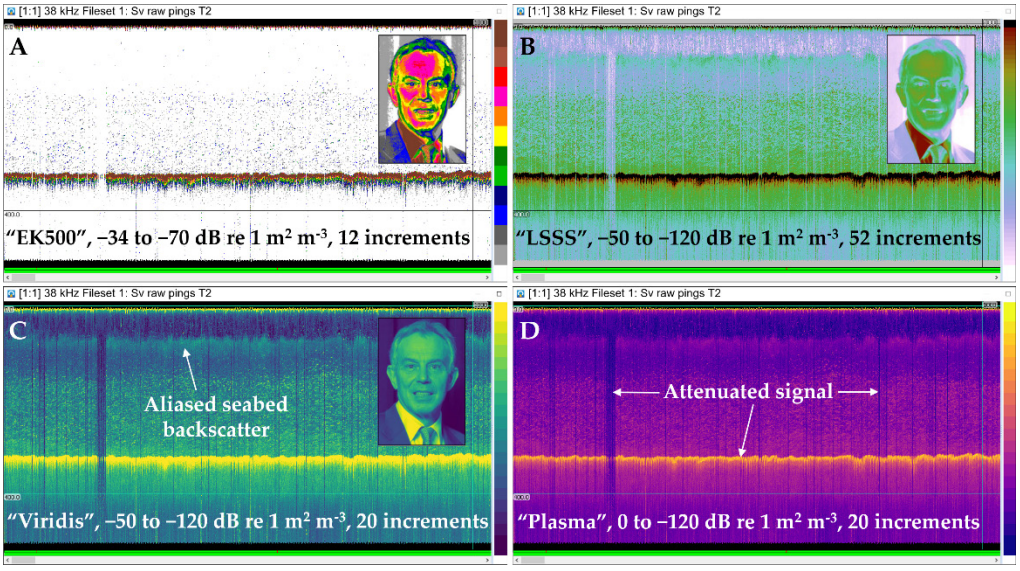

Figure 7.7. The first 1000 pings of the Simrad EK60 38-kHz calibrated S_v shown in Figure 4.14 panel A, visualized with different colour schemes and display ranges. Insets show the colour scheme mapped to a human face to illustrate the visual effectiveness of each. (A) The default colour scheme (EK500) and narrow display range for EK60 data in Echoview software; (B) the default colour scheme (LSSS) for EK60 data in LSSS software; (C) the Viridis colour scheme shown here with an intermediate display range; and (D) the Plasma colour scheme with a wide display range. The image of Tony Blair, adapted for our figures from Blackwell *et al.* (2020), is courtesy of the World Affairs Council and is licensed under the terms of the Creative Commons Attribution 2.0 Generic license. Data provided by IMR/DEFF.

Blackwell *et al*. (2020) showed how the colourfulness, perceptual uniformity, and luminance sequence of a colour scheme can affect the visual interpretation of an echogram. Of the four colour schemes shown in Figure 7.7, the "EK500" scheme (panel A) is highly colourful, but neither perceptually uniform nor sequential. Along with the narrow default S_v display range, it masks much of the important information in the data, including much of the water column backscatter, an aliased seabed echo, and weakly attenuated pings. The other three colour schemes are better designed, in that they are colourful, perceptually uniform, and sequential

[especially "Viridis" (panel C) and "Plasma" (panel D)]. Intermediate S_v display ranges (panels B and C) can highlight variance in the backscatter of different components of the echogram. In this case, a range of −50 to −120 dB works well for visualizing the water column backscatter, but misses much of the variance in the seabed echo. A wider display range of 0 to −120 dB (panel D) reveals a fuller picture, but starts to miss the variance within the different quantiles of the S_v distribution. A colour scheme that maps within the different quantiles, rather than uniformly across the entire distribution, might assist with this problem (Peña, 2021).

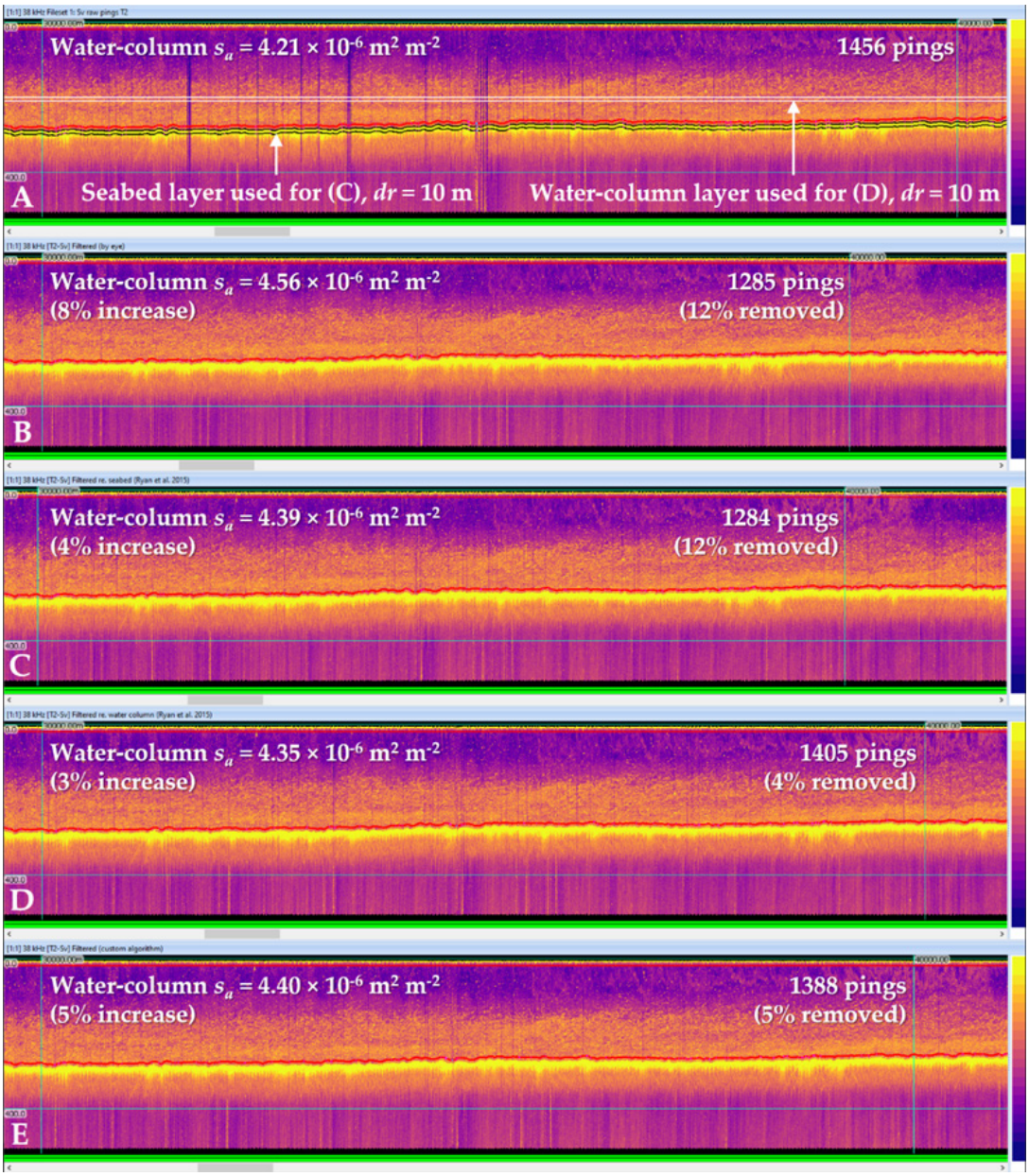

Figure 7.8. Results of four different algorithms for identifying and removing attenuated pings. The echograms represent S_v (colour scale −50 to −120 dB). (A) The raw data. (B) Data after subjective removal by eye. (C) The Ryan *et al.* (2015) algorithm with Echoview default settings applied (n = 31 pings, δ = 10 dB) based on the seabed-scattering layer indicated in panel A. (D) The Ryan *et al.* (2015) algorithm with Echoview default settings applied (n = 31 pings, δ = 10 dB) based on the water column-scattering layer indicated in panel A. (E) A custom algorithm, conceptually similar to Ryan *et al.* (2015), but applied to the entire ping range so that a consistent scattering layer does not need to be identified.

It is clear from this exercise that subjective identification of attenuated pings can lead to very different results unless a consistent method can be established. An objective computer algorithm (e.g. Ryan *et al.*, 2015) would, therefore, seem like a preferable alternative. However, while concise and repeatable, such algorithms will likely contain biases in their design and are notoriously difficult to parameterize for any given situation. In lieu of a comprehensive sensitivity analysis, in which parameter interactions can be quantified (e.g. McKay *et al.*, 1979; Rose, 1983; Burgos and Horne, 2007), a basic investigation using Echoview software highlighted the variation between four different approaches for identifying attenuated pings (Figure 7.8). The difference in water column s_a between the subjective (panel B) and objective algorithms (panels C–E) could have been decreased by reducing the objective-algorithm thresholds (δ). Despite the different number of pings removed between panel C and panels D–E, there was little difference in the estimated water column s_a. Encouragingly, this may suggest that the overall result is relatively insensitive to the parameters as long as the algorithm is appropriately designed, and the parameters are roughly constrained to suit the data. Ultimately, this kind of detection problem may be better addressed with machine-learning techniques (e.g. Malde *et al.*, 2020).

7.5 Signal attenuation due to transducer motion

As outlined in Section 2.3.2, signal attenuation due to transducer motion increases as a function of range, and with the rate and magnitude of transducer motion. Correcting for signal loss due to transducer motion is done during post-processing, using motion data collected by the platform. The Dunford (2005) correction algorithm is often used for this purpose, and requires inputs of the original S_v echogram plus pitch and roll motion data. To apply the correction, the motion data must be time-synchronized to the S_v data. This condition occurs if motion data are recorded on the same computer as the acoustic data, and the computer time is used for both datasets. However, if recorded on separate computers, time-synchronization between the motion and echogram data must be confirmed. Further, the motion data should be sampled at a rate that can fully characterize the platform movement, to avoid temporal aliasing due to an inadequate sampling rate. Nyquist–Shannon sampling theory says a waveform (in this case, pitch and roll) can be reconstructed by sampling at a rate of twice the highest frequency component of the waveform to avoid temporal aliasing. If these criteria are met, then application of the Dunford (2005) correction factor will provide a first-order correction to the S_v data due to the effects of motion for circular transducers. Some residual errors may exist if 3-dB beam widths differ from the manufacturer's specified value (Reynisson, 1998; Jech *et al.*, 2005; Haris *et al.*, 2018; Renfree *et al.*, 2019), and it should also be noted that 3-dB beam widths should be adjusted for local sound speed at the transducer face (Bodholt, 2002). The Echoview implementation of the Dunford correction allows the user to define the separation factor (i.e. signal loss due to the difference between transmit and receive), where a maximum signal loss of 3 dB (factor of 2) is allowed. Allowing correction beyond this threshold becomes increasingly inaccurate, as the correction becomes greater than the well-characterized main beam of the transducer. In this way, the Echoview algorithm serves a dual purpose, by providing a correction to S_v values to account for signal loss due to motion effects, as well as flagging data as bad when motion compensation levels exceed the user-defined threshold.

Most motion sensors sample pitch and roll at rates higher than the acoustic transmission interval (i.e. ping rate). However, these data are often recorded at lower sampling rates by the platform's data acquisition system or by the echosounder acquisition software. For example, it is common for the echosounder acquisition software to record motion values at the time of

transmission. In that case, the motion sampling rate will be determined by the ping rate, which, in many cases, will be below the Nyquist rate of platform motion. More recently, the Simrad EK80 acquisition software allows recording of motion data at its full rate, or at a user-defined decimation rate, in addition to recording motion data at the time of transmission. For example, motion reference units used for multibeam surveys can output data at 100 Hz, which usually far exceeds the Nyquist rate of motion for most platforms, and users may choose to embed motion telegrams in the acoustic data at a decimated sample rate.

What is the sampling rate needed to correct data for transducer motion for a particular platform? The answer will depend on the design of the platform and its behaviour in a range of sea states (e.g. Lloyd, 1998; Lloyd *et al.*, 2011; Tello *et al.*, 2011). Smaller, more lively platforms (e.g. ASV) will have a faster motion, and, therefore, require a higher motion sampling rate than larger platforms (e.g. RV). An important task when collecting survey data is to characterize transducer motion through a range of sea-state conditions, including rough weather, to determine a suitable sampling rate for motion data that would give acceptable corrections during routine operations. The Welch's Power Spectral Density (PSD; Welch, 1967) or a Fast Fourier Transform (FFT) can be calculated from the motion data to determine the strength of the variations (energy) as a function of waveform frequency. In other words, PSD or FFT show at which frequencies variations are strong or weak. Figure 7.9 shows an example of PSD, using five days of motion data recorded by the RV Investigator at a sampling rate of 10 Hz in a range of weather conditions. The PSD plot shows most of the energy is below 0.5 Hz, which means that most of the motion occurs at 0.5 Hz or less, and contributions from more rapid movements are less significant. Frequency components above 3 Hz contribute insignificant amounts. This is to be expected, as large vessels have an overarching slow-moving motion with occasional short-duration rapid movements. A sample rate of ~6 Hz (double the highest frequency component) would be sufficient to characterize this vessel's motion throughout a range of conditions.

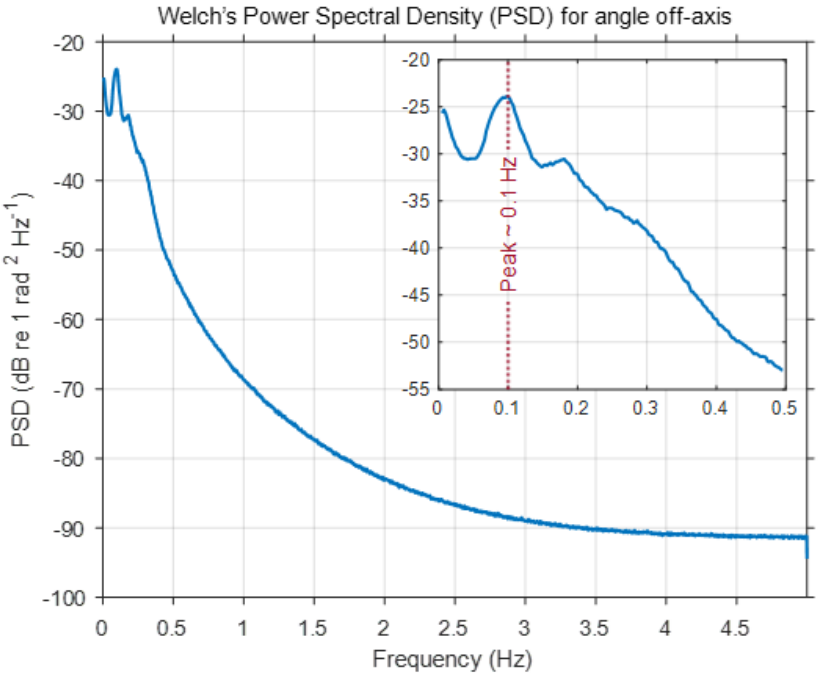

Figure 7.9. Welch's PSD for motion data recorded over a 5-day period by RV Investigator. The inset shows the peak ~ 0.1 Hz.

7.5.1 Motion correction evaluation and diagnostics

Before applying a motion correction, evaluating the magnitude of the potential error is worthwhile to better understand whether a motion correction is warranted. To evaluate the effect of motion, the following parameters must be known, measured, or estimated (Table 7.2): transducer beam width (total angular width as measured at the half-power points), acoustic frequency, speed of sound in water, acquisition range (i.e. maximum depth of data collection), maximum angle of vessel motion (i.e. the maximum angular deviation from zero as measured by the motion sensor, which is one-half the total angular movement), and the time-period of motion. The transducer properties are provided by the manufacturer, and the sound speed and data collection range are set during the survey. The platform motion characteristics (angular motion and periodicity) should be obtained from the vessel motion data. If motion data do not exist, motion characteristics can be estimated while at sea or can be calculated using published relationships between platform size and motion. The motion data can be analysed for the maximum angular motion, and a PSD or FFT can be applied to examine periodicity.

Table 7.2. Data and information needed to evaluate transducer motion effects on S_v data.

Data required	Where the information can be obtained
Transducer beam width	Transducer/echosounder manufacturer or independently measure
Acoustic frequency	Transducer/echosounder manufacturer
Speed of sound	CTD profile; temperature and salinity measurements at the transducer
Data range	Echosounder setup menu
Maximum angle of pitch and roll for the platform	Platform motion data; bubble level on the bridge; predicted values from platform motion characteristics
Periodicity of motion	Platform motion data; human measurements on the platform (e.g. stopwatch); theoretical relationships of platform dimensions to motion

In situations where below-Nyquist motion sample rates have been recorded, it might be possible to apply motion corrections, as long as there is a reasonable understanding of the typical behaviour of the platform. Ideally, to understand at what point lower motion sampling rates become unviable, the vessel should be characterized in a range of weather conditions, with motion data logged at the Nyquist rate or higher. As an example, a simulation was made with motion data from the RV Investigator to demonstrate the effect of below-Nyquist sampling rates on the motion correction algorithm (Figure 7.10). For the RV Investigator, the Nyquist sampling rate is ~ 6 Hz (as suggested by inspection of Figure 7.9). Using the motion correction factor at 10 Hz as the benchmark, the motion correction factor was unchanged down to sampling rates of 1 Hz, but below 1 Hz, the correction factor decreased solely as an artefact of sampling rate (Figure 7.10).

In general, it could be expected that a motion sampling rate greater than ~5 Hz will be adequate to capture the most significant component of a platform's motion. However, this will depend on the platform design, and the waters in which it works. To find a suitable sampling rate, a PSD analysis can be made using above-Nyquist motion data. When the required data are available, the methods described above to characterize the vessel with motion data above Nyquist, are recommended over using a rule of thumb value. This is particularly the case for small platforms where movement can be rapid. Further, these methods could be used to understand whether applying corrections to historic data with lower sampling rates would be viable.

As an example of using existing motion data collected independently of the echosounder, multifrequency S_v data were collected on the FSV Bigelow during an autumn bottom-trawl survey in 2016 (figures 7.11 and 7.12). In conjunction with the acoustic data, pitch-and-roll data were recorded at a nominal sampling rate of 1 Hz. While steaming between trawl stations, the 38-kHz echogram showed evidence of surface bubbles and a bottom echo that seemed to be affected by vessel motion, i.e. it was artificially rugose. The maximum pitch and roll values were 8 and 12°, respectively. The FFTs revealed bimodal periodicity of 6 and 8 s in pitch, and 8 and 9 s in roll. These motion characteristics can be used to generate diagnostic plots, using the Dunford correction, which show the effects of motion on S_v (Figure 7.13), and highlight the effect of range and motion periodicity on the S_v data. For the data collected in Figure 7.11, the maximum correction would be about 0.3 dB (linear factor of 1.07) for a periodicity of 6 s, and about 0.1 dB (linear factor of 1.02) for a periodicity of 9 s. These corrections are small, and may not require additional processing to correct motion effects. However, if this same motion is experienced in water masses up to 500 m deep, the effects are considerably greater with corrections of up to almost 9 dB (linear factor of 7.9). In this latter case, processing the data to correct for motion effects may be warranted.

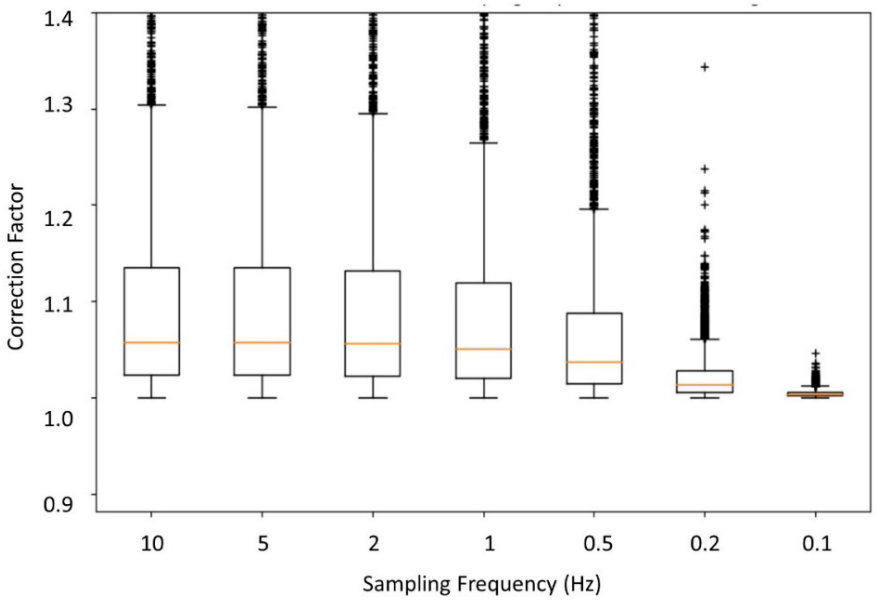

Figure 7.10. Difference in motion correction magnitude as a function of range between S_v data corrected with above Nyquist motion sample rates and a range of lower sampling rates.

When steaming, a ship's heading is often restricted to maintain the direction along a transect or transit between stations. In contrast, a ship's heading during trawling operations is often not restricted, and is selected based on seabed topography, currents, and sea state. In the case of sea state, less vessel movement is desired, as vessel motion can have deleterious effects on trawl performance (e.g. Tello *et al.*, 2011). Figure 7.12 shows an example of vessel motion during a bottom-trawl operation. In this case, pitch and roll were reduced relative to steaming (Figure 7.11), with < 4° maximum pitch (compared to 8° when steaming) and < 10° maximum roll (compared to 12°), and the periodicity was substantially slower, with most of the energy between 10 and 15 s for both pitch and roll (compared to between 5 and 10 s when steaming). The motion correction at 100 m, with a periodicity of 12.5 s and a maximum range of motion of 10°, was about 0.07 dB (linear factor of 1.02; not shown), suggesting negligible effects of vessel motion on S_v data during this trawl haul.

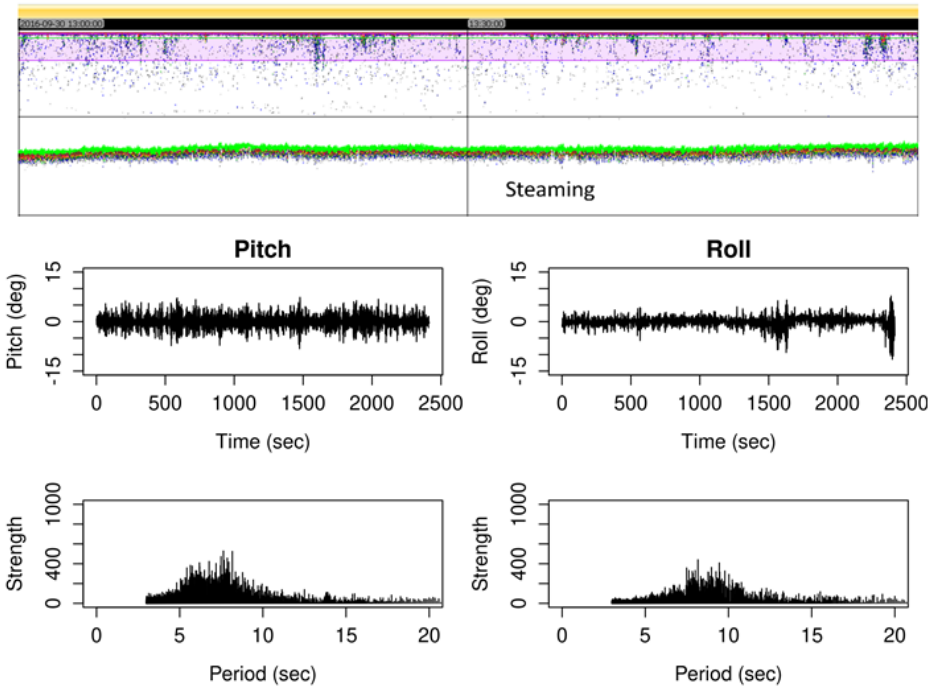

Figure 7.11. 38-kHz data collected on the FSV Bigelow in water depths of 60–70 m while steaming between bottom-trawl stations (echogram). Top panel: The purple shaded area in the echogram denotes aeration from surface bubbles, and the green line is 0.5 m above the seabed echo. Middle panels: The pitch-and-roll data show maximum pitch of about 7–8° (left) and about 11° (right) of roll. Bottom panels: The FFT results show modes of 6–7 s of pitch (left) and 7–10 s of roll (bottom right).

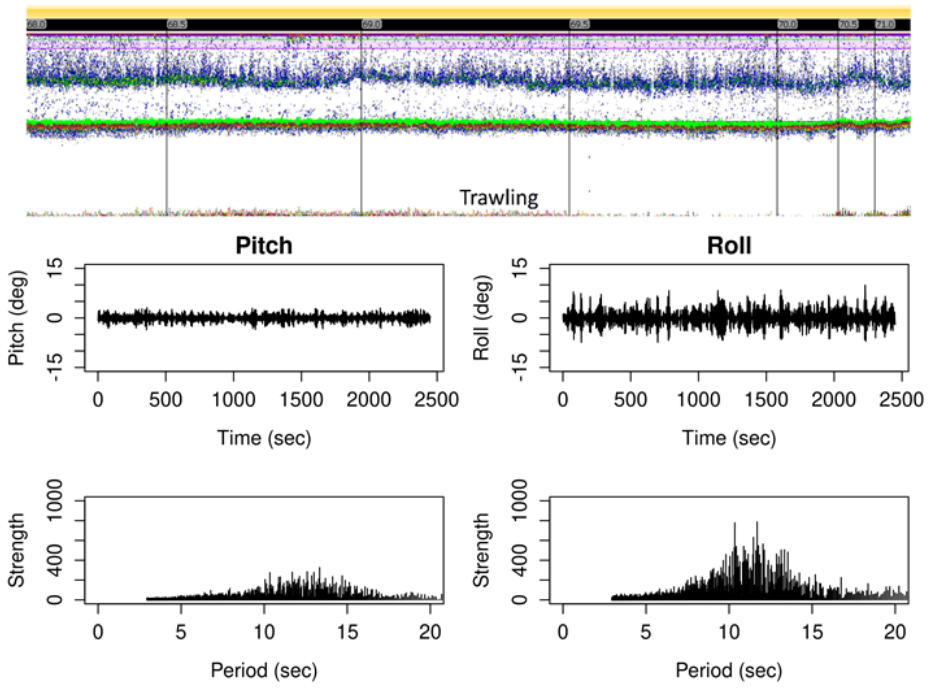

Figure 7.12. 38-kHz data collected on the FSV Bigelow in September 2016 in water depths of 60–70 m during bottom-trawl operations. Top panel: The purple shaded area denotes aeration from surface bubbles, and the green line is 0.5 m above the seabed echo. Middle panels: The pitch-and-roll data show maximum pitch of about 7–8° (left) and about 12–13° (right) of roll. Bottom panels: The FFT results show modes of 11–14 s and 12–13 s of pitch (left) and roll (right), respectively.

This evaluation can also be done during a survey, as a diagnostic tool to decide whether to continue with data collection. In this case, the vessel motion can be estimated by (1) extracting and graphing the *in situ* motion data and then using a PSD or FFT to estimate the periodicity, (2) watching the bubble level on the ship's bridge to measure angular motion (usually roll), and a stop watch to measure the periodicity, or (3) using relationships between ship length and roll and pitch period (e.g. Furusawa and Sawada, 1991).

The analysis of how a vessel responds to sea state is known as seakeeping, and measuring and predicting vessel motion is standard for shipbuilding and in the field of naval architecture. Generic relationships between vessel motion and vessel size have been developed, as part of predicting seaworthiness. Furusawa and Sawada (1991) provide relationships between ship length (L_{ship}, m), and pitch (T_{pitch}) and roll (T_{roll}) periods (s):

$$T_{pitch} = 0.45\sqrt{L_{ship}}0.91\sqrt{L_{ship}}$$

$$T_{roll} = 1.5T_{pitch}3.0T_{pitch}$$

The FSV Bigelow is about 62.5 m (L_{ship}), resulting in an estimated periodicity in pitch of 3.6–7.2 s, and in roll of 5.4–21.6 s. During steaming, the periodicity in pitch and roll was 6–7 s and 8–9 s, respectively (Figure 7.11), suggesting that the motion of FSV Bigelow can be characterized by these relationships. Interestingly, during trawling operations, the pitch-and-roll periodicities were similar at about 12 s each, suggesting that setting the vessel course relative to the sea state can mitigate pitch and roll movement.

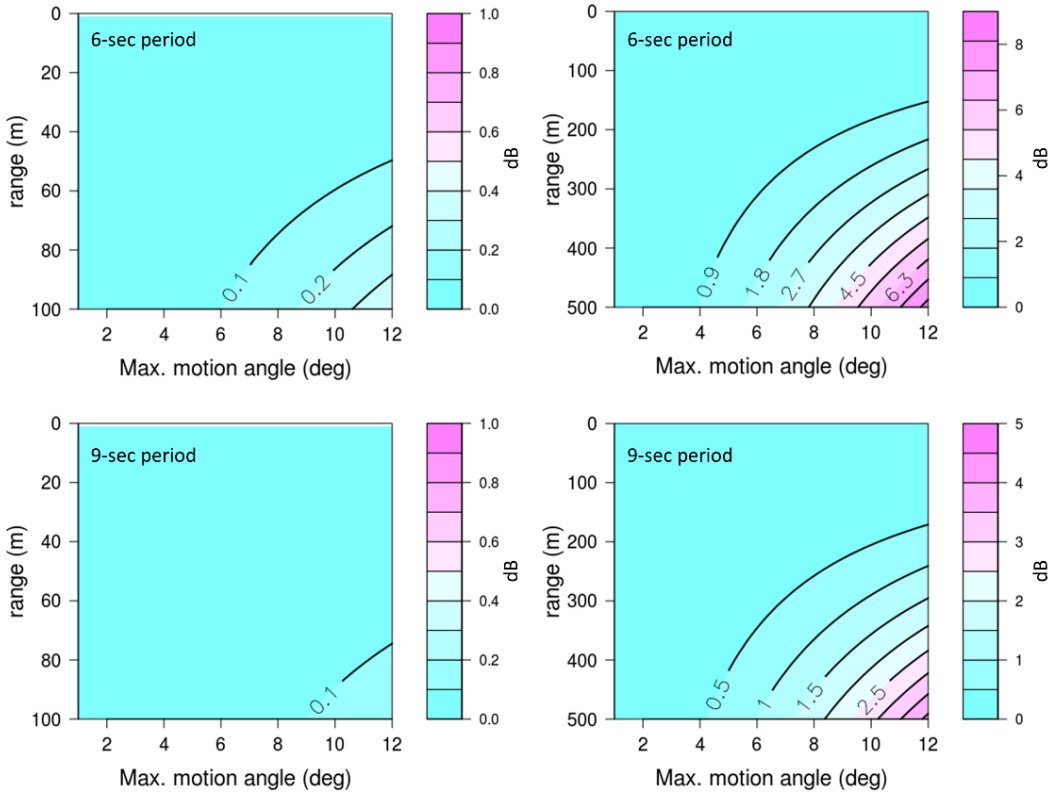

Figure 7.13. Diagnostic plots of the Dunford correction as a function of motion period (6 s periods in the top panels and 9 s periods in the bottom panels), range, and maximum degree of motion. Note that the ranges (e.g. depths) are different between the left and right plots.

As an example of a deep-water survey, an acoustic survey for smooth oreo (*Pseudocyttus maculatus*) was carried out on the RV Tangaroa in November 2009 on the South Chatham Rise, east of New Zealand. Some transects over flat areas were carried out with 38-kHz echosounders with hull-mounted transducers. Vessel motion and meteorological conditions were recorded, and corrections estimated based on Dunford's algorithm (Dunford, 2005). Because of the depth of this survey (800–1300 m), corrections were relatively large and variable (9–111%, equivalent to correction multipliers of 1.09–2.11) in moderate windspeeds of 13–28 knots (Table 7.3).

Calculated corrections were dependent on transect directions, with lower corrections when traveling with the wind/swell, due to reduced vessel motion (Figure 7.14).

Table 7.3. Motion corrections for New Zealand oreo acoustic surveys by stratum and transect direction.

Stratum	Windspeed (knots)	Motion correction (%)	
		North–south	South-north
2	13	18	20
22	10	16	22
3	19	22	21
4	16	19	47
42	27	69	23
5	26	87	18
52	27	69	23
8	20	66	61
82	28	111	41
9	20	9	31

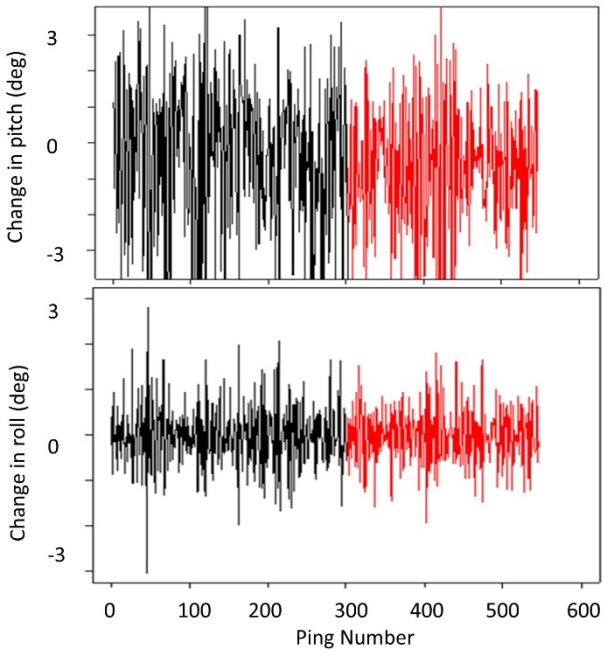

Figure 7.14. Approximate change in pitch (top) and roll (bottom) angle from transmit to receive for two transects in stratum 82, d86 (black) and d87 (red), which went in the opposite direction. Transect d86 had a motion correction of ~ 3.2 (217%) and d87 ~ 1.2 (23%).

7.6 Speckle noise

Speckle noise is a term mainly used in image processing to define granular interference that inherently exists in stochastic data. In acoustic data, speckle noise increases S_v data variance. Peña (2016) reduced speckle noise with a local smoothing kernel that was inversely proportional to the variance within the kernel samples. This application tends to preserve the edges of scattering features (e.g. layers and schools). Wavelet analysis is another method that has been used to reduce speckle noise. Wavelets project data into a new space where the noise component is more easily identified. Hard versions remove noise based on a threshold, while soft versions shrink coefficients close to zero by a given amount (see an example in Figure 7.15). The algorithm developed by Kovesi (1999) was successfully applied to acoustic data by Dunlop *et al.* (2018), although it may be too slow for a large dataset (Bazeille *et al.*, 2006).

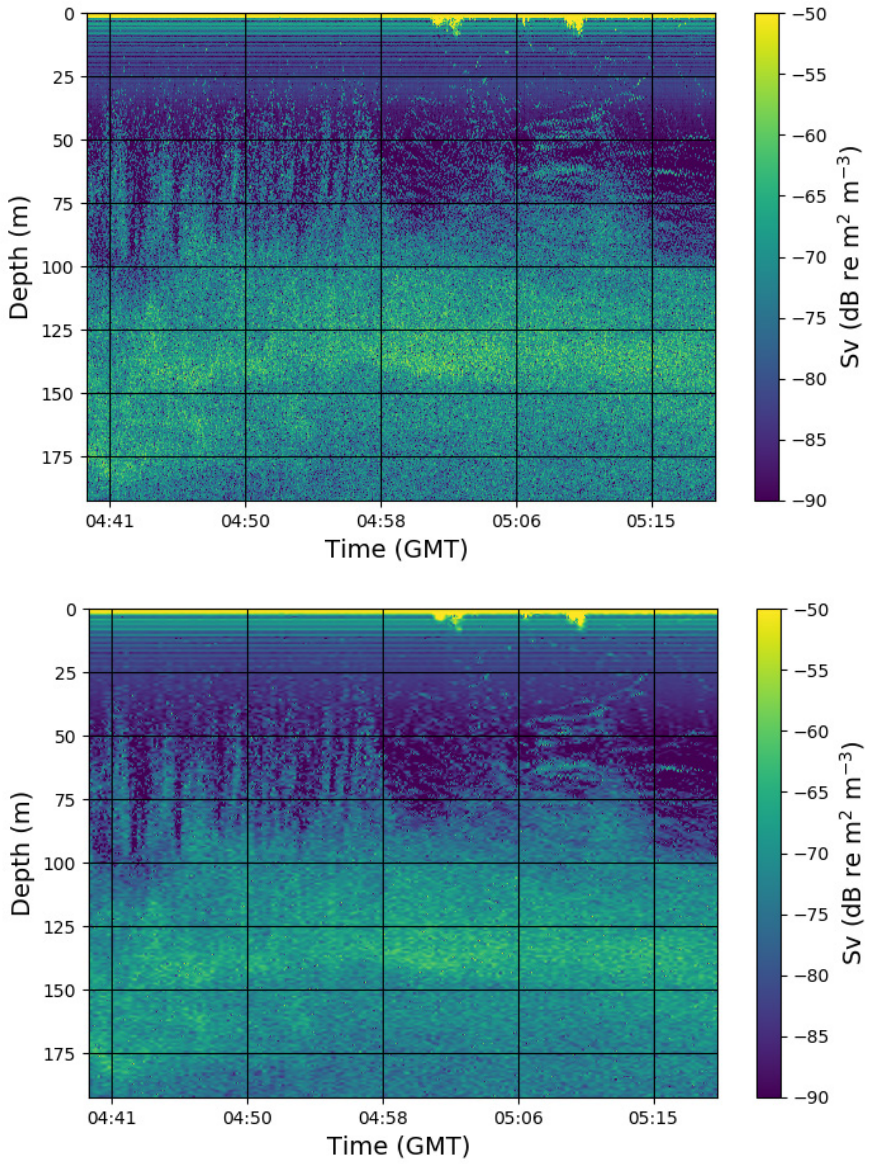

Figure 7.15. Wavelet denoising application. The original S_v echogram (top) is denoised from speckle with a soft wavelet algorithm (bottom).

7.7 Transducer ringing

Transducer ringing is caused by the vibration of the elements within the transducer, which produces a pulse of sound in the water. This vibration does not instantaneously start or end with the electrical input of the acoustic pulse. Rather, the elements ramp up and down at the beginning and end of the acoustic pulse, i.e. at the end of the acoustic pulse they vibrate for a short time after the pulse has been delivered, with the vibrations decreasing in amplitude over time. The ramp-down in vibration produces a noise area near the transducer that is evident in all transducers, but particularly noticeable for lower frequencies such as the Simrad 18-kHz transducer. Under normal conditions, S_v values within a portion of the transducer ringdown vary less than 0.1 dB. Abnormal values are indicative of issues in transmitted power, often due to air bubbles at the transducer face. The ringdown analysis in ESP3 software (Ladroit *et al.*, 2020) detects pings whose ringdown level deviates above a threshold from the local average level. The parameter has a default value of 0.05 dB. An example of transducer ringdown analysis is shown in Figure 7.16.

The ringdown analysis implemented in ESP3 takes the third power sample from Simrad EK60 data for each ping (corresponding to the end of the pulse, as EK60 pulses are divided to four samples), and looks for changes over time. This sample is used as a proxy for the impedance of the transducer, which should be matched for water. When the weather is good, the signal observed in this sample is stable, and any variation between pings can be attributed to quantization (i.e. precision) errors (changes < 0.01 dB). When aeration is observed in the echogram, the sample value will fluctuate, with sharp decreases observed in the sample value that may be attributed to changes in impedance, i.e. the contrast between the transducer and the medium (water, aerated water, or potentially only air).

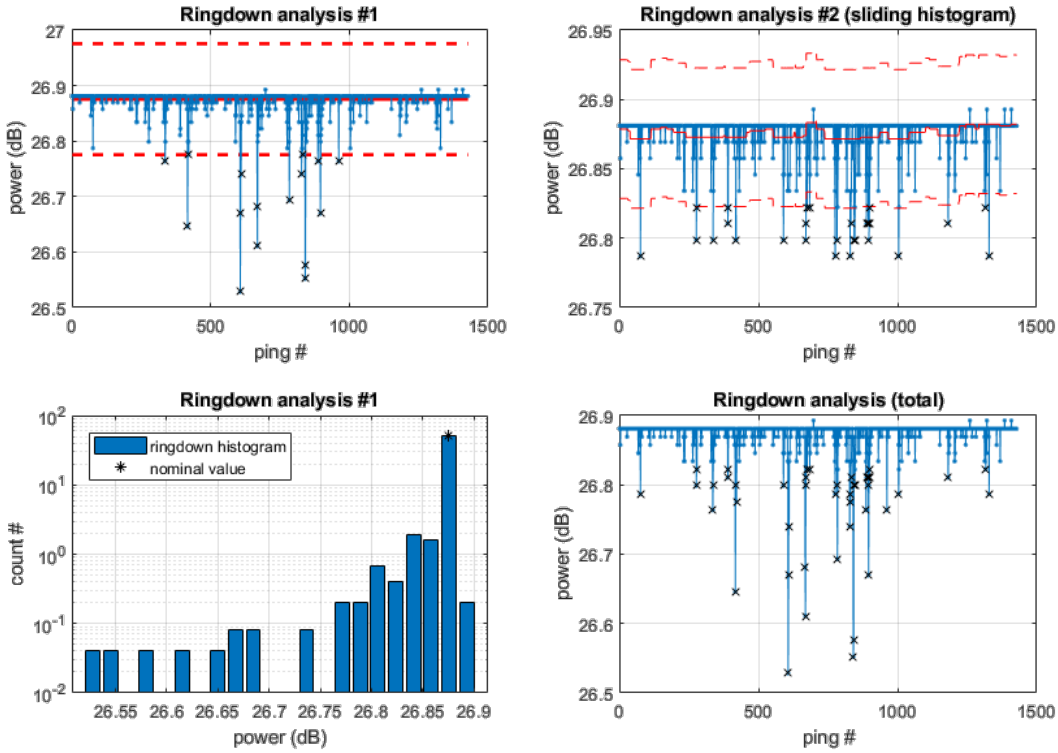

Figure 7.16. Example of results from a ringdown analysis of Simrad EK60 data in ESP3. Dashed red lines in the upper left panel indicate ± 0.1 dB thresholds and in the upper right panel ± 0.05 dB thresholds. The black criss-crosses indicate outliers, and the asterisk in the lower left panel indicates the mode of the distribution, i.e. the nominal value used in the analyses.

The ESP3 implementation is a two-step process. The first step (Figure 7.16, upper left panel) removes outliers from the power data, which are values less than a predefined threshold (here 0.1 dB) from the mode of the distribution (nominal value in the lower left panel of Figure 7.16). The second step increases resolution by applying a second threshold, equal to one half of the initial threshold, to the power data over a shorter time window, i.e. a sliding histogram of 11 pings (Figure 7.16, upper right panel). Pings with power values outside one of the two thresholds are flagged as "bad" by the ringdown analysis (Figure 7.16, lower right panel) and can be further evaluated by the user.

7.8 Multi-ping aliasing

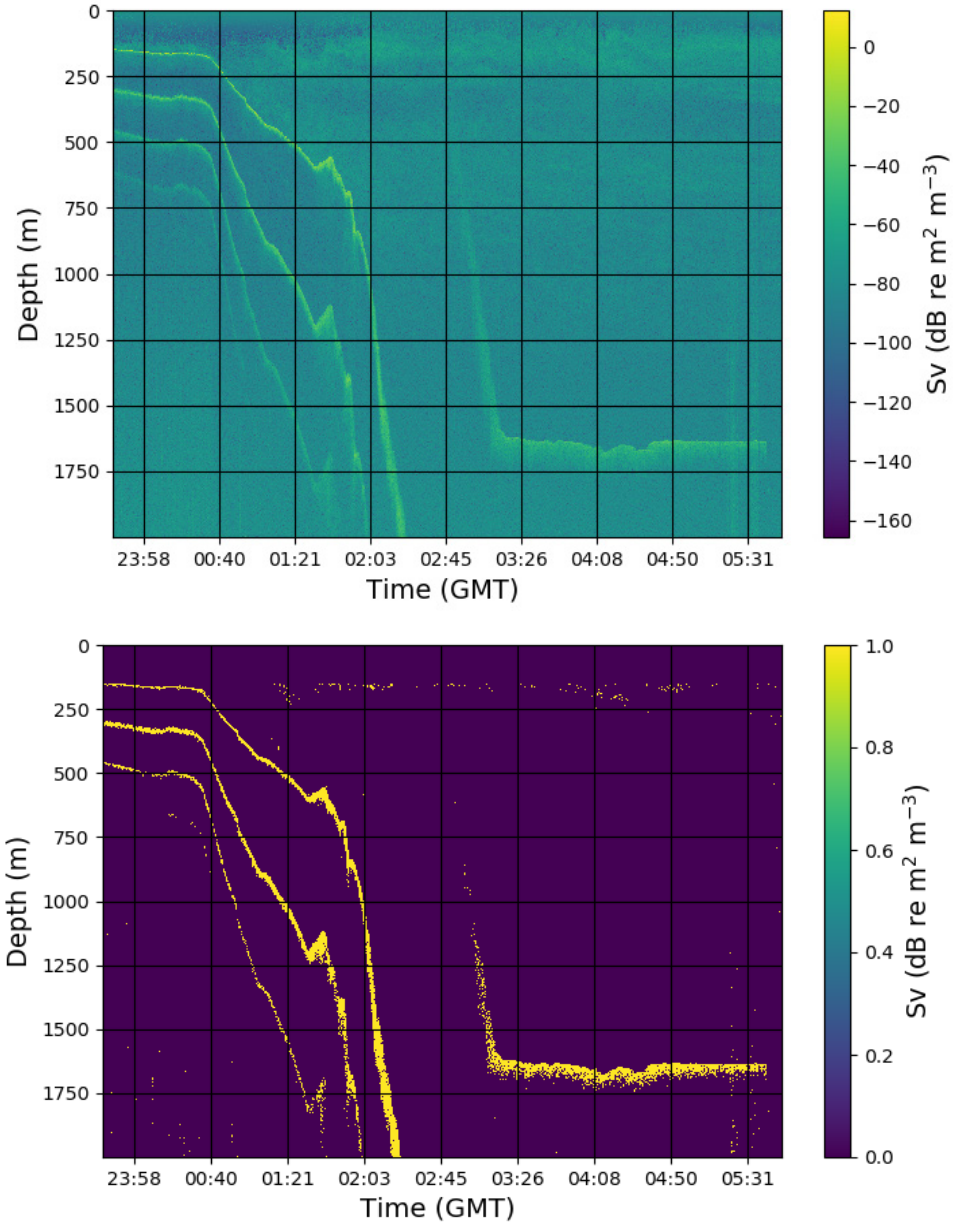

Figure 7.17. Aliased seabed detection example using the algorithm in Blackwell *et al.* (2019). The location of the real and aliased seabed scattering in the S_v echogram (top panel) is masked on the lower echogram (yellow pixels).

Aliased seabed echoes, also known as false bottom, second bottom echo or ghost echo (Tomczak *et al.*, 2002), are a form of echogram degradation caused by seabed reverberation from preceding pings coinciding with echoes from the current ping. A false bottom may appear above or below the real seabed echo, depending on the interplay between seabed depth and ping rate. The false bottom echo can be identified by changing the sampling rate, which will move the false bottom echo up or down. Renfree and Demer (2016) developed an algorithm that prevents this noise by calculating the needed sampling rate based on bottom depth. A Matlab executable is available[5]. The EAL can use high-resolution bathymetry maps to eliminate aliased seabed echoes when the seabed is deeper than the desired maximum logging range (provided with the algorithm). Blackwell *et al.* (2019) developed an algorithm that removes false bottom echoes through a double mask: the bottom steepness produces very high along-ship and athwart-ship angles when the second bottom starts to appear, which are useful to create both the real and the spurious bottom mask, together with the strong intensity of the bottom echo (Figure 7.17). This method does not require the use of bathymetry data.

[5] https://www.fisheries.noaa.gov/west-coast/science-data/ek80-adaptive-logger Last accessed 22 November 2021

8 Implications of results

Vessels of all sizes have traditionally been used to collect distribution and abundance data in support of fisheries stock assessments and ecological research. Days at sea for federal or state vessels are often scheduled up to a year in advance to balance the demands of institutional research mandates and targeted times during biological cycles (e.g. prespawning aggregations, seasonal migration), in an effort to maximize animal availability to survey platforms and data acquisition (e.g. acoustic technologies and direct capture gear). Population abundance/biomass surveys are conducted during scheduled days to maximize coverage of the population or stock spatial range, and to maintain data time-series. This scheduling is often independent of data collection conditions. Inclement weather during surveys potentially reduces both the quality and amount of data that are subsequently used in population abundance and biomass estimates. Autonomous platforms, both mobile and stationary, that sample for longer periods than survey vessel durations and/or can be deployed in locations that are not accessible to surface vessels (e.g. ice covered high latitudes) now supplement or replace vessels as data acquisition platforms. With autonomous deployments, continuous sampling occurs in all types of weather, with resulting data encompassing a wider range of meteorological conditions than those obtained from survey vessels. The same constraints on data quality exist for autonomous platforms, but data from these platforms may also be used to investigate effects of inclement weather on data quality. Additional research is required to determine how data from autonomous platforms differs from that obtained on survey vessels, and how biases change when estimating population abundance or biomass for a stock assessment using data from autonomous platforms (De Robertis *et al*., 2019).

8.1 Data quality flags and descriptors

To ensure that the identification of degraded data and the application of data corrections or filters are consistent within and among user groups, we advocate that metrics and threshold values be chosen and parameterized using local data. At this time, the sensitivity of each data-quality metric has not been quantified, and it is recommended that a sensitivity analysis be included when deciding which metric(s) are used in data quality evaluation. Analyses included in this report demonstrate that a single metric does not exist for data quality evaluation during inclement weather, and that the utility of each metric will depend on the survey platform and on the weather conditions during data acquisition. The use of metrics to evaluate acoustic data quality should become a routine part of data acquisition and pre-processing. We envision that real-time displays of data quality could be included in acquisition software, or tabulated and displayed while data are collected. Diagnostic metric values should also be included in acoustic processing software, and be available as a filter and/or mask during data processing.

8.2 Criteria for accepting or rejecting data

The analyst has the responsibility for defining the criteria, metrics, and corresponding metric thresholds, used to evaluate the extent of backscatter measurement degradation. It is beyond the scope of this report to recommend specific criteria, metrics, or threshold values, to accept, correct, or reject backscatter data. The choice of the metrics and threshold values used to evaluate signal degradation should be guided by the survey objective(s). As an example, comparing changes in seabed backscatter relative to bubble layer thickness is not relevant when

the seabed is beyond the detection range of the operating frequency used to acquire the acoustic data.

Despite the continuous strive to develop objective methods to monitor data quality, these quantitative efforts do not preclude visual inspection by an experienced operator or data scrutinizer. Visual inspection of echograms will continue to be a major component of the data-processing workflow for survey data. For example, the high dynamic range of noise is comparable to, or often greater than, the scattering by organisms, and can make visualizing and separating noise from biological scattering difficult. Colour maps based on data quantiles, objectively set thresholds, and colour scales that highlight scattering by organisms (in layers and single targets) as well as noise, may improve visual interpretation of echograms (Peña, 2021; Section 7.4.1). Visual inspection of echograms is feasible when experienced personnel are on board during data collection, or when data are processed shortly after the survey is completed. However, this task is exponentially more difficult when attempting to utilize years of historical data for a new purpose, such as estimating the abundance or distribution of non-focal species. In these cases, algorithms must be employed to process data. Most institutions have developed custom software, or tailored commercial software packages, to process large amounts of data. These processing routines are often designed for a single purpose, using specific data, and may not be applicable for other uses. Application of artificial intelligence and machine learning methods (AI and ML, respectively) are gaining traction in the fisheries acoustics community, and may provide advancements in the ability to process and analyse acoustic data (Malde *et a*l., 2020). The ability of AI and ML methods to incorporate indicators of data quality deserves further scrutiny.

8.3 How to determine threshold and diagnostics

Metrics, and associated threshold values, that indicate data degradation can be determined in many ways. Therefore, the criteria used to select metrics and thresholds need to be explicitly reported. As an example, an approach using the statistical properties of the data may set a threshold two standard deviations above or below a median value of a backscatter probability distribution function. This relative approach can be repeated among datasets, and will change thresholds depending on the dataset. However, it is not assumed to be an appropriate diagnostic metric in all circumstances, especially if the entire dataset was collected during inclement weather. In contrast, an absolute threshold approach would set a minimum signal-to-noise ratio for the backscatter data (i.e. maximum signal degradation), with data cells below the threshold being excluded from further analyses.

The consistency of any threshold value among surveys depends on the choice of a relative or absolute criterion, and how representative the data are for the range of conditions present during data acquisition. Any threshold value must be tuned to the specific platform and frequencies being collected. Metrics can be grouped into categories with diagnostic capability for particular attributes of the data (e.g. % attenuated ping, rate of change for roll, rate of change for pitch, deviation in seabed echo intensity, and windspeed). The choice of categories will be largely determined by which weather and platform factors are reducing data quality, and the availability of meteorological and platform motion data.

8.4 What do we do with the metrics

A primary goal of this report is to identify and provide examples where weather conditions reduced acoustic backscatter data quality acquired from surface platforms. An objective approach is advocated when evaluating and filtering low signal-to-noise-ratio acoustic data, as the choice of any diagnostic metric, and subsequent data treatment, will be influenced by data sources and the severity of data degradation. Setting diagnostic metric threshold values can be used to determine when data are (i) acceptable as collected, (ii) can be corrected, or (iii) should be excluded from further processing and analyses. The routine reporting of metric values will also serve as an index of data quality. Typically, the resolution of data quality metrics will match that of data exports, and can be used when evaluating the suitability of data for analytic tasks such as quantifying population abundance or biomass, with the associated uncertainty estimates. It is important to determine the required resolution of metric values, so that metric data matches the resolution of acoustic backscatter data (e.g. groups of pings, or EDSU).

The authors of this report envision that metrics will be used in future during data acquisition to evaluate if data should be collected when weather conditions deteriorate, and to decide, during data processing, if data can be corrected or if they need to be excluded from further processing and analyses (Dunford, 2005; Ryan *et al.*, 2015). Table 8.1 provides example metadata fields that could be adapted for use at sea and during processing. The final three rows identify strategies to be used during data acquisition when inclement weather occurs (diagnostics, criteria, and thresholds for assessing data quality; and actions to be taken when data quality has been compromised - e.g. reject or correct data). This table can be adapted for individual surveys, or used to set or modify standards currently used in international surveys (e.g. ICES, 2015; ICES, 2020).

Table 8.1. Metadata example for a specific survey.

Survey name	International Blue Whiting Survey
Region (e.g. North Sea)	West of the British Isles
Platform name	RV Tridens
Frequencies (e.g. 18/38/70/120/200 kHz)	38/120/200 kHz
Key species (e.g. Atlantic herring)	Blue whiting
Key habitat (e.g. seabed recorded in most cases)	Offshore, no seabed
Operational speed (e.g. 8 knots)	8 knots
Platform motion recorded (heave, pitch/roll)	Yes
Inclement weather likelihood (unlikely, some years, very likely)	Very likely
Meteorological recordings available (if yes which ones)	No
Strategy in case of bad weather (e.g. use deep-towed body, shelter, or ignore)	slow down survey speed and shelter if slowing down is not sufficient
How is data quality assessed (e.g. when fishing is not possible, wind force > 10 beaufort, or attenuated pings occur)	if windspeed > 10 beaufort or fishing is not possible anymore
Signal degradation correction factor applied (yes/no - if yes, what, etc.)	No

8.5 Quality flags relative to data uses

The impact of reduced data quality depends on which use those data are intended for. Relative estimates or data comparisons may tolerate higher levels of signal degradation and still be quantitatively or qualitatively relevant (Section 7). However, for mandated abundance or biomass estimates of commercially important species, small reductions in data quality can severely affect harvest allocations, and are, therefore, less tolerant of introduced noise and signal degradation. Data-quality flags that are part of acoustic metadata help users (data collectors or data analysts) understand the constraints of a dataset. These indices should include measures of the severity of data quality reduction, and the time-period over which quality is reduced. Abundance/biomass estimation surveys can run from days to months, and poor weather conditions will hopefully affect only a portion of the dataset. It may also be possible to use some or all of the reduced quality data in comparative analyses (e.g. relative density changes over time at the same location). Therefore, categorical classifications of data quality are recommended:

- 1: high – acceptable for abundance/biomass estimates;
- 2: good – acceptable for quantitative comparisons;
- 3: low – acceptable for qualitative comparisons; and
- 4: poor – cannot be used for any analysis.

It should be noted, that data quality classification can vary over time throughout the data acquisition, with changing sea states.

9 Conclusions and recommendations

9.1 Conclusions

1. Platforms respond to inclement weather differently. As a consequence, there does not appear to be consistent criteria, metrics, or thresholds that can be used to assess acoustic data quality on all platforms.
2. Platform-specific criteria, metrics, and thresholds need to be developed to determine when to modify data acquisition and/or accept/reject data for use in abundance/biomass estimates.
3. There are common diagnostics and evaluation methods for all platforms that can and should be applied to evaluate data quality during acquisition and/or processing.
4. Attenuated pings metrics (e.g. number, and proportion) were consistent indicators of data quality. A larger number and proportion of attenuated pings indicated degraded data quality. However, results from case studies strongly indicated that data degradation occurs before pings become attenuated below a S_v threshold (depending on specified value and operating frequency) and attenuated pings appear on the echograms.
5. Although seabed echoes are variable, even in calm weather, the results obtained suggest that seabed echo metrics can be used as indicators of water column acoustic data quality.

9.2 Recommendations

1. Collect platform motion data (heave, pitch, roll, speed, and heading) at appropriate sampling frequencies (sections 2.3.2, 5.3, and 7.5).
2. Conduct studies to verify theoretical data corrections for transducer motion. Platform motion data (pitch, roll, heave, and heading) collected during surveys at appropriate sampling rates can be used in comparisons with theoretical predictions, and the results obtained can be used to augment theory and to develop additional diagnostics (Section 2.3.2).
3. Collect meteorological data (windspeed, wind direction, sea state, wave height, and wave direction) for analyses of acoustic data quality (Section 5).
4. Develop platform-specific data quality metrics and indicators (Section 6).
5. Develop platform-specific motion relationships for data quality metrics and indicators (Section 7.5).
6. Compare seakeeping relationships of platform motion to platform size (Section 7.5.1).
7. Collect acoustic data using transducers that are independent of platform motion (e.g. mounted on moorings, buoys, towed vehicles, or nets) and compare these to data collected by survey platforms to quantify the effects of inclement weather on data quality (Section 4.4).
8. Investigate transducer impedance as a metric or indicator of data quality (Section 4.3).

References

Andersen, L. N. 2001. The new Simrad EK60 scientific echosounder system. Journal of the Acoustical Society of America, 109: 2336. https://doi.org/10.1121/1.4744207

Anderson, C. I., Brierley, A. S., and Armstrong, F. 2005. Spatio-temporal variability in the distribution of epi-and meso-pelagaic backscatter in the Irminger Sea, North Atlantic, with implications for predation on *Calanus finmarchicus*. Marine Biology, 146: 1177–1188. https://doi.org/10.1007/-s00227-004-1510-8

Baschek, B., Farmer, D. M., and Garrett, C. 2006. Tidal fronts and their role in air-sea gas exchange. Journal of Marine Research, 64: 483–515. https://doi.org/10.1357/002224006778715766

Bazeille, S., Quidu, I., Jaulin, L., and Malkasse, J-P. 2006. Automatic underwater image pre-processing. *CMM'06*, Oct 2006, Brest, France. ⟨hal-00504893⟩

Benoit-Bird, K. J., Moline, M. A., and Southall, B. L. 2017. Prey in oceanic sound scattering layers organize to get a little help from their friends. Limnology and Oceanography, 62: 2788–2798. https://doi.org/10.1002/lno.10606

Benoit-Bird, K. J., Welch, T. P., Waluk, C. M., Barth, J. A., Wangen, I., McGill, P., Okuda, C., *et al.* 2018. Equipping an underwater glider with a new echosounder to explore ocean ecosystems. Limnology and Oceanography Methods, 16: 734–749. https://doi.org/10.1002/lom3.10278

Blackwell, R., Harvey, R., Queste, B., and Fielding, S. 2019. Aliased seabed detection in fisheries acoustic data, Cornell University, Ithaca, NY, USA. 9 pp. https://arxiv.org/abs/1904.10736

Blackwell, R., Harvey, R., Queste, B., and Fielding, S. 2020. Colour maps for fisheries acoustic echograms. ICES Journal of Marine Science, 77: 826–834. https://doi.org/10.1093/icesjms/fsz242

Bodholt, H. 2002. The effect of water temperature and salinity on echosounder measurements, ICES Symposium on Acoustics in Fisheries. Montpellier, FR, June 2002. Presentation 123. https://courses.washington.edu/fish538/resources/Bodholt 2002 water temp.pdf

Bourguignon, S., Berger, L., Scalabrin, C., Fablet, R., and Mazauric, V. 2009. Methodological developments for improved bottom detection with the ME70 multibeam echosounder. ICES Journal of Marine Science, 66: 1015–1022. https://doi.org/10.1093/icesjms/fsp089

Burgos, J. M., and Horne, J. K. 2007. Sensitivity analysis and parameter selection for detecting aggregations in acoustic data. ICES Journal of Marine Science, 64: 160–168. https://doi.org/10.1093/-icesjms/fsl007

Chu, D., Parker-Stetter, S., Hufnagle, J., L. C., Thomas, R., Getsiv-Clemons, J., Gauthier, S., and Stanley, C. 2019. 2018 Unmanned surface vehicle (Saildrone) acoustic survey off the west coasts of the United States and Canada. 2019MTS-IEEE Oceans2019. 8 pp. https://doi.org/-10.23919/OCEANS40490.2019.8962778

Clay, C. S., and Medwin, H. 1977. Acoustical Oceanography: Principles and Applications, John Wiley and Sons, Inc., New York. 544 pp. https://doi.org/10.1017/S0025315400028228

Cutter, G. R. J., and Demer, D. A. 2014. Seabed classification using surface backscattering strength versus acoustic frequency and incidence angle measured with vertical, split-beam echosounders. ICES Journal of Marine Science, 71: 882–894. https://doi.org/10.1093/icesjms/fst177

Dalen, J., and Løvik, A. 1981. The influence of wind-induced bubbles on echo integration surveys. Journal of the Acoustical Society of America, 69(6): 1653–1659. https://doi.org/10.1121/1.385943

De Robertis, A., and Handegard, N. O. 2013. Fish avoidance of research vessels and the efficacy of noise-reduced vessels: a review. ICES Journal of Marine Science, 70: 34–45. https://doi.org/10.1093/-icesjms/fss155

De Robertis, A., and Higginbottom, I. 2007. A post-processing technique to estimate the signal-to-noise ratio and remove echosounder background noise. ICES Journal of Marine Science, 64: 1282–1291. https://doi.org/10.1093/icesjms/fsm112

De Robertis, A., Lawrence-Slavas, N., Jenkins, R., Wangen, I., Mordy, C. W., Meinig, C., Levine, M., *et al*. 2019. Long-term measurements of fish backscatter from Saildrone unmanned surface vehicles and comparison with observations from a noise-reduced research vessel. ICES Journal of Marine Science, 76: 2459–2470. https://doi.org/10.1093/icesjms/fsz124

Delacroix, S., Germain, G., Berger, L., and Billard, J-Y. 2016a. Bubble sweep-down occurrence characterization on research vessels. Ocean Engineering, 111: 34–42. https://doi.org/10.1016/-j.oceaneng.2015.10.040

Delacroix, S., Germain, G., Gaurier, B., and Billard, J-Y. 2016b. Experimental study of bubble sweep-down in wave and current circulating tank: Part I—Experimental set-up and observed phenomena. Ocean Engineering, 120: 78–87. https://doi.org/10.1016/j.oceaneng.2016.05.003

Demer, D. A. 2004. An estimate of error for the CCAMLR 2000 survey estimate of krill biomass. Deep-Sea Research II, 51: 1237–1251. https://doi.org/10.1016/s0967-0645(04)00077-3

Demer, D. A., Berger, L., Bernasconi, M., Bethke, E., Boswell, K., Chu, D., Domokos, R., *et al*. 2015. Calibration of acoustic instruments. ICES Cooperative Research Reports, Vol. 326. 133 pp. https://doi.org/10.17895/ices.pub.5494

Demer, D. A., Andersen, L. N., Bassett, C., Berger, L., Chu, D., Condiotty, J., Cutter, G. R., *et al*. 2017. 2016 USA–Norway EK80 Workshop Report: Evaluation of a wideband echosounder for fisheries and marine ecosystem science. ICES Cooperative Research Reports, Vol. 336. 69 pp. https://doi.org/10.17895/ices.pub.2318

Dunford, A. J. 2005. Correcting echo-integration data for transducer motion. Journal of the Acoustical Society of America, 118: 2121–2123. https://doi.org/10.1121/1.2005927

Dunlop, K. M., Jarvis, T., Benoit-Bird, K. J., Waluk, C. M., Caress, E. W., Thomas, H., and Smith, K. L. 2018. Detection and characterisation of deep-sea benthopelagic animals from an autonomous underwater vehicle with a multibeam echosounder: A proof of concept and description of data-processing methods. Deep Sea Research Part I: Oceanographic Research Papers, 134: 64–79. https://doi.org/10.1016/j.dsr.2018.01.006

Fleischer, G. W., Cooke, K. D., Ressler, P. H., Thomas, R. E., de Blois, S. K., Hufnagle, J., L. C., Kronlund, A. R., *et al*. 2005. The 2003 integrated acoustic and trawl survey of Pacific hake, *Merluccius productus*, in U.S. and Canadian waters off the Pacific coast. U.S. Department of Commerce, NOAA Technical Memorandum, NMFS-NWFSC-65. 45 pp.
https://www.webapps.nwfsc.noaa.gov/assets/25/192_06272005_114457_haketm65final.pdf

Foote, K. G. 1999. Extinction cross-section of Norwegian spring-spawning herring. ICES Journal of Marine Science, 56: 606–612. https://doi.org/10.1006/jmsc.1999.0479

Foote, K. G., Knudsen, H. P., Vestnes, G., MacLennan, D. N., and Simmonds, E. J. 1987. Calibration of acoustic instruments for fish density estimation: A practical guide. ICES Cooperative Research Reports, Vol. 144. 69 pp. https://doi.org/10.17895/ices.pub.8265

Fraser, S. 2017. Acoustic Investigation of the hydrodynamics and ecology of a tidal channel and the impacts of a marine renewable energy installation. Doctoral Dissertation, Aberdeen University. https://abdn.primo.exlibrisgroup.com/discovery/collectionDiscovery?vid=44ABE_INST:44ABE_VU1&collectionId=81151712890005941&sortItemsBy=author&query=any,contains,Fraser

Furusawa, M., and Sawada, K. 1991. Effects of transducer motion on quantifying single fish echoes. Nippon Suisan Gakkaishi, 57: 857–864. https://doi.org/10.2331/suisan.57.857

Grömping, U. 2007. Estimators of relative importance in linear regression based on variance decomposition. The American Statistician, 61: 139–147. https://doi.org/10.1198/000313007x188252

Haris, K., Kloser, R. J., Ryan, T. E., and Malan, J. 2018. Deep-water calibration of echosounders used for biomass surveys and species identification. ICES Journal of Marine Science, 75: 1117–1130. https://doi.org/10.1093/icesjms/fsx206

ICES. 1990. Hull mounted, protruding transducer for improving echo integration in bad weather. ICES Document CM. 1990/B: 31. 10 pp.

ICES. 2007. Acoustic seabed classification of marine physical and biological landscapes. ICES Cooperative Research Reports, Vol. 286. 183 pp. https://doi.org/10.17895/ices.pub.5453

ICES. 2015. Manual for International Pelagic Surveys (IPS). Series of ICES Survey Protocols, SISP 9-IPS. 92 pp. https://doi.org/10.17895/ices.pub/7582

ICES. 2020. Working Group of International Pelagic Surveys (WGIPS). ICES Scientific Reports, 2:46. 473 pp. https://doi.org/10.17895/ices.pub.6088

Jech, J. M., Foote, K. G., Chu, D., and Hufnagle, J. L. C. 2005. Comparing two 38-kHz scientific echosounders. ICES Journal of Marine Science, 62: 1168–1179. https://doi.org/10.1016/-j.icesjms.2005.02.014

Kieser, R., Reynisson, P., and Mulligan, T. J. 2005. Definition of signal-to-noise ratio and its critical role in split-beam measurements. ICES Journal of Marine Science, 62: 123–130. https://doi.org/10.1016/-j.icesjms.2004.09.006

Klevjer, T. A., Torres, D. J., and Kaartvedt, S. 2012. Distribution and diel vertical movements of mesopelagic scattering layers in the Red Sea. Marine Biology, 159: 1833–1841. https://doi.org/10.1007/s00227-012-1973-y

Kloser, R. J. 1996. Improved precision of acoustic surveys of benthopelagic fish by means of a deep-towed transducer. ICES Journal of Marine Science, 53: 407–413. https://doi.org/10.1006/jmsc.1996.0057

Kloser, R. J., Sutton, C., Krusic-Golub, K., and Ryan, T. E. 2015. Indicators of recovery for orange roughy (*Hoplostethus atlanticus*) ineastern Australian waters fished from 1987. Fisheries Research, 167: 225–235. https://doi.org/10.1016/j.fishres.2015.02.017

Kornelliussen, R. J. 2000. Measurement and removal of echo integration noise. ICES Journal of Marine Science, 57: 1204–1217. https://doi.org/10.1006/jmsc.2000.0806

Kovesi, P. 1999. Phase preserving denoising of images. *In* Conference Proceedings DICTA '99 Digital Image Computing: Techniques and Applications, pp. 212–217. Ed. by A. Pearce and M. Robey. APRS (Australian Pattern Recognition Society). https://doi.org/10.1109/dicta.2012.6411698

Ladroit, Y., Escobar-Flores, P. C., Schimel, A. C., and O'Driscoll, R. L. 2020. ESP3: An open-source software for the quantitative processing of hydro-acoustic data. SoftwareX, 12: 100581. https://doi.org/10.1016/j.softx.2020.100581

Levine, M., and De Robertis, A. 2019. Don't work too hard: Subsampling leads to efficient analysis of large acoustic datasets. Fisheries Research, 219: 105323. https://doi.org/10.1016/j.fishres.2019.105323

Lloyd, A. R. J. M. 1998. Seakeeping: Ship behaviour in rough weather, A.R.J.M. Lloyd., UK. 396 pp.

Lloyd, A. R. J. M., Hosoda, R., Robinson, D. W., Nicholson, K., and Victory, G. 2011. Seakeeping [and Discussion]. Philosophical Transactions of the Royal Society of London. Series A: Physical and Engineering Sciences, 334: 1634. https://doi.org/10.1098/rsta.1991.0012

MacLennan, D., Copland, P., Armstrong, E., and Simmonds, E. J. 2004. Experiments on the discrimination of fish and seabed echoes. ICES Journal of Marine Science, 61: 201–210. https://doi.org/10.1016/-j.icesjms.2003.09.005

MacLennan, D., and Simmonds, E. J. 1992. Fisheries Acoustics. Springer, The Netherlands. 325 pp. https://link.springer.com/book/10.1007/978-94-017-1558-4

MacLennan, D. N., Fernandes, P. G., and Dalen, J. 2002. A consistent approach to definitions and symbols in fisheries acoustics. ICES Journal of Marine Science, 59: 365–369. https://doi.org/10.1006/-jmsc.2001.1158

Malde, K., Handegard, N. O., Eikvil, L., and Salberg, A-B. 2020. Machine intelligence and the data-driven future of marine science. ICES Journal of Marine Science, 774: 1274–1285. https://doi.org/10.1093/icesjms/fsz057

Manik, H. M., Furusawa, M., and Amakasu, K. 2006. Measurement of sea bottom surface backscattering strength by quantitative echo sounder. Fisheries Science, 72: 503–512. https://doi.org/10.1111/-j.1444-2906.2006.01178.x

McKay, M., Beckman, R., and Conover, W. 1979. A comparison of three methods for selecting values of input variables in the analysis of output from a computer code. Technometrics, 21: 239–245. https://doi.org/10.1080/00401706.1979.10489755

Mitson, R. B. 1995. Underwater noise of research vessels, ICES Cooperative Research Reports, Vol. 209. 65 pp. https://doi.org/10.17895/ices.pub.5317

Novarini, J. C., and Bruno, D. R. 1982. Effects of the sub-surface bubble layer on sound propagation. Journal of the Acoustical Society of America, 72: 510–514. https://doi.org/10.1121/1.388107

Novarini, J. C., and Bruno, D. R. 1983. Erratum: "Effects of the sub-surface bubble layer on sound propagation" [J. Acoust. Soc. Am. 72, 510-514 (1982)]. Journal of the Acoustical Society of America, 74: 1845. https://doi.org/10.1121/1.389598

Novarini, J. C., Keiffer, R., and Norton, G. 1998. A model for variations in the range and depth dependence of the sound speed and attenuation induced by bubble clouds under wind-driven seas. IEEE Journal of Ocean Engineering, 23: 423–438. https://doi.org/10.1109/48.725236

Nunnallee, E. P. 1990. An alternative to thresholding during echo-integration data collection. Rapports et Procès-Verbaux des Réunions du Conseil International pour l'Exploration de la Mer. 189: 92-94. https://doi.org/10.17895/ices.pub.8754

O'Driscoll, R. L., Dunford, A. J., and Dunn, A. 2016. Industry acoustic surveys of spawning southern blue whiting on the Bounty Platform, New Zealand. Fisheries Research, 178: 61–70. https://doi.org/10.1016/j.fishres.2015.05.007

O'Driscoll, R. L., Dunford, A. J., and Ladroit, Y. 2014. Acoustic estimates of southern blue whiting from the Campbell Island Rise, August-September 2013 (TAN1309). New Zealand Fisheries Assessment Report 2014/22. 46 pp.

Peña, M. 2016. Incrementing data quality of multi-frequency echograms using the Adaptive Wiener Filter (AWF) denoising algorithm. Deep-Sea Research I, 116: 14–21. https://doi.org/10.1016/-j.dsr.2016.07.008

Peña, M. 2021. Full customization of colour maps for fisheries acoustics: visualizing every target. Fisheries Research, 240: 105949. https://doi.org/10.1016/j.fishres.2021.105949

R-Core-Team 2020. R: A language and environment for statistical computing. R Foundation for Statistical Computing, Vienna, Austria., URL https://www.R-project.org.

Renfree, J. S., and Demer, D. A. 2016. Optimizing transmit interval and logging range while avoiding aliased seabed echoes. ICES Journal of Marine Science, 73: 1955–1964. https://doi.org/10.1093/icesjms/fsw055

Renfree, J. S., Sessions, T. S., Murfin, D., Palance, D. G., and Demer, D. A. 2019. Calibrations of wide-bandwidth transceivers (WBT mini) with dual-frequency transducers (ES38-128/200-18C) for Saildrone surveys of the California current ecosystem during summer 2018. NOAA-Technical Memorandom NMFS-SWFSC-608. 29 pp.

Reynisson, P. 1998. Monitoring of equivalent beam angles of hull-mounted acoustic survey transducers in the period 1983–1995. ICES Journal of Marine Science, 55: 1125–1132. https://doi.org/10.1006/-jmsc.1998.0369

Rose, K. A. 1983. A simulation comparison and evaluation of parameter sensitivity methods applicable to large models. Developments in Environmental Modelling, 5: 129–140. https://doi.org/10.1016/-b978-0-444-42179-1.50019-5

Ryan, T. E., Downie, R. A., Kloser, R. J., and Keith, G. 2015. Reducing bias due to noise and attenuation in open-ocean echo integration data. ICES Journal of Marine Science, 72: 2482–2493. https://doi.org/10.1093/icesjms/fsv121

Ryan, T. E., and Kloser, R. J. 2016. Improved estimates of orange roughy biomass using an acoustic-optical system in commercial trawlnets. ICES Journal of Marine Science, 73: 2112–2124. https://doi.org/10.1093/icesjms/fsw009

Ryan, T. E., Kloser, R. J., and Macaulay, G. J. 2009. Measurement and visual verification of fish target strength usingan acoustic-optical system attached to a trawlnet. ICES Journal of Marine Science, 66: 1238–1244. https://doi.org/10.1093/icesjms/fsp122

Shabangu, F. W., Ona, E., and Yemane, D. 2014. Measurements of acoustic attenuation at 38 kHz by wind-induced airbubbles with suggested correction factors for hull-mounted transducers. Fisheries Research, 151: 47–56. https://doi.org/10.1016/j.fishres.2013.12.008

Simmonds, E. J., and MacLennan, D. 2005. Fisheries Acoustics: Theory and Practice, 2nd ed., Blackwell Science., Oxford, UK. 437 pp.

Spence, J. H., and Fischer, R. W. 2017. Requirements for reducing underwater noise from ships. IEEE Journal of Oceanic Engineering, 42: 388–398. https://doi.org/10.1109/joe.2016.2578198

Stanton, T. K. 1982. Effects of transducer motion on echo-integration techniques. Journal of the Acoustical Society of America, 72: 947–949. https://doi.org/10.1121/1.388175

Tello, M., Ribeiro e Silva, S., and Soares, C. G. 2011. Seakeeping performance of fishing vessels in irregular waves. Ocean Engineering, 38: 763–773. https://doi.org/10.1016/j.oceaneng.2010.12.020

Tesler, W. D. 1989. Bias and precision in acoustic biomass estimation. Proceedings of the Institute of Acoustics, 11: 201–211.

Tomczak, M., Haffner, G., and Frønæs, E. 2002. False-bottom acoustic echo in mid water? A note on how to evaluate and prevent the interference. IEEE Journal of Oceanic Engineering, 27: 870–-872. https://doi.org/10.1109/joe.2002.804059

Trevorrow, M. V. 2003. Measurements of near-surface bubble plumes in the open ocean with implications for high-frequency sonar performance. Journal of the Acoustical Society of America, 114: 2672–2684. https://doi.org/10.1121/1.1621008

Wang, X., Zhang, J., and Zhao, X. 2016. A post-processing method to remove interference noise from acoustic data collected from Antarctic krill fishing vessels. CCAMLR Science, 23: 17–30.

Watkins, J. L., and Brierley, A. S. 1996. A post-processing technique to remove background noise from echo integration data. ICES Journal of Marine Science, 53: 339–344. https://doi.org/10.1006/jmsc.1996.0046

Weber, T. C. 2008. Observations of clustering inside oceanic bubble clouds and the effect on short-range acoustic propagation. Journal of the Acoustical Society of America, 124: 2783–2792. https://doi.org/10.1121/1.2990707

Welch, P. D. 1967. The use of fast Fourier transform for the estimation of power spectra: A method based on time averaging over short, modified periodograms. IEEE Transactions on Audio and Electroacoustics, 15: 70–73. https://doi.org/10.1109/tau.1967.1161901

Whitton, T. A., Jackson, S. E., Hiddink, J. G., Scoulding, B., Bowers, D., Powell, B., D'Urban Jackson, T., *et al*. 2020. Vertical migrations of fish schools determine overlap with a mobile tidal stream marine renewable energy device. Journal of Applied Ecology, 57: 729–741. https://doi.org/10.1111/1365-2664.13582

Williamson, B. J., Fraser, S., Blondel, P., Bell, P. S., Waggitt, J. J., and Scott, B. E. 2017. Multisensor acoustic tracking of fish and seabird behavior around tidal turbine structures in Scotland. IEEE Journal of Oceanic Engineering, 42: 948–965. https://doi.org/10.1109/joe.2016.2637179

Wittje, R. 2020. Noise: from nuisance to research subject. Physics Today, 73: 43–48. https://doi.org/10.1063/pt.3.4409

Annex 1: Author contact information

All authors contributed to all sections.

Name	Institution	e-mail	Postal Address
Martin Cox	Australian Antarctic Division	martin.Cox@aad.gov.au	Australian Antarctic Division, 203 Channel Hwy, Kingston, TAS 7050, Australia
Pablo Escobar-Flores	NIWA	pablo.escobar-flores@niwa.co.nz	NIWA, 301 Evans Bay Parade Hataitai, Wellington, New Zealand
Sven Gastauer	Thünen Institute of Sea Fisheries	sven.gastauer@thuenen.de	Thünen Institute of Sea Fisheries, Herwigstraße 31, 27572 Bremerhaven, Germany
John Horne	University of Washington	jhorne@uw.edu	University of Washington, School of Aquatic and Fisheries Sciences, Box 355020, Seattle, WA 98195 USA
Toby Jarvis	Echoview Software	toby.jarvis@echoview.com	Echoview Software Pty Ltd, GPO Box 1387, Hobart, Tasmania 7001, Australia
Michael Jech	NOAA/ NEFSC	michael.jech@noaa.gov	NEFSC, 166 Water St., Woods Hole, MA 02543 USA
Haris Kunnath	CSIRO	haris.kunnath@csiro.au	CSIRO Oceans and Atmosphere, GPO Box 1538, Hobart, Tasmania 7001, Australia
Yoann Ladroit	NIWA	yoann.ladroit@niwa.co.nz	NIWA, 301 Evans Bay Parade Hataitai, Wellington, New Zealand
Richard O'Driscoll	NIWA	richard.odriscoll@niwa.co.nz	NIWA, 301 Evans Bay Parade Hataitai, Wellington, New Zealand
Geir Pedersen	IMR	geir.pedersen@hi.no	Havforskningsinstituttet/Institute of Marine Research, Postboks 1870 Nordnes, NO-5817 Bergen, Norway
Marian Peña	IEO	marian.pena@ieo.es	Centro Oceanográfico de Baleares (IEO, CSIC), Muelle de Poniente s/n, 07015 Palma de Mallorca, Spain
Tim Ryan	CSIRO	tim.ryan@csiro.au	CSIRO Marine Laboratories, Castray Esplanade, Battery Point TAS 7004
Serdar Sakinan	WUR	serdar.sakinan@wur.nl	Wageningen Marine Research, PO Box 68, 1970 AB Ijmuiden, Netherlands

Matthias Schaber	Thünen Institute of Sea Fisheries	matthias.schaber@thuenen.de	Thünen Institute of Sea Fisheries, Herwigstraße 31, 27572 Bremerhaven, Germany
Rebecca Thomas	NOAA/ NWFSC	rebecca.thomas@noaa.gov	NWFSC, 2725 Montlake Blvd. E, Seattle, WA 98115, USA
Haley Viehman	Echoview Software	haley.viehman@echoview.com	Echoview Software Pty Ltd, GPO Box 1387, Hobart, Tasmania 7001, Australia
Carrie Wall	NOAA/ NCEI	carrie.wall@noaa.gov	University of Colorado Boulder, Cooperative Institute for Research in Environmental Sciences, NOAA NCEI, 325 Broadway, Boulder, CO, 80305 USA
Timothy Whitton	University of Bangor	t.whitton@bangor.ac.uk	Centre for Applied Marine Sciences, School of Ocean Sciences, Bangor University, Askew Street, Menai Bridge, Isle of Anglesey, Wales, UK LL59 AB

Annex 2: Glossary

This is not a comprehensive list of all terms used in this report. The terms listed here are those that were not defined in the report.

Band	In this report, band is used as the span of frequencies in a signal.
Bandpass	Signal processing term, where the frequency band of interest is retained in the signal and the frequencies outside of that band (higher and lower) are removed from the signal.
Bandwidth	The frequency content of a signal measured by the difference between the maximum and minimum frequencies. For example, the bandwidth of a signal between 90 and 100 kHz is 10 kHz.
Cross-talk	The reception of acoustical energy transmitted by one sonar system and received by another sonar system. Most common as impulse noise.
Heading	The compass direction in which the longitudinal axis of a platform points.
Narrowband	When the frequency bandwidth of a transmit pulse is less than or equal to 10%
Ping	The transmit pulse.
Wideband	When the frequency bandwidth of a transmit pulse is greater than 10%.

Annex 3: List of acronyms and abbreviations

ABC	Area backscattering coefficient
AC	Alternating current
AcMeta	Metadata convention for processed acoustic data from active acoustic systems https://github.com/ices-publications/AcMeta
ADCP	Acoustic doppler current profiler
AI	Artificial intelligence
AOS	Acoustic optical system
ASV	Autonomous surface vehicle
AUV	Autonomous underwater vehicles
AWF	Adaptive Wiener Filter
CSIRO	Commonwealth Scientific and Industrial Research Organization, Australia
CW	Continuous wave
DC	Direct current
DEFF	Department of Environment, Forestry and Fisheries, South Africa https://www.environment.gov.za
EDSU	Equivalent distance sampling unit
ESP3	Echo Sounder package; https://sourceforge.net/p/esp3/wiki/ESP3
FAD	Fish attraction device
FFT	Fast Fourier transform
FORCE	Fundy Ocean Research Centre for Energy, Canada; https://fundyforce.ca
FV	Fishing vessel
GAM	Generalized additive model
GLM	Generalized linear model
ICES	International Council for the Exploration of the Sea
IMR	Institute for Marine Research, Norway; https://www.hi.no
IESNS	International Ecosystem Survey in Nordic Sea
LMG R2	Lindeman, Merenda, Gold relative importance of statistical r-squared value
Loess	Locally estimated scatterplot smoothing
LSSS	Large Scale Survey System; https://www.marec.no
ML	Machine learning
NEFSC	NOAA Northeast Fisheries Science Centre, USA https://www.fisheries.noaa.gov/about/northeast-fisheries-science-center

NIWA	National Institute of Water and Atmospheric Research, New Zealand https://niwa.co.nz
NOAA	National Oceanic and Atmospheric Administration, USA https://www.noaa.gov
NWFSC	NOAA Northwest Fisheries Science Centre, USA https://www.fisheries.noaa.gov/about/northwest-fisheries-science-center
PSD	Power spectral density
ROV	Remote-operated vehicle
RV	Research vessel
S_a	Area backscatter
S_v	Volume backscatter
s.d	Standard deviation
SNR	Signal-to-noise ratio
SWFSC	NOAA Southwest Fisheries Science Centre, USA https://www.fisheries.noaa.gov/about/southwest-fisheries-science-center
TGQUAD	ICES Topic Group on Collecting Quality Underwater Acoustic Data in Inclement Weather
TS	Target strength
TVG	Time-varied-gain
USV	Unoccupied surface vessel
UxV	Unoccupied Vehicle, with the x representing surface, underwater, or aerial
WBAT	Wideband autonomous transceiver
WGFAST	ICES Working Group on Fisheries Acoustics, Science, and Technology
WKQUAD	ICES Workshop on Collecting Quality Underwater Acoustic Data in Inclement Weather

Annex 4: Platform metadata

Table A3.1. Platform relevant metadata for all platforms included in this report - Part 1 of 3. FV: fishing vessel; RV: research vessel; FSV: fisheries survey vessel. NA: unknown or information not available.

Platform	FV Amaltal Explorer	FSV Bell M. Shimada	RV Dana	RV Dr Jorge Carranza	FSV Henry B. Bigelow	RV Investigator
Nation	New Zealand	USA	Denmark	Mexico	USA	Australia
Length (m)	65	63.6	78.4	59	63.6	93.9
Width (m)	16	15	14.7	13	15	18.5
Displacement (tonne)	1386	2479	2483	NA	2479	6082
Draft (m)	NA	5.9	5.6	NA	5.9	6.2
Motoring						
Main engine	NA	Diesel-electric	Alpha diesel type 16 V 23 LU	NA	Diesel-electric	Diesel-electric
Power (kW, HP)	NA	2 x 1150 kW (1542 HP)	2 x 2.320 HP @ 800 rmp	NA	2 x 1150 kW (1542 HP)	2 x L3 AC reversible propulsion motors rated at 2600 kW each, and 1200 kW bow Azimuth thruster
Location of acoustic equipment						
Main location of acoustic equipment	Hull	Hull, drop keel	Maine equipment is towed body; Hull mounted equipment is used as auxiliary	Hull	Hull, drop keel	Hull, drop keel

Table A3.1 (cont.)	FV Amaltal Explorer	FSV Bell M. Shimada	RV Dana	RV Dr Jorge Carranza	FSV Henry B. Bigelow	RV Investigator
Location of acoustic equipment (cont.)						
Retractable drop keel	NA	Yes	No	NA	Yes	Yes
Retractable drop keel max depth (m)	NA	9.15	NA	NA	9.1	4
Retractable drop keel operational depth (m)	NA	9.15	NA	NA	7.5	2
Towed body	NA	NA	Yes. From portside; lowered to between 3 and 7 m depth	NA	NA	NA
Deep-towed body	NA	NA	NA	NA	NA	NA
Acoustic equipment						
Acoustic equipment	Simrad ES60	Simrad EK60 (replaced by EK80), ME70	Simrad EK60	Simrad EK60	Simrad EK/ES60, ME70; RDI ADCP	Simrad EK60 (replaced by EK80), SH90, and ME70 Kongsberg EM 122, EM710, EM2040c, and SBP120 RDI Ocean Surveyor 75 and 150 kHz ADCP

Table A3.1 (cont.)	FV Amaltal Explorer	FSV Bell M. Shimada	RV Dana	RV Dr Jorge Carranza	FSV Henry B. Bigelow	RV Investigator
Acoustic equipment (cont.)						
EK60/EK80 frequencies (kHz)	38	18, 38, 70, 120, 200	18, 38, 120	38	18, 38, 70, 120, 200	18, 38, 70, 120, 200, 333
Motion recording						
Pitch and roll	NA	Applanix Pos MV V4	NA	NA	Applanix Pos MV V5	Kongsberg Seapath 330+ MRU 5+ (for EK80), Applanix POSMV (for multibeam systems)
Heave	NA	Applanix Pos MV V4	NA	NA	Applanix Pos MV V5	Kongsberg Seapath 330+ MRU 5+ and Applanix POSMV
Motion compensation	NA	Yes (no Dunford correction)	NA	NA	Yes for depth recording	Yes for depth recording

Table A3.2. Platform relevant metadata for all platforms included in this report - Part 2 of 3. FV: fishing vessel; RV: research vessel. NA: unknown or information not available.

Platform	FV Janas	RV Kaharoa	RV L'Astrolabe	FV Saxon Onward	RV Tangaroa	FV Tomi Maru
Nation	New Zealand	New Zealand	France	Australia	New Zealand	New Zealand
Length (m)	45	28	65	32	70	68
Width (m)	10	8	12.8	7	14	11
Displacement (tonne)	1079	236	2028	209	2291	1230
Draft (m)	6.5	NA	NA	NA	NA	NA
Motoring						
Main engine	NA	NA	2 x 2270 kW; 2 shafts; 2 variable pitch propellers	NA	NA	NA
HP	NA	NA	NA	NA	NA	NA
Location of acoustic equipment						
Main location of acoustic equipment	Hull	Hull	Hull	Hull	Hull	Hull
Drop keel	No	No	No	No	No	No
Drop keel max depth (m)	NA	NA	NA	NA	NA	NA
Drop keel general operational depth (m)	NA	NA	NA	NA	NA	NA
Towed body	NA	NA	NA	NA	NA	NA
Deep-towed body	NA	NA	NA	NA	NA	NA
Acoustic equipment						
Acoustic equipment	Simrad ES60	Simrad EK60	Simrad EK60	Simrad ES60	Simrad EK60	Simrad ES60
EK60/EK80 frequencies	38	38	38	38	38	38

Table A3.2 (cont.)	FV Janas	RV Kaharoa	RV L'Astrolabe	FV Saxon Onward	RV Tangaroa	FV Tomi Maru
Motion recording						
Pitch and roll	No	No	No	No	Yes	No
Heave	No	No	No	No	Yes	No
Motion compensation	No	No	No	No	Yes	No

Table A3.3. Platform relevant metadata for all platforms included in this report - Part 3 of 3. NA: unknown or information not available.

Platform	Saildrone
Nation	USA
Length (m)	7
Width (m)	0.74
Displacement (tonne)	NA
Draft (m)	2.5
Motoring	
Main engine	NA (wind powered)
HP	NA
Location acoustic equipment	
Main location of acoustic equipment	Keel
Drop keel	No
Drop keel max depth (m)	NA
Drop keel general operational depth (m)	NA
Towed body	NA
Deep-towed body	NA
Acoustic equipment	
Acoustic equipment	Simrad WBT mini (EK80)
EK60/EK80 Frequencies	38, 200
Motion recording	
Pitch and roll	VectorNav VM300
Heave	VectorNav VM300
Motion compensation	No (gimbaled transducer)